

UNIVERSITY OF OKLAHOMA

GRADUATION COLLEGE

INVESTIGATION OF HYDRAULIC AND MECHANICAL CEMENT INTEGRITY: AN
ADVANCED COMPUTATIONAL STUDY

A DISSERTATION

SUBMITTED TO THE GRADUATE FACULTY

in partial fulfillment of the requirements for the

Degree of

DOCTOR OF PHILOSOPHY

By

YUXING WU

Norman, Oklahoma

2021

INVESTIGATION OF HYDRAULIC AND MECHANICAL CEMENT INTEGRITY: AN
ADVANCED COMPUTATIONAL STUDY

A DISSERTATION APPROVED FOR THE
MEWBOURNE SCHOOL OF PETROLEUM AND GEOLOGICAL ENGINEERING

BY THE COMMITTEE CONSISTING OF

Dr. Saeed Salehi, Chair
Dr. Ramadan Ahmed,
Dr. Catalin Teodoriu
Dr. Hameed Karami
Dr. Harold Stalford

© Copyright by YUXING WU 2021
All Rights Reserved.

Acknowledgment

I would like to express my deep acknowledgment to my Ph.D. advisor Dr. Saeed Salehi for his continuous support of my study. His patient, immense, and priceless academic guidance helped me in all times of research and writing of this thesis as well as other technical articles. His class, Advanced Well Integrity, presented a new research area and provided many valuable ideas in my Ph.D. study. He was not only an excellent academic advisor for me but also a friend, helping me a lot in my study and daily life. Thanks to his encouragement, professional guidance, and continuous financial support, I can finish this work, obtain my Ph.D. diploma, own my current scholarly achievements. I am very proud that he can be my mentor.

I am grateful that Dr. Ramadan Ahmed, Dr. Catalin Teodoriu, Dr. Hameed Karami, and Dr. Harold Stalford are members of my Ph.D. committee. Their help and supports improve my theory background and research skills, which are valuable treasures in my future investigation. I also want to thank all of my committee members for their comments on my general exam. These comments allowed me to have a more insightful understanding of the topic, consolidating my knowledge background.

Many thanks to the partial support from the U.S. Department of Energy, National Energy Technology Laboratory under Award Number DE- FE0031575\ (Tuscaloosa Marine Shale Laboratory). I would also like to appreciate to the University of Oklahoma (OU), especially the Mewbourne School of Petroleum and Geological Engineering (MPGE) and Well Construction Technology Center (WCTC), for providing necessary study sources, financial supports, academic guidance, and career consultations. I would also present my

gratitude to Pegasus Vertex, Inc. for a 4-month internship. The experience taught me precious skills for my future career.

I want to extend my special appreciation to Dr. Chinedum Ezeakacha, Dr. Raj Kiran, Dr. Harshkumar Patel, Dr. Shawgi Ahmed, Dr. Musaab Elhag, Dr. Mustafa Ramadan, Mr. Nabe Konate, Mr. Raymos Kimanzi, and other colleagues. Discussion with them always inspired many fantastic ideas to have a significant improvement in my work. I appreciate Ms. Yuanjie Li, Ms. Wanyue Zhang, Ms. Weiyue Han, Ms. Shuyu Lu, Ms. Jing Fu, Mr. Yu Yan, Mr. Yurong Ma, Mr. He Zhang, Dr. Hao Xiong, and other friends who always faced difficulties together with me. Their encouragement and support make me confident to solve any challenges during my life and study.

Finally, I am profoundly grateful to my family, without whom I cannot persist such a long time to finish my doctoral study. Thanks to their understanding, love, and care, I can focus on my academic journey over the years. May almighty God bless everyone mentioned above and also those people not mentioned but have contributions. I am grateful for the assistance.

Table of Contents

Acknowledgment	iv
Table of Contents	vi
List of Tables	xi
List of Figures	xiii
Abstract	xix
Chapter 1: Introduction	1
1.1. Background	1
1.2. Problem Statement and Motivation.....	4
1.3. Objectives.....	7
1.4. Research Methodology.....	8
1.4.1. Analytical Calculation	9
1.4.2. Experimental Study.....	9
1.4.3. FEA Model.....	10
1.4.4. Mud Displacement Model.....	10
1.5. Scope of Study	11
1.6. Overview of Dissertation	12
Chapter 2: Literature Review: Current Standard, Industrial Report, And Previous Study	14

2.1.	Well Barrier System.....	14
2.2.	Potential Leakage Pathways.....	16
2.2.1.	Drilling.....	17
2.2.2.	Completion.....	18
2.2.3.	Production.....	18
2.2.4.	P&A	19
2.3.	Indicators of Gas Migration from Leakage Pathways.....	19
2.4.	Current Standards and Regulations of Maintaining Well Integrity.....	21
2.4.1.	API RP 65-2: Isolating Potential Flow Zones During Well Construction..	23
2.4.2.	API RP 96: Deepwater Well Design and Construction	25
2.4.3.	API RP 90 and API RP 90-2: Annular Casing Pressure Management for Offshore and Onshore Wells.....	26
2.4.4.	NORSOK D-010: Well Integrity in Drilling and Well Operations & Norwegian Oil & Gas 117: Recommended Guidelines for Well Integrity.....	27
2.4.5.	ISO 16530-1: Well Integrity - Part 1: Lifecycle Governance Manual.....	27
2.5.	Field Studies for Gas Leakage in Wellbores	28
2.6.	Previous Studies On Wellbore Leakage Pathway	31
2.6.1.	Wellbore Leakage Pathway – General Well.....	34
2.6.2.	Wellbore Leakage Pathway – HTHP Well.....	38

2.6.3.	Wellbore Leakage Pathway – High-Temperature Well.....	41
2.6.4.	Wellbore Leakage Pathway – CO ₂ Sequestration.....	42
2.7.	Cement Failure Mechanism	44
2.7.1.	Hydraulic Integrity Concerns.....	44
2.7.2.	Mechanical Integrity Concerns	51
Chapter 3: Experimental and Numerical Investigation of Cement Mechanical Integrity		62
3.1.	Experimental Setup.....	62
3.1.1.	Sample Preparation	63
3.1.2.	DIC and Diametric Compression Test Setup.....	64
3.2.	Numerical Model Setup	65
3.3.	Diametric Compression Test Result	68
3.3.1.	Neat Class H and Nano-Modified Cement	68
3.3.2.	Neat Class H and Geopolymer Cement	70
3.4.	Numerical Simulation Verification	72
3.5.	Stress Distribution in The Base Scenario.....	75
3.6.	Influence of Young’s Modulus and Poisson’s Ratio.....	78
3.7.	Chapter Summary.....	81
Chapter 4: Numerical Investigation of Temperature and Pressure Impacts on Cement Integrity (A Parametric Study).....		84

4.1. Numerical Setup.....	85
4.2. Analytical Verification.....	87
4.3. Failure Analysis of Two Heat Flow Directions	89
4.4. Sensitivity Analysis.....	91
4.4.1. Heat Flow from Formation to Casing ($\Delta T < 0$)	93
4.4.2. Heat Flow from Formation to Casing ($\Delta T > 0$)	95
4.5. Chapter Summary.....	98
Chapter 5: Numerical Investigation of Cement Hydraulic Integrity Impacted by	
Displacement Factors.....	100
5.1. CFD Simulation Setup	100
5.2. Result and discussion	103
5.2.1. WBM Displaced by Neat Class G and Geopolymer.....	104
5.2.2. Effect of Density Ratio	105
5.2.3. Effect of Cement Injection Rate	107
5.2.4. Effect of Mud Contamination	108
5.3. Chapter Summary.....	110
Chapter 6: Conclusion, Recommendations, And Future Work	
6.1. Conclusions	113
6.2. Recommendations	114

6.3. Future Work	116
Nomenclature	118
Reference	122
Appendix: Biography.....	147

List of Tables

Chapter 2

Table 2.1 Major primary and secondary well barriers during drilling, completion, production, and P&A stage.	16
Table 2.2 Summary of objectives and scopes for API, NORSOK, Norwegian Oil & Gas, and ISO standards.	22
Table 2.3 Statistical analysis of well integrity and barrier failures around the world (failure barriers are marked with red font).	28
Table 2.4 Summary of the literature studied in this dissertation.	32
Table 2.5 Model setup of Radonjic and Oyibo (2015) investigating effect of OBW on bond and cement strength.	45

Chapter 3

Table 3.1 Details of cement slurry design.	63
Table 3.2 Components of nano-synthetic graphite.	64
Table 3.3 Material properties of the casing, cement, and formation in the base case.	67
Table 3.4 Young's modulus and Poisson's ratio were used for evaluating the effect of elastic properties on cement performances.	68

Chapter 4

Table 4.1 The properties of FORGE geothermal wellbore (from Moore et al. 2019).	85
Table 4.2 Material properties for the base case.	87
Table 4.3 Temperature of casing and formation used for sensitivity analysis.	89
Table 4.4 The studied parameters for sensitivity response analysis.	93

Table 4.5 Comparison of mechanical stress sensitivity to various parameters..... 97

Chapter 5

Table 5.1 Properties of cement slurries and drilling muds used in the model..... 103

List of Figures

Chapter 1

- Figure 1.1 Schematic of mud-cement displacement for hydraulic well integrity considerations. 2
- Figure 1.2 Voids in cement because of poor drilling fluid displacement (Khalifeh et al., 2016). 2
- Figure 1.3 An example of loss well integrity in Macondo. Integrity failure can lead to catastrophic health, safety, and environmental consequences (BOEMRE, 2011). 3
- Figure 1.4 Schematic of the enlarged and narrow wellbore (also call over-gauge and under-gauge wellbore). 6
- Figure 1.5 Two heat flow patterns in geothermal wells. For the shallow depth of production wells, heat flows far away from the wellbore. For the deep depth of injection wells, heat flows towards the wellbore. 7
- Figure 1.6 Graphical overview of research methodology in this study. 9

Chapter 2

- Figure 2.1 Classification of wellbore safety barrier (after Skalet, 2005). 15
- Figure 2.2 Sketch map of potential wellbore leakage pathways (red lines indicate the channels). 17
- Figure 2.3 Cross-section schematic of three common wellbore configurations: a) a fully cemented well with a closed outer annulus, b) a partially cemented well with drilling fluid and a closed outer annulus, and c) a partially cemented well with formation fluids and a closed outer annulus, and c) a partially cemented well with formation fluids and an open

outer annulus (casing directly contacts with formation fluids). Light green arrows indicate the potential leakage pathways (Lackey and Rajaram, 2019).....	21
Figure 2.4 Left sketch illustrates fluid migration outside of the casing. Right sketch shows different mechanisms for failure initiation. i.e., from top to bottom, they are radial cracking, plastic deformation, casing-cement debonding, cement-formation debonding, incomplete cementing, and channelization.....	36
Figure 2.5 Typical creep deformation curve for salt formation. Jandhyal et al. (2013) evaluated salt deformation assuming steady-state creep behavior (red zone).	37
Figure 2.6 Non-uniform field stresses model: (i) uniform inner and outer pressure with thermal effect; and (ii) non-uniform external pressure (blue color is casing, gray color indicates cement, yellow color represents formation, and red arrows present the directions of loads).	41
Figure 2.7 Graphically explanation of the challenges when supercritical CO ₂ injects into the wellbore.....	43
Figure 2.8 Bond failure under shear stress conditions. a) Continuous bond model complete failure, b) Discontinuous bond model (interfacial lock-up) partially but still intact.	46
Figure 2.9 Drilling fluid displaced by cement slurry in the eccentric annulus. Casing eccentricity is calculated by $e = \varepsilon R1 - R2$, where e is casing eccentricity, R1 and R2 are wellbore radius and casing radius.	47
Figure 2.10 Mud displacement efficiency influenced by enlarged wellbore due to washout.	51

Figure 2.11 Schematic showing six typical cement failure modes. Casing, cement, and formation are represented by blue, gray, and orange colors. Red lines indicate the failure in each case (modified from Wang and Taleghani, 2014).....	53
Figure 2.12 Stresses influencing the failure modes of set cement.....	54
Chapter 3	
Figure 3.1 Dimension of the casing-cement-formation system used in diametric compression tests. Blue, gray, and yellow colors indicate steel casing, cement sheath, rock formation, respectively.	64
Figure 3.2 a) Casing-cement-formation system before and after painting; b) Graphically explanation of the measurement of full-field strain and deformation using DIC technique.	65
Figure 3.3 a) Geometry of the casing-cement-formation system compressing diametrically with a curved loading platen; b) Magnified sketch of load platen. Red line represents the contact surface between load platen and sample. The contact angle is 23°	66
Figure 3.4 a) Strain distribution of the neat class H cement at different times; b) Strain distribution of the nano-modified class H cement at different times. Pictures in the first row illustrate the horizontal strain distribution, while the second row is the vertical strain distribution.	69
Figure 3.5 Comparison of the neat class H to nano-modified cement under a diametric compression test.....	70
Figure 3.6 Strain distribution of the casing-geopolymer-formation at different times.	71

Figure 3.7 Comparison of the neat class H to geopolymers cement under a diametric compression test.....	72
Figure 3.8 Comparison of the numerical solution to DIC diametric compression test results. Yellow, blue, and green mark out the elastic, failure initiation, and fully debonding zone, respectively.	73
Figure 3.9 Comparison of the horizontal and vertical strain distribution obtained from a) DIC experiment and b) numerical simulation.....	74
Figure 3.10 Radial and hoop stress distribution around the wellbore. Because of the symmetricity of the model, the stress in θ of 0° - 90° is shown. Blue and orange solid lines indicate stress in the casing-cement and cement-formation interfaces, respectively. Red and purple dash lines indicate compressive and tensile strengths.	76
Figure 3.11 Radial and hoop stress distribution in different orientations. a) The comparison of hoop stress in 0° (y-axis), 45° , and 90° (x-axis); b) The comparison of radial stress in 0° (y-axis), 45° , and 90° (x-axis). Blue area indicates the casing, gray area is cement and red area is formation.	77
Figure 3.12 Effect of Young's modulus and Poisson's ratio along 0° on a). radial stress at the casing-cement interface, b). hoop stress at the casing-cement interface, c). radial stress at cement-formation interface, and d). hoop stress at cement-formation interface.	79
Figure 3.13 Effects of Young's modulus and Poisson's ratio along 45° on a). radial stress at the casing-cement interface, b). hoop stress at the casing-cement interface, c). radial stress at cement-formation interface, and d). hoop stress at cement-formation interface.	80

Figure 3.14 Effects of Young’s modulus and Poisson’s ratio along 90° on a). radial stress at the casing-cement interface, b). hoop stress at the casing-cement interface, c). radial stress at cement-formation interface, and d). hoop stress at cement-formation interface. 81

Figure 3.15 Flowchart of the extensive investigation of cement performance using a numerical approach. 82

Chapter 4

Figure 4.1 a) Schematic of the 2D numerical model with boundary conditions. b) Actual model with mesh elements (left) and the dimension of casing and cement (right). 86

Figure 4.2 Comparison of radial and hoop stresses at casing-cement and cement-formation interface between analytical and simulating results: a) radial and b) hoop stress distribution when heat flow toward casing; c) radial and d) hoop stress distribution when heat flows away from the casing. 88

Figure 4.3 a) Radial stress and b) hoop stress in variable differential temperature (ΔT) in the casing-cement and cement-formation interfaces at 0° and 90° 91

Figure 4.4 Radial stress in the casing-cement interface when heat transfers from formation to casing ($\Delta T < 0$) a) at 0° and b) at 90°; hoop stress in the casing-cement interface c) at 0° and d) at 90° 94

Figure 4.5 Radial stress in the casing-cement interface when heat transfers from the casing to the formation ($\Delta T > 0$) a) at 0° and b) at 90°; hoop stress in the casing-cement interface c) at 0° and d) at 90° 96

Chapter 5

Figure 5.1 Flowchart of using an integrated rock-fluid model to investigate the mud displacement characterization in enlarged wellbores (Caliper log of TMS is used for the develop annulus geometry).....	102
Figure 5.2 a) Caliper log of one well in TMS from 12020.5 ft to 12032.5 ft; b) Verified fine mesh used in the model.....	103
Figure 5.3 a) Snapshot of a class G cement-WBM displacement in the annulus. Comparison of cement volume fraction after displacement between neat class G and Geopolymer b) in the upper and c) lower annulus.	105
Figure 5.4 a) Comparison of cement volume fraction of the middle of the enlarged section in the upper annulus with different density ratios. b) Snapshots of mud displaced by the cement slurries with 1.2, 1.4, 1.6, and 1.8 of density ratios (from top to bottom) after displacement.	106
Figure 5.5 a) Comparison of cement volume fraction of the middle of the enlarged section in the upper annulus with different flow rates. b) Snapshots of mud displaced by the cement slurries with 0.1, 0.2, 0.3, 0.4, and 0.5m/s of flow rate (from top to bottom) after displacement.	107
Figure 5.6 Relationship between shear stress and shear rate for a) geopolymer and b) class G cement contaminated with different amounts of WBM.....	108
Figure 5.7 Cement volume fraction of middle point in the enlarged section (red “X” mark) of geopolymer and class G cement contaminated with different amounts of WBM.....	109

Abstract

Cement sheath is a significant barrier to maintain the zonal isolation of wells, preventing severe consequences such as kick (or influx) accidents, environmental contaminations, and safety threats. Many previous investigations have assessed the performance of cement via experimental and analytical studies based on several setups. However, further advanced studies should be conducted to solve the severe challenges posed by the increased exploration activities in harsh operational environments and advanced stimulation in long lateral wells.

To achieve this goal, mechanical and hydraulic cement integrity considerations should be involved during the analysis. Mechanical considerations should satisfy the requirements of structural failure prevention in the cement under different wellbore conditions, such as high-temperature high-pressure (HTHP). Hydraulic integrity needs quality evaluations of cement slurry. This dissertation aims to evaluate cement quality by analyzing the mechanical stresses around the set cement and the fluid mechanics in the cement displacement processes using a numerical approach. The specific objectives are to (i) investigate the performance of cement under various designs, operations, and loading conditions, (ii) identify the influencing parameters which affect the cement performance, and (iii) evaluate the influence of enlarged wellbore on the mud displacement efficiency via a numerical approach.

Diametric compression simulation indicates that cement sheath is likely to fail at the casing interface before the formation interface. Along with the casing-cement interface,

failure would initiate at the location parallel to the direction of applied load ($\theta = 0^\circ$). High hoop stresses exceeding the limiting strength are the primary cause of the cement failure. HTHP wellbore conditions have a significant influence on cement integrity due to high thermal loads. Heat flow direction away from the wellbore ($\Delta T > 0$) generates approximately 65% higher magnitudes of radial and hoop stresses in the cement sheath compared to heat flow direction toward the wellbore ($\Delta T < 0$). Sensitivity analysis indicates that regardless of the heat transfer direction, radial and hoop stresses in cement have a higher sensitivity to temperature changes than internal pressure load. For heat flow toward the wellbore ($\Delta T < 0$), temperature difference, internal casing pressure, and in-situ horizontal stresses are three main predictors of stresses in cement. For heat flow toward the formation ($\Delta T > 0$), there is no precise predictor of stresses in cement. Radial stress primarily depends on temperature difference and internal casing pressure, followed by the cement's Young's modulus and in-situ stresses. On the other hand, Hoop stress mainly depends on the cement's Young's modulus and Poisson's ratio, followed by temperature difference and in-situ stress. For the cement hydraulic integrity study, an incomplete mud removal has a high risk of occurring at the top of the annulus.

Technical novel information of this research is to (i) investigate the performance of different cement under subsurface conditions by an experimentally validated finite element analysis (FEA) model, (ii) use the casing-cement-formation system to represent a more realistic wellbore condition, and (iii) study the influence of fluid dynamics during mud removal.

Chapter 1: Introduction

1.1. Background

In recent decades, the increasing energy requirements and depletion of conventional wells force the petroleum industry to focus on explorations and drilling activities in complex environments. Advanced stimulation methods such as hydraulic fracturing, wellbore acidizing, and explosives are commonly used to maximize the recovery, achieving the financial balance. These operations pose a more challenging problem concerning well integrity. A worldwide study reported that more than 380,000 wells in Canada, China, Netherland, offshore Norway, the U.K., and the U.S. had wellbore integrity issues (Davies et al., 2014). Lack of wellbore integrity can induce negative economic impacts, environmental consequences (i.e., groundwater contamination, greenhouse gas emission, etc.), and safety threats.

Many wellbore barriers are used to prevent the loss of integrity, such as drilling fluids, casing, wellhead, Blowout Preventer (BOP), and cement (NORSOK D-010, 2013). Cement sheath, placed between casing and formation, is an important barrier to maintaining zonal isolation and preventing fluid communication because of its extremely low permeability and porosity (Wang and Taleghani, 2014). A survey shows that cement design is a top technical challenge in well construction (Oil & Gas IQ, 2015). Herein, the performance of cement sheath plays a vital role in wellbore integrity analysis. Two aspects are necessary for an excellent cement design – hydraulic and mechanical considerations. Hydraulic integrity considerations mainly focus on mud displacement, while mechanical concerns structural failures.

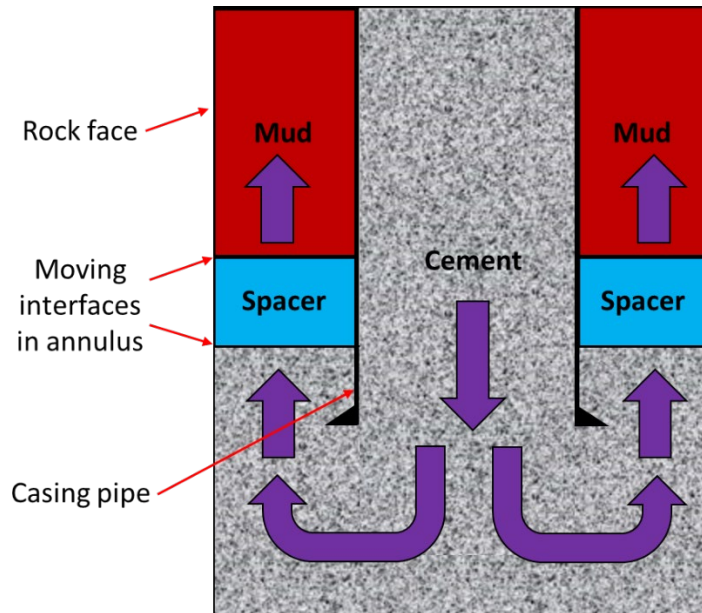


Figure 1.1 Schematic of mud-cement displacement for hydraulic well integrity considerations (mud displaced by cement and spacer).

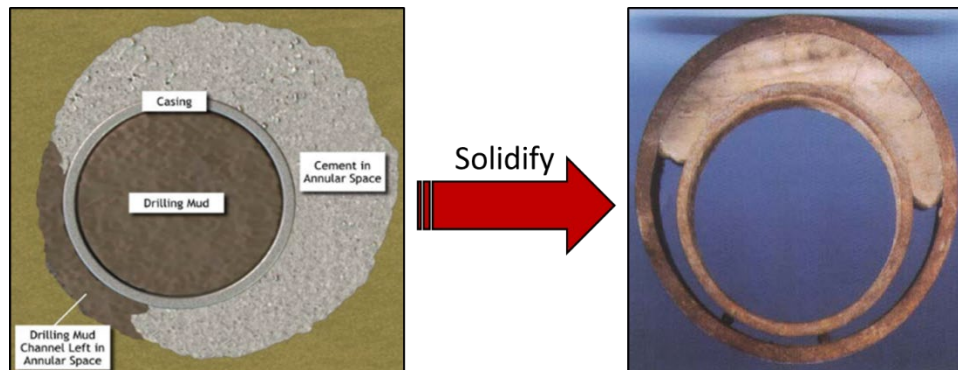


Figure 1.2 Voids in cement because of poor drilling fluid displacement induced by casing eccentricity (Khalifeh et al., 2016).

Hydraulic well integrity requires the evaluation of drilling fluid displacement (Figure 1.1). Many factors can significantly affect the density ratio of fluid, rheology, and pumpability. (Kleef and van Vliet 1993; Colmenares et al., 1997; Khalifeh et al., 2016; Bai et al., 2016; Kiran et al., 2017; Teodoriu and Bello, 2020; Kamali et al., 2020; Kimanzi et

al., 2020). More details will be discussed in the next several sections. Improper mud removal can lead to cement void problems, resulting in surface debonding (**Figure 1.2**).

Mechanical integrity should consider structural failures of the cement sheath under different well conditions, such as high-temperature and high-pressure (HPHT) and pressure and thermal cycle loading. For example, the Macondo accident on April 20th, 2010, resulted in the death of 11 workers and severe injuries to 16 others. The cause of the incident was the negligence of the rig crew to restore the defects in the cement sheath detected during the negative pressure test. It made the cement and casing barriers fail (BP, 2010; BOEMRE, 2011; CCR, 2011, DHSG, 2011). Gases propagated along the leakage pathway to induce an underground blowout (**Figure 1.3**).

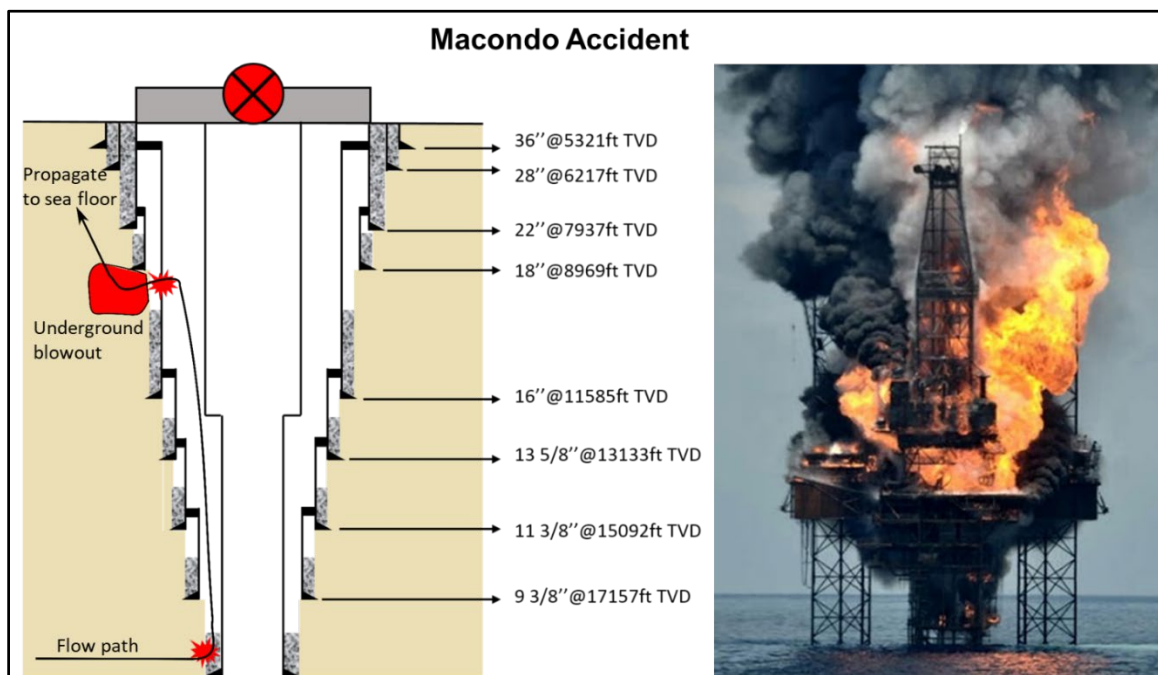


Figure 1.3 An example of loss well integrity in Macondo. Integrity failure can lead to catastrophic health, safety, and environmental consequences (BOEMRE, 2011).

1.2. Problem Statement and Motivation

The complexity of modern oil and gas requires a more comprehensive understanding of the mechanisms of barrier systems. Although the industry has published many regulations and standards to ensure the quality of cement sheath, many accidents still happened. A statistic report in 2017 presented 156 loss of control (LOC) events that occurred in 2000-2015. Approximately 54.5% of the LOC event are in the Gulf of Mexico. Drilling, workover, and production are recognized as high-risk activities, which are 45%, 21%, and 17% of LOC events happened, respectively. Blowout (or kick) has the highest potential for consequences (Holand et al., 2017). Therefore, the investigation of the barrier is crucial to increase production efficiency.

Cement sheath is a critical barrier to permanently shut off water penetration into the well and establish zonal isolation after a casing string has been run into a wellbore. The reliability of the cement sheath, especially in some complex formation and stimulating conditions, is becoming a critical challenge. Three types of mechanisms typically lead to the loss of cement integrity – hydraulic, mechanical, and chemical degradation (Bois et al., 2012). The hydraulic mechanism involves inefficient displacement of mud/cement due to casing eccentricity or improper cement estimation, this resulting in the channeling of cement in the wide side and slow-moving or immobile mud in the narrow region (Ermila et al., 2013). Mechanical degradation occurs when the compressive or tensile loadings on the cement are higher than the corresponding limiting strength (Patel et al., 2019). Chemical degradation is the cement damage because of the interaction between cement and the fluid, such as drilling fluid/mud or formation fluids (Brandi et al., 2011; Walsh et al.,

2013). Each failure mechanism can be interactional with the other. For example, a cement sheath is subjected to mechanical damage accelerated by chemical exposure leading to fluid penetrate deeper into the cement sheath. The mechanical damage can be due to mud contamination triggering by improper displacement (Carroll et al., 2016). Details of the literature review are presented in the next Chapter. In this dissertation, hydraulic and mechanical degradation is mainly focused on, and chemical degradation will be briefly discussed. Three knowledge gaps aim to be solved – (i) mud displacement in an enlarged wellbore; (ii) more realistic simulation using casing-cement-formation system; (iii) cement integrity evaluation in HTHP wells.

Mud displacement is the procedure that using cement slurry or other fluids remove drilling fluid from the casing-formation annulus. For a complex formation (i.e., shale), the wellbore size is different from the drill bit due to swelling and dispersion. Therefore, the irregular wellbore shape plays a vital role in displacement efficiency (**Figure 1.4**). However, the effect is not fully understood and required more investigations.

Another knowledge gap is the improvement of the investigation method. Previous studies have published many methods to test cement and its bond strength (see Chapter 2). In the field conditions, a casing-cement-formation is an integrated system. An advanced testing method considering the interactions of casing, cement, and formation should be developed.

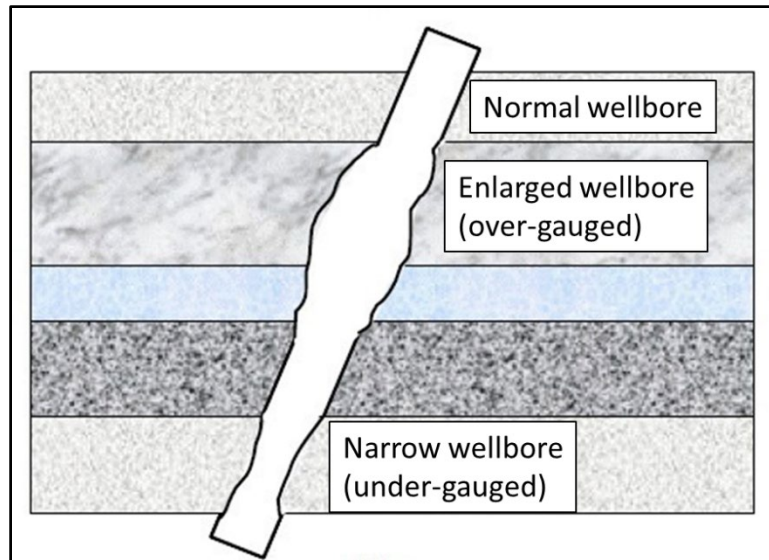


Figure 1.4 Schematic of a wellbore with enlarged (over-gauge) and narrow (under-gauge) segments.

The last knowledge gap focuses on the cement integrity evaluation in HTHP wells. In this condition, expansion and shrinkage induced by thermal loads cannot be negligible. This dissertation also highlights the difference of mechanical properties in two kinds of heat flow patterns – (i) heat flows from casing to formation and (ii) heat flows from formation to casing. The investigation has guiding significance in cement integrity evaluation of HTHP wells, such as geothermal wells (**Figure 1.5**).

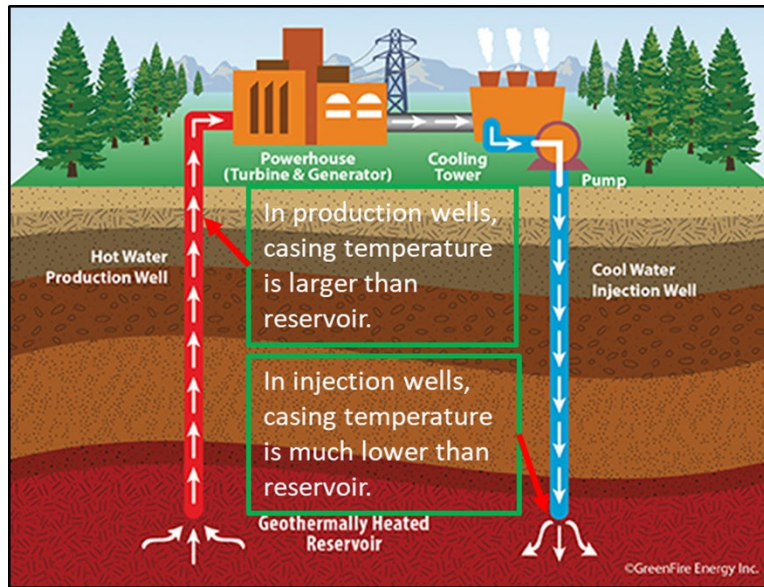


Figure 1.5 Two heat flow patterns in geothermal wells. For the shallow depth of production wells, heat flows far away from the wellbore. For the deep depth of injection wells, heat flows towards the wellbore.

1.3. Objectives

In this dissertation, the quality of cement sheath is evaluated from mechanical and hydraulic perspectives using validated numerical simulations. Furthermore, all of the models can be extended to other cement systems if cement properties are known. Following are the specific objectives:

- Investigate cement mechanical performance in lab-scale under diametric compression using a realistic configuration, casing-cement-formation system.
- Advance the cement integrity evaluation using a numerical simulation approach.
- Extend the lab-scale test to field-scale and consider the influence of HTHP to find the influencing parameters.
- Understand the influence of heat flow patterns and identify critical parameters affecting the performance of cement sheath.

- Analyze cement hydraulic behavior (mud removal) in the annulus between casing and formation.

This dissertation presents (i) a computational fluid dynamics (CFD) model to test displacement efficiency of different fluid systems (i.e., water-based mud displaced by Geopolymer and class G cement) and influence of mud contamination; (ii) diametric compression test evaluate the effect of elastic properties on the integrity using a casing-cement-formation system; (iii) a real-scale FEA model with thermal considerations is developed to simulate the mechanical stresses under HTHP conditions; (iv) identify the critical parameters affecting hydraulic and mechanical degradation of cement by the conduction of sensitivity response curves.

1.4. Research Methodology

This study uses analytical calculation, experimental investigation, and numerical models to evaluate cement performance from hydraulic and mechanical perspectives. Literature, field reports, regulations, and standards, such as API, NORSOK, Norwegian Oil & Gas Standard, and ISO are reviewed to identify the knowledge gaps for the well integrity (details are shown in Chapter 2). For hydraulic investigations, a CFD model is developed to assess the mud removal in enlarged wellbores. FEA models are used for mechanical degradation studies. Diametric compression and HTHP simulation are validated by analytical and experimental results, respectively (**Figure 1.6**).

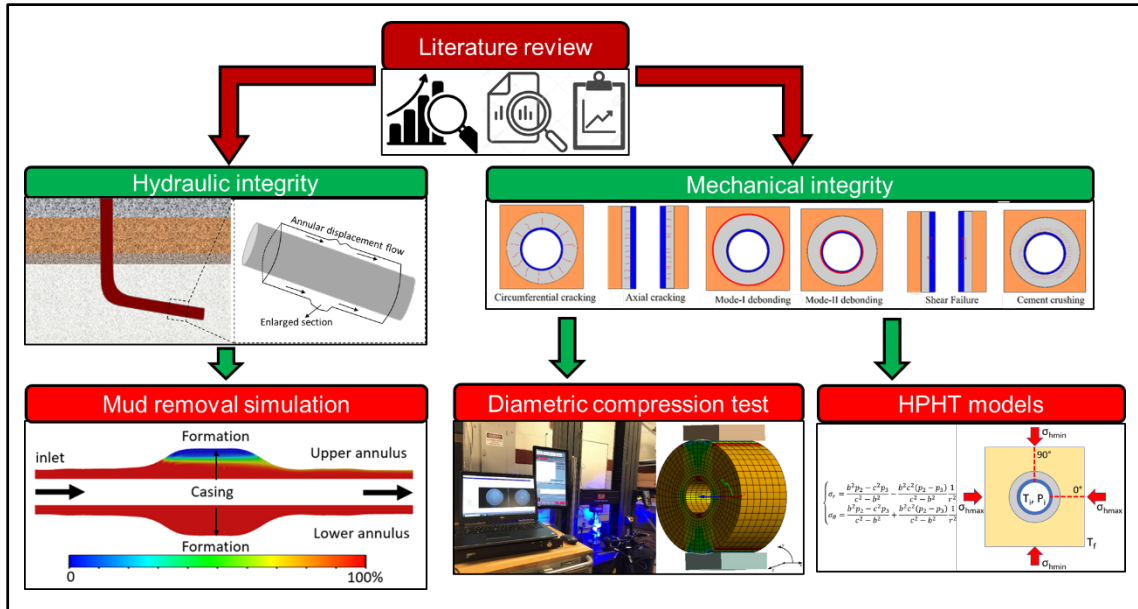


Figure 1.6 Graphical overview of research methodology in this study.

1.4.1. Analytical Calculation

Previous studies have published many analytical models to investigate cement integrity by evaluating mechanical stresses near cement (see Chapters 2 and 5). After comparing elastic, poroelastic, thermoelastic, and elastoplastic models, the study uses a modified thermoelastic solution to validate the true-scale HTHP model. Some parameters are selected based on the analytical calculation equations. These parameters are identified as the target data to perform sensitivity analysis in future numerical modeling.

1.4.2. Experimental Study

A digital image correlation (DIC) experiment is conducted to measure the strain distribution of the casing-cement-formation system under diametric compression (see Chapter 3). The objective of this experiment is to verify the FEA model. Strain map and load-time relationship from DIC and FEA are compared. Reviewing the experimental

results also can provide preliminary results, which are helpful to understand the FEA model. Additionally, the input data for simulation are also tested in the lab.

1.4.3. FEA Model

FEA models are utilized to simulate the performance of cement sheath under different mechanical properties, in-situ conditions, and operations (see Chapters 4 and 5). Models are developed using commercial software – ANSYS Mechanical. Two models aim to evaluate the cement under diametric compression and HTHP, respectively. The former model is verified by the DIC experiment, while the last one is validated using analytical calculations. These validated models perform parametric and sensitivity studies by simulating various cement systems, applied load, and well condition scenarios.

1.4.4. Mud Displacement Model

As mention before, mud displacement is recognized as a crucial procedure to determine the quality of cement sheath. Improper mud removal can result in a mixture of cement and mud, leading to low cement strength, called mud contamination. In the worst case, drilling fluids remain in the annulus, and voids will develop after the solidification of the cement. Formation fluid and gas can escape from the channel to have a blowout accident. In this study, a CFD model is developed to predict the displacement quality (see Chapter 6). The model is conducted using Ansys Fluent based on the multiphase finite-volume theory. It would be a helpful tool for optimizing the displacement by testing different cement receipts and operational scenarios. Mud contamination on cement displacement efficiency is also investigated.

1.5. Scope of Study

Hydraulic and mechanical degradations of cement sheath are discussed in this dissertation. For the hydraulic degradation analysis, Displacement of WBM using geopolymer and class G cement are compared. The rheological properties and density of mud and cement systems are measured in the lab. Cement with 0.1, 0.2, 0.3, 0.4, and 0.5 m/s of flow rate are simulated to evaluate the effect of cement injection rate. Geopolymer and class G cement are contaminated with 5%, 10%, 15%, and 20% of WBM, respectively. The contaminated cement is used to perform the mud contamination investigation on the displacement. The properties of contaminated cement are measured.

For the mechanical degradation analysis, diametric compression simulation is used to simulate the casing-cement-formation integrity. The cement is assumed to be solid with linear elastic properties and treated as an impermeable and non-porous material. After verifying the diametric compression test, the model was further extended to varying cement Young's modulus and Poisson's ratio. Inputting these data to the model can indirectly investigate the effect of different cement recipes, aging, curing temperature, and curing time on cement performance.

Investigation of HTHP well integrity is based on a true-scale FEA model. Analytical calculations are utilized for verification. To simplify the model and save the calculating time, the model follows plane strain assumptions. Two kinds of heat flow directions are considered in the simulation. A parametric study is applied to investigate the relative influence of temperature difference, cement material properties, and operational factors on stresses within the cement. The risk of cement failure is evaluated by the six

common failure modes of cement introduced by Schreppers (2015) – circumferential cracking, axial cracking, inner and outer debonding, shear failure, and cement crushing.

1.6. Overview of Dissertation

The dissertation is separated into ten chapters. Following is the topic that will be involved in each chapter:

- Chapter 1 introduces the knowledge background and structure of this dissertation. Research background, problem statement and motivation, objectives, research methodology, and scope of the study are involved.
- Chapter 2 presents a literature review to understand well integrity and potential wellbore leakage pathways. The review covers current standards, industrial reports, conference papers, and journal publications. Failure mechanisms, analytical solutions, modeling, experimental studies, cement properties, and characterizations are discussed.
- Chapter 3 shows an introduction to the DIC experiment and simulation. DIC experiments section shows the experimental setup and bond strength evaluation. Numerical studies extend the results to evaluate Young's modulus and Poisson's ratio on cement mechanical performances.
- Chapter 4 discusses the procedure for the investigation of cement integrity under HTHP conditions using a numerical model. Details of the model are presented. Two different temperature modes are compared. A sensitivity study is conducted to compare the influence of several parameters, such as thermal conductivity, expansion coefficient, differential temperature, internal casing pressure, Young's

modulus, Poisson's ratio, and in-situ stresses ratio. This chapter also mentions failure modes for evaluating the risk of losing integrity.

- Chapter 5 presents the numerical setup of mud displacement simulation. The influence of wellbore enlargement cement receipt, mud contamination, and flow rate is discussed.
- Chapter 6 summarizes all results of this dissertation and presents major conclusions, recommendations, and future work of this study.

Chapter 2: Literature Review: Current Standard, Industrial Report, And Previous Study

Well integrity is defined as “the application of technical, operational, and organizational solutions to reduce risk of uncontrolled release of formation fluids and well fluids throughout the lifecycle of a well” (NORSOK D-010, 2013). To control the well, a barrier system is used to prevent the unintended communication of fluids within the well and preventing unplanned emissions to the environment. Although many standards and regulations have been published, oil and gas wells accidents due to loss of integrity still occurred in past decades. Following will introduce i) overview of well barrier systems, ii) potential leakage pathways, iii) indicators of gas migration, iv) standards and regulations review, v) field studies, vi) previous studies on wellbore leakage pathways, and vii) cement failure mechanism study.

2.1. Well Barrier System

Barriers are impermeable objects preventing the uncontrolled release of fluids. NORSOK D-010 (2013) classify the safety barrier into two types based on the prevention sequence. When the fluids migrate, the first physical barriers stopping the movement are primary barriers such as mud (or drilling fluids). If the primary barrier fails, the next obstacles that fluids encounter are secondary barriers such as casing, packer, wellhead, and drilling BOP (NORSOK D-010, 2013). Sklet (2005) presented a classification of wellbore safety barriers (**Figure 2.1**). Physical barriers are functional in the whole lifecycle of wells, while technical barriers are initiated during the gas migration. Administrative (or procedural) barriers indicate normative management procedures. Human factor (or

organizational/operational) barriers refer to few mistakes in human actions during different operations.

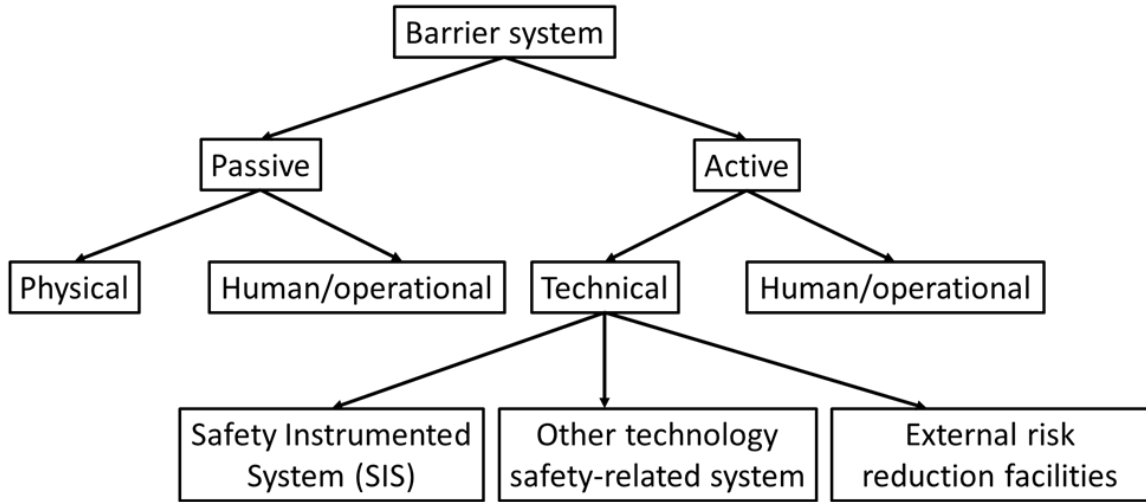


Figure 2.1 A common method to classify wellbore safety barriers (after Skalet, 2005).

The selection of barrier elements is significantly dependent on well type and life stage. **Table 2.1** presents an example of a barrier system used during drilling, completion, production, and P&A stages (Khalifeh and Saasen, 2020). Drilling fluid is a primary barrier providing hydraulic isolation during drilling operations. It creates an overbalance condition between the fluid column and rock formation to prevent kicks (or influx) of formation fluids in the wellbore. Cement is another common barrier consisting of Portland cement with special additives. It is set in the column of casing strings and casing-formation to provide a continuous, permanent, and impermeable hydraulic seal. The sealability of cement is dependent on its tensile and compressive strength, porosity, permeability, bond strength, and reactions with fluids (Carey et al., 2010; Williams et al., 2011; Thomas et al., 2014; Jafariesfad et al., 2017; Kimanzi et al. 2020). In addition, fatigue properties should be considered when casing and cement are set in a well with cycle pressure and temperature

(Ugwu, 2008; Yuan et al., 2013; Shadravan et al., 2014; Shadravan et al., 2015a and 2015b; Vralstad et al., 2015; Wu et al., 2020). For other barriers such as wellhead, BOP, packer, and tubing hanger, the purpose is to support a physical hindrance for controlling formation fluids or injected fluids (Sklet 2005).

Table 2.1 Major primary and secondary well barriers during drilling, completion, production, and P&A stages.

<i>Stage of Wellbore Lifecycle</i>	<i>Primary Well Barriers</i>	<i>Secondary Well Barriers</i>
Drilling	Drilling fluid	Annulus cement, casing, wellhead, and BOP
Completion	Drilling fluid	Annulus cement, casing and string, hanger, wellhead, and BOP
Production	Production/completion string	Annulus cement, casing, hanger, wellhead, and BOP
P&A	Plug, casing or liner, cement in perforation zone	Annulus cement, casing, surface plug, and wellhead

2.2. Potential Leakage Pathways

Leakage pathways are a primary challenge to damage wellbore by gas migration. Previous studies have presented ten common locations – at the casing-plug interface, through a plug of Plugging and abandonment (P&A), at the casing-cement interface, through casings, through cement, at cement-formation interface, through fractures within the cement, through dual barrier system (i.e., liner packer), at the wellhead (either via Xmas tree and valves), and through the Blowout preventer (BOP) (**Figure 2.2**). As mentioned in the last section, the selection of barrier elements depends on the stage of wellbore life. The

following presents the details of wellbore leakage pathways during the drilling, completion, production, and P&A stage.

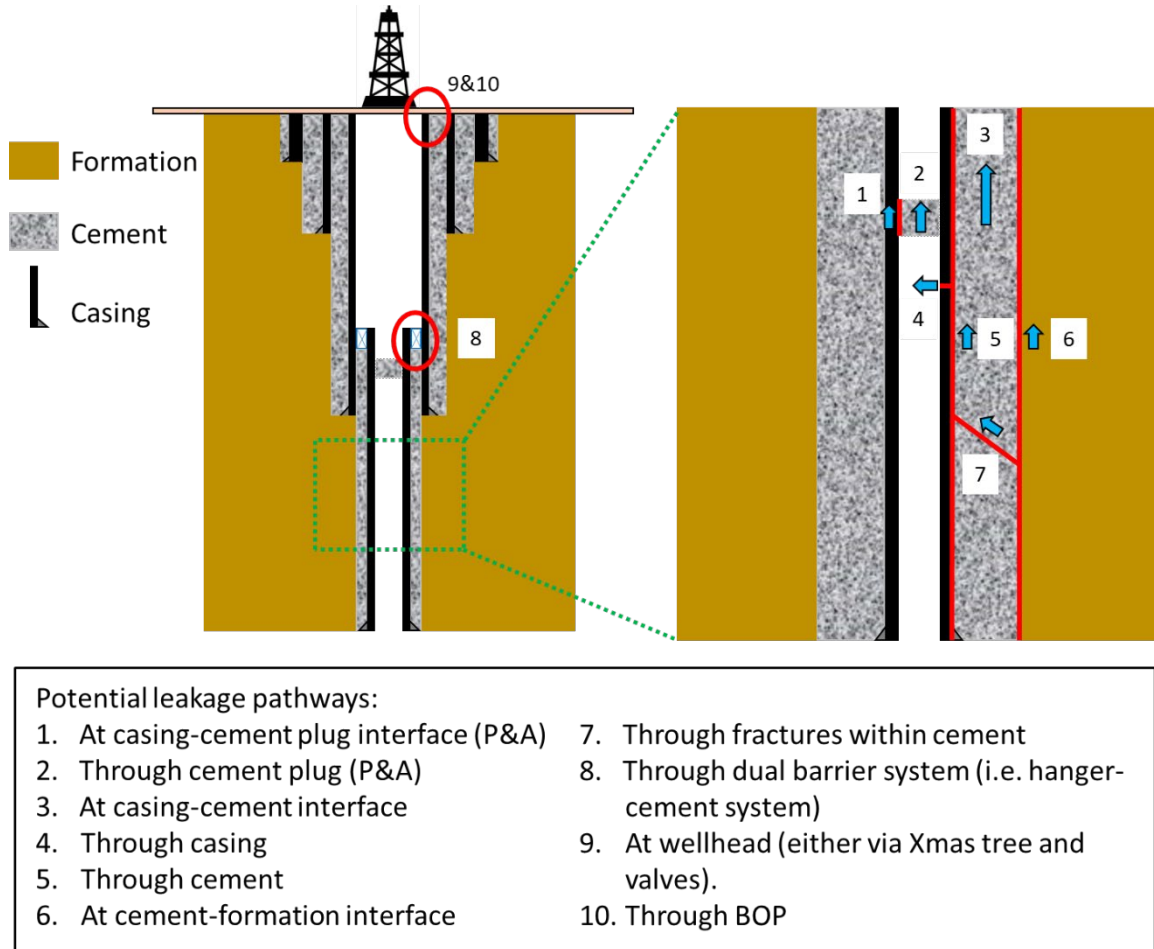


Figure 2.2 Ten common potential wellbore leakage pathways in a wellbore (red lines and circles locate the possible channels).

2.2.1. Drilling

When an insufficient mud weight is applied during the drilling stage, gas (or kick) is developed due to a lack of overbalance between wellbore and formation. Drilling fluid is recognized as the primary barrier to stop gas migration. Last casing sets, annulus cement, wellheads, and drilling BOPs are secondary barriers to maintain zonal isolation. Otherwise, the release of pressure during gas leaking to the surface would result in severe

consequences. The potential leakage pathways are at casing-cement and cement-formation interfaces, within annulus cement, through the last casing sets, wellheads, and BOPs (Type #3, #4, #5, #6, #7, #9, #10 in **Figure 2.2**). It is noted that at the beginning of drilling, before the installment of BOP, drilling fluid is the only barrier in the wellbore. The potential leakage pathway is through the fluid column.

2.2.2. Completion

The objective of well completion is the preparation of production or injection after drilling. The standard procedures include casing, cementing, perforating, and stimulating. Leakage can occur through annulus cement, interfaces, casing, wellhead, and drilling BOP (Type #3, #4, #5, #6, #7, #9, #10 in **Figure 2.2**). Especially for some production wells, a liner is installed with a hanger. The hanger with the annular cement can develop a dual barrier system to prevent gas movement (Type #8 in Figure 2.5). Besides, to cement the annulus, completion strings are used for pumping cement to displace mud. Improper cement design can result in influx leaking through the string.

2.2.3. Production

Production string (or completion string) is the primary barrier during production due to drilling fluid removed by cement in well completion procedures. When the well loses control, gas tends to transport to the surface via the string. Other locations are mainly near annular cement, casing, liner hanger (if applicable), wellhead, and BOP (Types #3, #4, #5, #6, #7, #8, #9, #10 in **Figure 2.2**).

2.2.4. P&A

P&A is used for permanent close wells or abandonment of a section of the well for sidetracking. Casings and other equipment are recycled. Cement plugs are placed across any open hydrocarbon-bearing formations, casing shoes, and aquifers. The selection of cement plugs is crucial for the adaptation of different environments. Besides leakage pathways near annulus cement, casing, surface plug, and wellhead, gas can also leak through the plug and its interface to the casing (Type #1 and #2 in **Figure 2.2**). P&A also requires cementing the reservoir perforation zone. The low quality of the cementing works leads to leakages.

2.3. Indicators of Gas Migration from Leakage Pathways

Sustained casing pressure (SCP) and surface casing vent flow (SCVF) are two typical indicators of loss integrity. Gases move along the wellbores to the surface via leakage pathways. The migration leads to gas either accumulating pressure at the wellhead or escaping to the atmosphere from the wellhead. **Figure 2.3** illustrates the three primary mechanisms of developing SCP and SCVF (Harrison, 1983 and 1985; Watson and Bachu, 2009; Bair et al., 2010; Nowamooz et al., 2015; Roy et al., 2016; Sherwood et al., 2016; Conley et al., 2016; Lackey et al., 2017; Bachu, 2017; Lackey and Rajaram, 2019).

Figure 2.3a presents the gas leakage in a fully cemented well with a closed outer annulus. In this situation, casing failure is the primary barrier to prevent leakage channels. A casing with defects may result in fluid transferring to the external cement. Due to the non-uniformity of cement degradation, gases tend to flow to the interface between the high- and low-quality cement, then circumvent from the low-quality cement to the formation. In

this case, gases may flow to the surface through formation, but no SCP and SCVF are observed.

Figure 2.3b shows gas migration within a partially cemented well with drilling fluid and a closed outer annulus. Gases go to the cemented annulus via leakage casing. Because of partially cementation, gases tend to migrate via low-quality cement. At the cement-mud interface, gases continue to move to the wellhead through mud and develop an SCP.

Figure 2.3c and Figure 2.3d are the situations with a partially cemented well with formation fluids and an open outer annulus (casing directly with formation fluids). Gas communication with adjacent formations can result in gas invasion or groundwater crossflow because of the open annulus. Gas invasion occurs at the high pressure hydrocarbon-bearing intermediate formation, while the groundwater crossflow is that gases are dissolved into annular liquid and move to the surrounding subsurface. If the surface casing vent is open, the pressure is released by SCVF (**Figure 2.3c**). If the surface casing vent is closed, SCP occurs and increases annulus pressure to form pathways in the formation (**Figure 2.3d**).

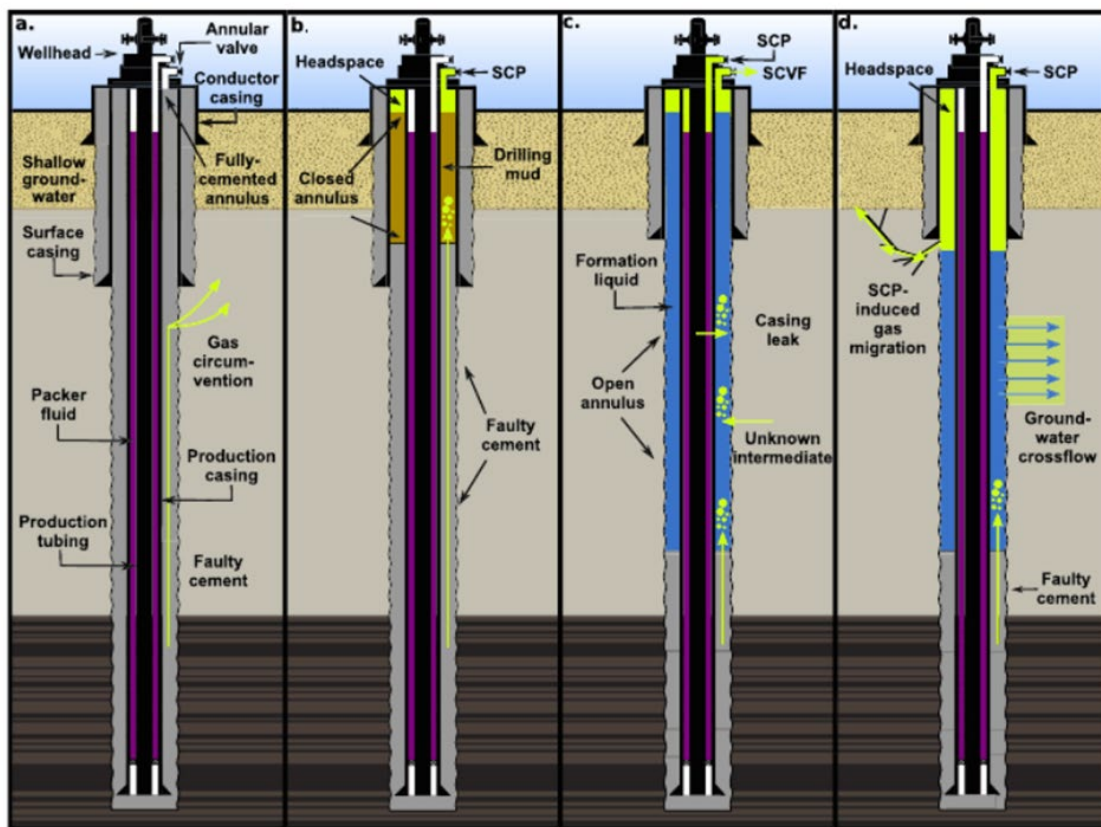


Figure 2.3 Cross-section schematic of three common wellbore configurations: a) a fully cemented well with a closed outer annulus, b) a partially cemented well with drilling fluid and a closed outer annulus, and c) a partially cemented well with formation fluids and a closed outer annulus, and d) a partially cemented well with formation fluids and an open outer annulus (casing directly contacts with formation fluids). Light green arrows indicate the potential leakage pathways (Lackey and Rajaram, 2019).

2.4. Current Standards and Regulations of Maintaining Well Integrity

Many industrial standards and regulations have been published to guide the well's safety. In this section, standards from four popular organizations – API, NORSOK, Norwegian Oil & Gas, and ISO are reviewed. **Table 2.2** summarizes the objectives and scopes of each document. Section 2.4.1 to 2.4.5 presents more details.

Table 2.2 Summary of the objective of API, Norsok, Norwegian Oil & Gas, and ISO standards.

<i>Code</i>	<i>Standard Name</i>	<i>Objectives</i>
API RP 65-2 (2010)	Isolating Potential Flow Zones During Well Construction	<ol style="list-style-type: none"> 1. Control flows during cementing operations and setting casing and liner pipe strings. 2. Prevent sustained casing pressure (SCP).
API RP 96 (2011)	Deepwater Well Design and Construction	<ol style="list-style-type: none"> 1. Identify barriers in deepwater wells for maintaining well integrity. 2. Discuss details of each barrier and evaluate requirements for maintaining well control. 3. Analyze the effect of near-wellbore loads on the reliability of wellbores. 4. Describe the risk and remedial operations in deepwater wells.
API RP 90 (2012)	Annular Casing Pressure Management for Offshore Wells	<ol style="list-style-type: none"> 1. Control annular casing pressure (ACP) such as SCP, thermal casing pressure, and operation-imposed pressure for offshore wells. 2. Cover monitoring, diagnostic testing, the establishment of a maximum allowable wellhead operating pressure, and documentation of ACP for the various types of offshore well. 3. Recognize ACP results in various levels of risk to safety and environments.
API RP 90-2 (2016)	Annular Casing Pressure Management for Onshore Wells	<ol style="list-style-type: none"> 1. Provide monitoring and managing methods for ACP in onshore wells. 2. Control ACP such as SCP, thermal casing pressure, and operation-imposed pressure for onshore wells. 3. Include criteria for establishing diagnostic thresholds, diagnostic testing, and documentation of ACP. 4. Discuss risk management considerations for different well situations.
	Well Integrity in Drilling and	<ol style="list-style-type: none"> 1. Define the minimum requirements and guidelines to maintain well integrity.

NORSOK D-010 (2013)	Well Operations	<p>2. Provide minimum requirements of barrier design for different well operations, such as drilling, well testing, sidetracks, etc.</p> <p>3. Provide acceptance criteria of different barriers.</p>
Norwegian Oil & Gas 117 (2017)	Recommended Guidelines for Well Integrity	<p>1. Understand well integrity in the whole lifecycle from well design, well behavior, and operational limits.</p> <p>2. Not only focus on general regulations and standards but also include field-specific procedures and internal requirements.</p> <p>3. Cover offshore and onshore wells in drilling, completion, intervention, and P&A operations.</p> <p>4. Separate the guideline based on the different requirements in service-company engineers and personnel with responsibilities within well integrity.</p>
ISO 16530-1 (2017)	Well Integrity - Part 1: Lifecycle Governance Manual	<p>1. Maintain well integrity during the lifecycle for all kinds of oil and gas well, including subsea, onshore, offshore wells.</p> <p>2. Discuss the integrity details from the design, construction, operational, intervention, and abandonment phase.</p> <p>3. Consider the effect of corrosion and erosion when wells are in some harsh environments.</p> <p>4. Provide a risk evaluation system to control, prevent, and mitigate unintended fluid migrations.</p>

2.4.1. API RP 65-2: Isolating Potential Flow Zones During Well Construction

Overview: API RP 65-2 (2010) standard provides suggestions of physical barriers in isolating potential flow zones during well construction. This standard aims to prevent or mitigate flows before, during, and after primary cementing operations and use an optimized

barrier system to solve SCP issues. A successful cement design should have good compatibility associating with wells by the optimization of pre-flush operations, mechanical properties, rheology, casing centralization, and pore pressure – fracture gradient window (Roustaei et al., 2015; Busahmin et al., 2017; Choi et al., 2018; Wu et al., 2020; Kimanzi et al., 2020). This standard summarizes the influencing parameters or operations on the quality of cementing work, such as hole quality, drilling fluid properties, casing setting, mud displacement, cement slurries design, and post cementing operations. Float preventing backflows, cement plug (i.e., top and bottom plug), cement design considerations, and normative casing setting procedure are introduced to enhance the cementing operations. Specifically, for cement design, the standard suggests nine performance parameters should be considered – 1) rheological properties, 2) hydrostatic pressure control, 3) fluid loss control, 4) free fluid and sedimentation control, 5) static gel strength development, 6) resistance to the invasion of gas or fluid, 7) compressive or sonic strength development, 8) shrinkage/expansion, 9) long-term cement sheath integrity.

Knowledge gaps: The standard analyzes the function of different barriers to maintaining zonal isolation. However, cement failure due to fatigue is not involved. After cementing, hydraulic fracturing is an effective stimulating method to enhance production. Fluids are injected alternatively to avoid negative environmental impacts (i.e., seismic activities). The fast-slow-fast injection rates result in high – low – high pressures in the wellbore. In high-temperature wells, when cold fluids are injected, it triggers high – low – high temperatures. The cycle pressure and temperature lead to fatigue failure of cement (De Andrade et al., 2015; De Andrade and Sangesland, 2016). Another gap is verifying the reliability of

integrity. The standard suggested using the leak-off test (LOT) and formation integrity test (FIT) to predict lost circulation and cement losses. However, no recommended methods for cement bond testing.

2.4.2. API RP 96: Deepwater Well Design and Construction

Overview: API RP 96 (2011) is an industrial guideline for deepwater well design and construction. Because of the high pressure in the downhole, barrier elements need to overcome severe environments. This standard is more focused on the acceptance criteria of each barrier and loads surrounding the wellbore to ensure integrity. It is noted that because of the deep depth and high hydraulic pressure, deepwater wells are always with high pressure. Barriers under such conditions are easy to fail due to high differential pressure between the wellbore and rock formation. Therefore, this standard emphasizes integrity management.

Compared with conventional wells, maintaining the integrity of deepwater wells is a challenge due to mudline depth, well depth, temperatures, and downhole pressures. The standard mentions some specific difficulties: a) salt zone and rubble zones, b) subsurface geology including shallow water flow hazards, c) abnormal pore pressure, d) weather challenges (i.e., hurricanes and typhoon), e) thermal fluid expansion and trapped annular pressure loads, f) wellhead and hanger load capacities, g) BOP limitations, h) directional drilling, and i) hazards of acidic gas (i.e., H₂S). To manage the integrity, some methods for verifying hydrostatic barriers (fluids within the well), annular cement barriers (mainly focus on the procedure of drilling fluid displaced by cement slurry), and operational barriers (well monitor) are presented.

Knowledge gaps: The purpose of this recommendation is to minimize the risk of well integrity loss for deepwater wells by well design, operational planning, and risk management. Many barriers are introduced, such as subsea wellheads, production liners, casings, etc. Cement sheath, as an essential barrier, is not fully understood. The cementing log is suggested to verify the quality of cement placement. However, the method only can present conditions near the casing-cement interface. For defects within the cement, it is hard to be observed in the log. In addition, P&A, as an essential operation for non-production well treatment, is not discussed.

2.4.3. API RP 90 and API RP 90-2: Annular Casing Pressure Management for Offshore and Onshore Wells

Overview: API RP 90 (2012) and 90-2 (2016) provide annular pressure management recommendations for offshore and onshore wells, respectively. Workflow of annular pressure management for fixed platform wells, subsea wells, and hybrid wells are presented. The standards highlight an empirical method to calculate the maximum allowable wellhead operating pressure for avoiding casing collapse and burst.

Knowledge gaps: Many analytical and experimental investigations have been verified that overlapping of the previous casing shoe with cement (some publications also call it “dual barrier system”) is a common method to mitigate abnormal annulus pressure issues (Ramadan et al., 2019; Ahmed et al., 2020). However, the liner hanger is recognized as neither a major barrier nor an element of a dual barrier system in these standards.

2.4.4. NORSOK D-010: Well Integrity in Drilling and Well Operations & Norwegian Oil & Gas 117: Recommended Guidelines for Well Integrity

Overview: NORSOK D-010 (2013) provides acceptance criteria of barrier elements and barrier systems. The schematics of barriers in different wellbore life stages are presented. The standard focuses on evaluating barrier performance and killing wells (or barrier re-establishment) for risk management.

Norwegian Oil & Gas 117 (2017), on the other hand, emphasizes integrity training. The standard suggests operators and engineers should understand well integrity fundamentals, relevant regulations and standards, and procedures or reactions for different cases. A guideline of well handover documentation is provided to improve the cooperation of several companies or organizations. Similar to the other standards, Norwegian Oil & Gas 117 also involves acceptance criteria of barriers and risk management.

Knowledge gaps: Two standards do not cover the influence of different downhole conditions (i.e., HPHT, deepwater, onshore, offshore, etc.) on the barrier performance. Understanding these conditions benefits the wellbore design and reduces the risk of lost integrity.

2.4.5. ISO 16530-1: Well Integrity - Part 1: Lifecycle Governance Manual

Overview: ISO 16530-1 (2017) discusses the requirements and recommendations for managing well integrity throughout design, construction, operation, intervention, and abandonment phases. It presents a wellbore integrity management system, including risk assessment, organizational structure (i.e., roles and responsibilities), barriers, performance

standards, verification of the obstacles, reporting and documentation, barrier maintenance procedures, and auditing.

Knowledge gaps: This standard highlights the maintenance of integrity for general wells. More specific specialties in some applications, such as HPHT wells, deepwater wells, and H2S hazards, still need further consultations.

2.5. Field Studies for Gas Leakage in Wellbores

Well integrity and barrier failure is a common issue for wellbore maintenance. **Table 2.3** is a statistical analysis of integrity and barrier failures around the world. Field studies show that failure of casing and cement are two primary reasons for loss of integrity. The failures are occurred due to chemical corrosion, wellbore stresses, cementing work quality, degradation, fatigue, formation type, and initial defects of the casing.

Table 2.3 Statistical analysis of worldwid well integrity and barrier failures (failure barriers are marked with bold font).

<i>Country</i>	<i>Type</i>	<i>Location</i>	<i>Total wells in the study</i>	<i>Percentage of wells with integrity issues</i>	<i>Comments</i>	<i>Publication</i>
USA	Onshore	Santa Fe Springs Oilfield, California	52	75%	Well integrity failure observed by gas bubble seeping to the surface.	Chillingar and Endres (2005)
USA	Onshore	Ann Mag Field, South Texas	18	61%	Most barrier failures have occurred in the shale zone.	Yuan et al. (2013)
USA	Offshore	GoM	15,500	43%	26.2% of barriers fail in	Brufatto et al. (2003)

					surface casing.	
Norway	Offshore	Unknown	193	38%	Gas leak to surface in 2 wells.	Vignes (2011)
China	Onshore	Kenxi Reservoir	160	31%	Casing and tubing failure is the major reason for the loss of well integrity.	Peng et al. (2007)
China	Onshore	Gudao Reservoir	3,461	30%	Barriers fail in the oil-bearing zone.	Peng et al. (2007)
Norway	Offshore	Unknown	217	25%	32% of leakage occurs at the wellhead.	Randhol and Carlsen (2007)
Canada	Onshore	Saskatchewan	435	22%		Erno and Schmitz (1996)
Norway	Offshore	Unknown	711	20%	Low cement quality has been observed.	Nilsen (2007)
Norway	Offshore	Unknown	406	18%	1% has failure issues at the wellhead.	Vignes and Aadnoy (2010)
China	Onshore	Daqing Field	6,860	16%	42% of well integrity failure is at old wells.	Lan et al. (2000)
Bahrain	Onshore	Bahrain	750	13%	Failures are at the surface casing. Gas migration in some wells leaks to the surface.	Sivakumar and Janahi (2004)
Holland	Onshore	Unknown	31	13%		Vignes (2011)
UK	Offshore	UK Continental Shelf	6,137	10%		Burton (2005)
USA	Onshore	Marcellus Shale, Pennsylvania	8,030	6.3%	1.27% of failures are leaking to the surface.	Davies et al. (2014)

China	Onshore	Gunan Reservoir	132	6.1%	Most wells with integrity issues are old wells (the wells' age is more than 40 years).	Peng et al. (2007)
USA	Onshore	Unknown	6,953	6.1%		Marlow (1989)
China	Onshore	Hetan Reservoir	128	5.5%	Casing and tubing failure is a major reason for the loss of integrity.	Peng et al. (2007)
USA	Onshore	Marcellus Shale, Pennsylvania	4,602	4.8%		Ingraffea (2012)
Canada	Onshore	Alberta	316,439	4.6%		Watson and Bachu (2009)
Indonesia	Onshore & Offshore	Malacca Strait	164	4.3%	41.4% of wells are identified as high risk of failure.	Calosa and Sadarta (2010)
USA	Onshore	Pennsylvania	6,466	3.4%	0.24% of wells leak to surface.	Vidic et al. (2013)
China	Onshore	Kenli Reservoir	173	2.9%	Barriers fail in the oil-bearing zone.	Peng et al. (2007)
USA	Onshore	Marcellus Shale, Pennsylvania	3,533	2.6%		Considine et al. (2013)
USA	Onshore	Unknown	470	1.9%	Failures of cement are identified as a significant reason for gas migration.	IPCC (2005)

Many field studies have shown that casing and tubing failure could bring SCP issues and fail well integrity (Brufato et al., 2003; Peng et al., 2007; Yuan et al., 2013; King and King, 2013). The pathways can be developed with a poor connection, casing-fluid

corrosion, thermal and mechanical loads. If the tubing fails, the outer casing can be a secondary barrier to continue main the isolation. However, if the leakage is at the outer casing, blowouts occur due to pressurization.

The selection of cement slurries should satisfy the hydraulic integrity requirements, including cement rheology and pumpability during cementation (Shahriar, 2011; De Paula et al., 2014; Shahriar and Behdi, 2015; Vipulanandan and Mohammed, 2015; Sun et al., 2017; Ma and Kawashima, 2019). Cement is injected into the annulus as a liquid phase. It transfers from fluid to gel and finally to a set condition. The duration of the process is significantly dependent on the curing temperature, pressure, and additives of cement slurries. Ineffective mud displacement by cement may result in low-quality cement sheath due to residual mud contamination and voids. Complex rock formation, improper selection of cement slurries and displacement operations, poor wellbore conditions, and eccentric setting casing are all challenges during the displacement.

After cement placement, well activities can pose a challenge in integrity for successful cementing wells. Stimulating operations change the stresses around the wellbore. If the stress exceeds the strength limitation, failure is developed, forming a gas migration channel. Additionally, some field observations indicate that gases may also migrate through other potential pathways, i.e., wellhead, cement plug, packer, liner hanger.

2.6. Previous Studies On Wellbore Leakage Pathway

Many studies have been published to discuss the development of wellbore leakage pathways (**Table 2.4**). Based on the wellbore types, these researches can be divided into

six categories – general well, HPHT well, high-temperature well, deepwater well, P&A well, and CO2 sequestration well. Following are the details of the review.

Table 2.4 Summary of selected literatures studied in this dissertation.

<i>Well Type</i>	<i>Reference</i>	<i>Model Type</i>	<i>Summary</i>	<i>Assumptions and Limitations</i>
<i>General</i>	Patel and Salehi (2019)	FEA and analytical model	Evaluate cement failure mechanism and conduct a parametric study on cement integrity.	Lack of failure criteria.
<i>General</i>	Wang and Taleghani (2014)	FEA	Investigate initiation and propagation of cement failure due to fluid leakage at the casing shoe	Assume a predefined leakage pathway at the casing-cement and cement-formation interfaces.
<i>General</i>	Jandhyala et al. (2013)	FEA	Evaluate the effect of the creep in salt on well integrity	Calculate creep deformation based on steady-state stage, and neglect transient and tertiary stages.
<i>General</i>	Fleckenstein et al. (2001)	FEA	Investigate casing expansion due to burst pressure and the formation of radial fractures in cement	Calculations are based on plane strain theory. Axial deformations are neglected.
<i>General</i>	De Andrade and Sangesland (2016)	FEA	Assess the effects of casing eccentricity, properties, initial defects, applied loads on cement integrity	The model is 2D, and the calculations are based on plane strain theory
<i>HPHT</i>	Li et al. (2010)	Analytical model	Analyze cement sheath coupling effects of temperature and pressure in a non-uniform in-situ stress field	Strength is assumed constant with different curing temperatures and pressures.

<i>HPHT</i>	Xu et al. (2015)	FEA and analytical model	Study the effect of wellhead casing pressure and downhole temperature	Strength is assumed constant with different curing temperatures and pressures.
<i>HPHT</i>	Yuan et al. (2013)	FEA	Study fatigue failure of cement under alternative high and low cycle pressure.	Model is occupied on a lab scale.
<i>HPHT</i>	Yuan et al. (2012)	FEA	Understand casing collapse failure in HPHT gas wells	The application of Von-Mises criterion may result in a high difference to the actual phenomenon.
<i>High-temperature</i>	Li et al. (2010)	Analytical model	Analyze cement sheath coupling effects of temperature and pressure in a non-uniform in-situ stress field	Strength is assumed constant with different curing temperatures and pressures.
<i>High-temperature</i>	Wu et al. (2020)	FEA and analytical model	Assess the effect of temperature distribution on the development of fracture in cement.	Strength is assumed constant with different curing temperatures and pressures.
<i>CO₂ Sequestration</i>	Celia et al. (2005)	FEA and analytical model	Evaluate the interfacial bond integrity of cement during CO ₂ sequestration.	The model is verified on a lab scale.
<i>CO₂ Sequestration</i>	Bai et al. (2015)	FEA	Evaluate the influence of injected supercritical CO ₂	Only assess shear failure at cement-salt interface. The investigation of casing-cement integrity and cement integrity is also required.

<i>CO₂ Sequestration</i>	Nygaard et al. (2014)	FEA	Propose a modeling approach to investigate the effect of dynamic loads on wellbore integrity.	Assume one cycle loads. A multiple cycle process should be considered for future improvements.
-------------------------------------	-----------------------	-----	---	--

2.6.1. Wellbore Leakage Pathway – General Well

Patel and Salehi (2019) presented a comprehensive analytical solution to calculate the stress distribution of cement in liner-cement-casing systems. Radial and hoop stresses were calculated by thick-walled cylinder theory. The calculations were used to verify an FEA simulation. A parametric study was conducted using the validated model to understand the effect of wellbore loads, geometrical, and properties on the risk of cement failure, such as wellbore pressure, annulus pressure, cement height and width, Young’s modulus, and Poisson’s ratio of cement. According to the results, interfacial bond failure (or debonding) and radial cracking were the most likely failure modes. The risk of failure was determined by the comparison between stress magnitude and strength limitation.

Wang and Taleghani (2014) realized that improper cementing jobs led to voids around the casing shoe (**Figure 2.4**). Excessive fluid pressure in the voids was a principal drive force for cement failure propagation. An FEA simulation was created to simulate cylindrical stresses and crack length. Stress analysis showed the initiation of cement failure while crack length presented the propagation. The cohesive zone (bonding at the interfaces) was assumed as a predefined failure path with zero width. Damages in the cement were determined based on traction separation law (Tvergaard 2001). The potential leakage pathways were at the casing-cement interface. Sensitivity analysis showed that rigidity,

interfacial normal and shear strength, and Young's modulus of formation were the most influencing parameters. One major assumption for this study was that a predefined leakage pathway at the casing-cement and cement-formation interfaces had been created before applying loads. Debonding could not be treated as re-fractures. Wang and Hu (2019) presented that the load required to re-open the fracture was lower than initiation within intact cement. The measured values of the maximum load before debonding in this study should be less than the actual value. In other words, the cement bond should be stronger in reality than in the simulations.

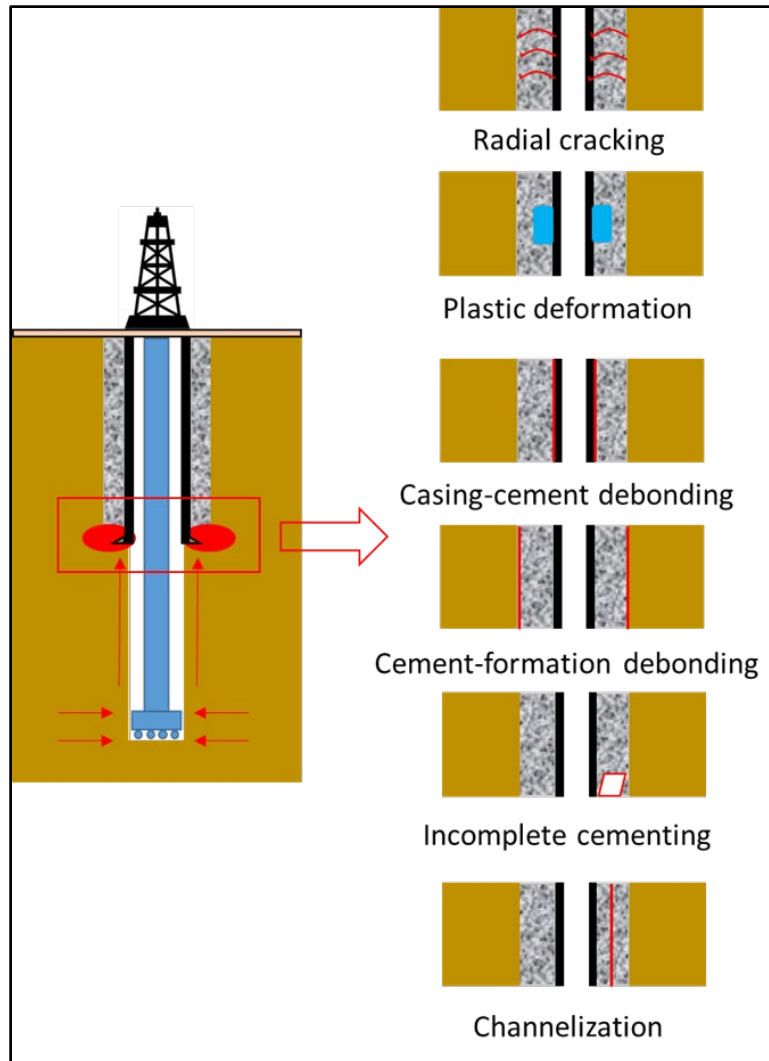


Figure 2.4 Left sketch illustrates fluid migration outside of the casing. Right sketch shows different mechanisms for failure initiation. i.e., from top to bottom, they are radial cracking, plastic deformation, casing-cement debonding, cement-formation debonding, incomplete cementing, and channelization.

Regardless of the cementing job quality, a time-varying load generated from salt formation poses a unique challenge. Jandhyala et al. (2013) evaluated the integrity of elastic and conventional cement sheath in salt formation by numerical models. Creep deformation was calculated by the secondary creep (or steady-state) theory. However, creep is a time-dependent material property. It can be separated into three stages – transient,

steady-state, and tertiary. In the transient stage, the strain rate is high. Then the rate decreases and remains constant. It is called steady-state creep. Strain rates in the tertiary stage increases again. The limitation of the study is that the difference of deformation calculated by transient, steady-state, and tertiary creep was not considered (**Figure 2.5**).

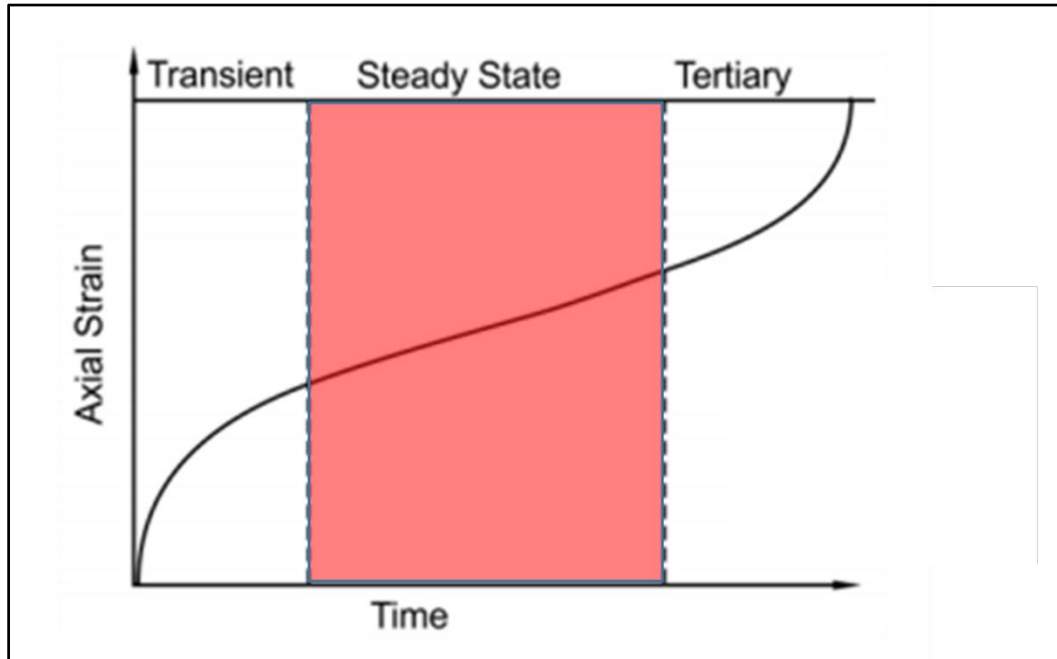


Figure 2.5 Typical creep deformation curve for salt formation. Jandhyal et al. (2013) evaluated salt deformation assuming steady-state creep behavior (red zone).

Casings are another barrier to prevent unintended fluid migrations. Failure due to exceeding internal casing pressure is the main reason for the casing failure. Fleckenstein et al. (2001) investigated casing resistance to internal burst pressure using a 2D FEA model. Deformation in the axial direction was neglected due to the application of plane strain in calculating stresses. Von-Mises failure criterion was the standard to determine casing failure. The results showed that an intact cement sheath significantly enhanced casing burst resistance. Confining pressure at the rock formation had positive impacts on casing burst

resistance. The effect on casing-cement-formation systems was obvious than casing-cement-casing systems.

Eccentric casing poses a primary technical challenge. Akgun et al. (2004) investigated the relationship between casing eccentricity and inclination angle. De Andrade and Sangesland (2016) presented a numerical study to predict the high-risk zone within a cement sheath. Effect of mechanical properties, initial geometrical defects, thermal properties, different loads was evaluated. Increasing casing eccentricity led to a high risk of radial cracks. Regardless of the casing eccentricity, initial geometrical defects decreased the cement strength. Cement thermal and mechanical properties, expansion coefficient, Young's modulus, and Poisson's ratio have significant effects on the performance of cement.

2.6.2. Wellbore Leakage Pathway – HTHP Well

HPHT wells are defined as the bottom hole temperature is more than 150°C or 300°F and wellhead pressure is greater than 69 MPa or 10,000 psi (Shadravan and Amani, 2012). The compression of fluids in high pressure makes the HPHT wells are an effective reservoir for hydrocarbon storage. However, the high-temperature and high-pressure nature of the well may trigger many integrity issues. Li et al. (2010) developed a 2D analytical model to calculate the stress of the casing-cement-formation system under non-uniform in-situ field stresses. Plane strain theory was assumed. Casing pressure and wellbore temperature were imposed on the inner surface of the casing, while field stresses and formation temperature were applied at the outer boundary of the formation. The author solved the equation by separating the complex loading into two situations – situation I:

uniform inner and outer pressure with thermal and mechanical loads; situation II: non-uniform external pressure (**Figure 2.6**). The results showed that increasing casing temperature led to tension in the cement. The highest stress was at the casing-cement interface. The risk of failure was low when the stress was becoming uniform (or homogeneous). Xu et al. (2015) used a similar analytical model to validate the numerical simulation and extended the research to study the influence of the wellhead casing pressure on cement integrity. High wellhead casing pressure increased the risk of cement failure. A major assumption for both studies was the strengths were assumed constant under different downhole temperatures and pressures. High magnitude of stress referred to a high risk of failure. However, as Fink (2015) presented, the strength of cement tends to increase with higher curing temperature and pressure.

Mechanical failure of cement under static HPHT environments plays a crucial role in forming leakage pathways, but also fatigue failure due to dynamic pressure and temperature cycles is common. The cycles are experienced in the process of hydraulic fracturing, steam injection, and production. Yuan et al. (2013) studied the fatigue failure of cement sheath under alternative high and low cycle pressure using a 3D FEA model. The effect of confining pressure, temperature, and elastic properties on cement stress distribution was investigated. However, the model was based on a lab scale. It was because fatigue behaviors in this model were determined by the Stress-N theory generated from laboratory experiments.

Since casings are a significant barrier of wells, casing failure probably triggers unexpected fluid communications. Especially in HPHT conditions, the high pressure and

temperature difference between wellbore and formation during production could cause a decrease of casing collapse resistance. Yuan et al. (2012) study casing collapse failure in HPHT wells using an FEA model. Casing eccentricity, cement voids, and the presence of initial cement channels were assessed to show how did the cementing complications affect casing integrity. Other parameters such as in-situ stresses, elastic cement properties, wellbore geometries, temperature were also evaluated. The authors simulated maximum Von-Mises equivalent stress in casing and cement as the reference value for the analysis. However, the Von-Mises criterion is only valid for ductile materials with equal compressive and tensile strength (Choi et al., 2003). The application of the criterion on cement sheath might have a difference from the actual phenomenon.

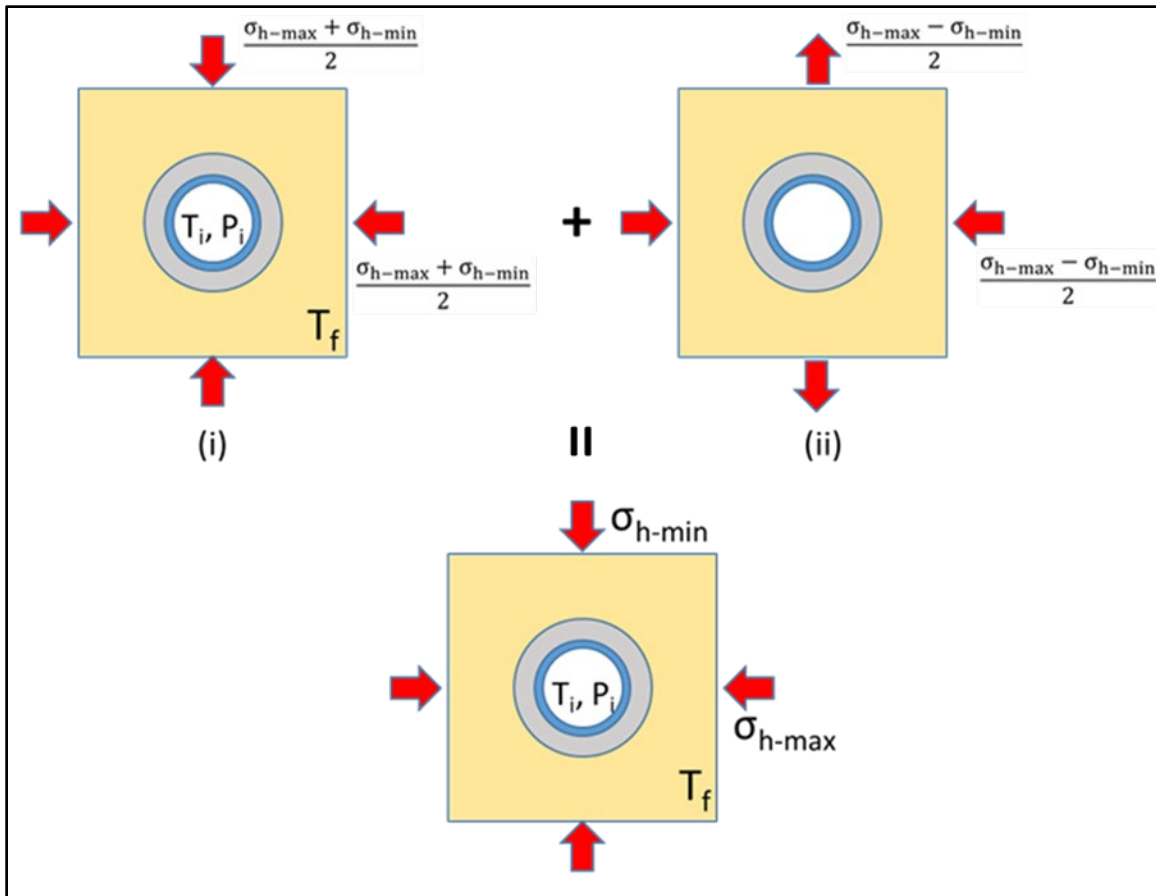


Figure 2.6 Non-uniform field stresses model: (i) uniform inner and outer pressure with thermal effect; and (ii) non-uniform external pressure (blue color is casing, gray color indicates cement, yellow color represents formation, and red arrows present the directions of loads).

2.6.3. Wellbore Leakage Pathway – High-Temperature Well

High-temperature conditions, such as those found in geothermal wells, pose a unique challenge for cement design. Unlike oil and gas wells, geothermal wells do not generate any revenue until nearby facilities such as power plants and electric grids have been constructed. Thus, their long-term integrity is significantly essential. Li et al. (2010) used an analytical model to calculate the stress distribution near the wellbore under a non-uniform in-situ stress field considering thermal loads in high-temperature conditions. A

numerical simulation verified by the analytical solutions was published by Wu et al. (2020). The objective of the study was to assess the effect of temperature changes on the development of fracture in cement systems. For both publications, as mentioned before, strength was assumed constant with different curing temperatures and pressures (details shown in the last section).

2.6.4. Wellbore Leakage Pathway – CO₂ Sequestration

CO₂ sequestration in depleted reservoirs, coal seams, and the saline aquifer is an effective method to mitigate greenhouse effects on our planet. Pathways for possible leakage include diffuse leakage across caprock formations, concentrated leakage through natural faults and fractures, and leakage through human-made features such as wells. In this review, the wellbore pathways induced by structural failure focus on preventing CO₂ escape from the reservoir to the surface through the channels and avoiding inefficient storage. Celia et al. (2005) conducted an analytical model to evaluate the interfacial bond integrity of cement quantitatively. The model was validated by numerical simulation. Both FEA and analytical models are on lab scale, which might not be applicable in the field.

Bai et al. (2015) focused on investigating the influence of supercritical CO₂ on well integrity. When CO₂ is injected into the wellbore, because of its compressible nature, CO₂ tends to become the supercritical condition. Well integrity is required to be considered with respect to low temperature and corrosion of the supercritical CO₂ (**Figure 2.7**). In this research, experiments were used to evaluate the effect of corrosion on casing and cement integrity, while numerical simulations aimed to simulate the performances when the temperature dropped down. The study also assessed casing-cement-salt formation integrity.

Displacement of cement sheath near the cement-salt interface, at the interface, and within the salt rock near the interface were compared to identify shear failure at the cement-salt interface. However, casing-cement integrity and cement integrity are also crucial during CO₂ injection.

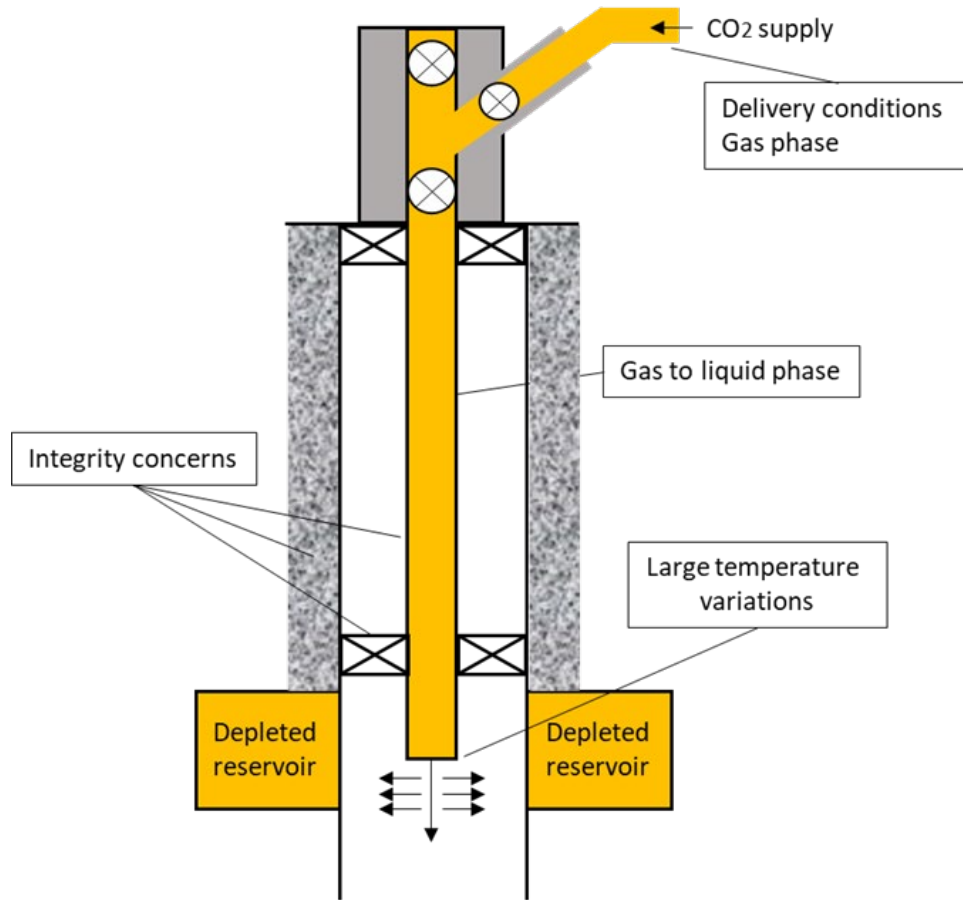


Figure 2.7 Graphically explanation of the challenges when supercritical CO₂ injects into the wellbore. Due to the change of pressure, CO₂ transfer from gas to liquid phase during the injection.

Nygaard et al. (2014) studied dynamic loading on wellbore leakage in the Wabamun area CO₂ sequestration project in Canada. The numerical model was considered both thermal and pressure cycle loads. Stresses distribution was simulated after one cycle. For future improvements, a multiple cycle process should be considered.

2.7. Cement Failure Mechanism

As shown in the previous section, cement is one of the major barriers to maintaining zonal isolation of the wellbore. In this section, the cement failure mechanism will be introduced from hydraulic and mechanical aspects. The mechanical design considers structural integrity, while the hydraulic is influenced by the fluid dynamics of the wellbore fluids.


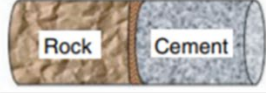

2.7.1. Hydraulic Integrity Concerns

Primary cementing has been identified as a major technical challenge affected by hole cleaning, mud contaminations, cement placement, and post-placement settling. Poor hole cleaning can contaminate the cement slurry affecting the bond and cement strength (Vivas et al., 2020. Busahmin et al., 2017).

Li et al. (2016) tested the effects of oil-based mud (OBM) and its components on the performance of cement slurries. The contaminated OBM reduced the liquidity of the class G cement slurries by the loss of a large number of free water slurries. Compressive and bond strengths decrease with increasing OBM contamination, while porosity and permeability will be increased. Broni-Bediako and Amorin (2019) conducted an experimental study to discuss the influences of cement contamination on a WBM. The findings showed that with more concentration of class G cement contaminated, yield point, gel strength, fluid loss, density, and pH value of the WBM increased with more concentration of class G cement contaminations. The changing of plastic viscosity was highly related to the amount of added cement. For the range of tests, it decreased slightly with cement concentration of 10 g and 20 g, while it increased when 30 g cement was

added. Eid et al. (2021) compared the geopolymer to neat class G cement contaminated with WBM and OBM. The neat class G cement with OBM contaminations had an increasing rheology profile, while it decreased with WBM. Geopolymer contaminated with both mud systems showed a reduced rheology profile.

Table 2.5 Model setup of Radonjic and Oyibo (2015) investigating effect of OBW on bond and cement strength.

Physical drilling fluid contamination	Chemical drilling fluid contamination	
Composite core with no drilling fluid contamination at the rock surface	Composite core with no drilling fluid contamination at the surface	
Composite cores (sandstone/cement & shale/cement) scraped off the dehydrated drilling fluid leaving a slight residue of drilling fluid at the	Composite core with 5% drilling fluid contamination at the surface	
Composite cores (sandstone/cement & shale/cement) washed off the drilling fluid leaving some drilling fluid particles at the interface, primarily lodged within the rock pores	Composite core with 10% drilling fluid contamination at the surface	

Radonjic and Oyibo (2015) investigated the impact of physical and chemical mud contamination on bond strength. Physical contamination occurs due to mud dehydration on the formation surface, while chemical contamination indicates mud mixed with cement slurry during the displacement (**Table 2.8**). Mud cake at the interface degraded the bond strength. The comparison between sandstone and shale bonds presented that the former had a relatively strong bond with the same amount of contaminated mud due to the discontinuous bond (or interfacial lock-up). Wilson et al. (2018) noted that the bond of continuous contact is either fully adhesive or fully disconnected, while the bond in discontinuous contact can be separated into many individual micro-bonds across the interface rather than a single macro-scale bond. As the increment of external loading, some

bonds fail while the others are remaining intact. Completely interfacial debonding occurs when all micro-bonds are broken (**Figure 2.8**). The interlocking bond was formed when the cement gel structure flowed into surface cavities or pores on the casing or formation surface (Kimanzi et al., 2020).

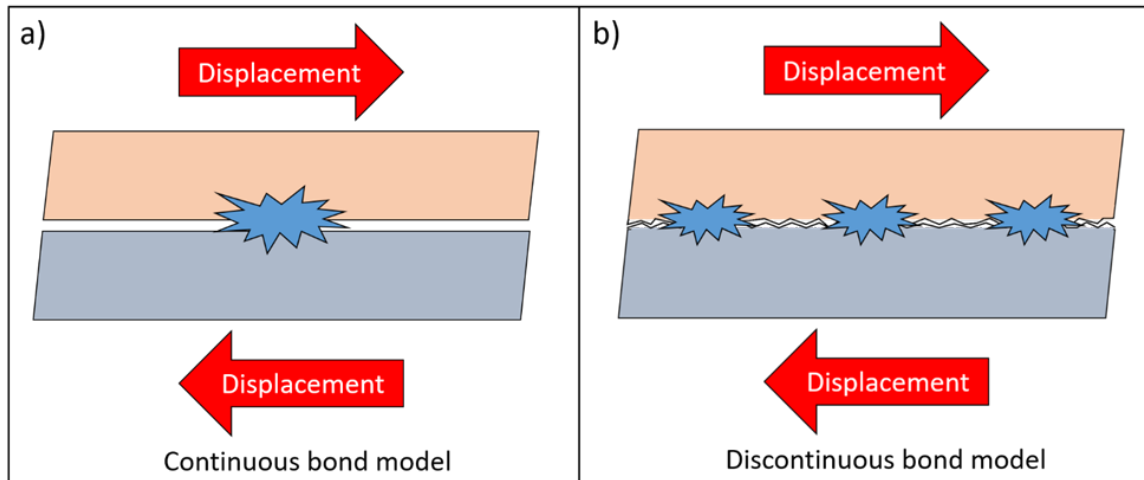


Figure 2.8 Bond failure under shear stress conditions. a) Continuous bond model complete failure, b) Discontinuous bond model (interfacial lock-up) partially but still intact.

To overcome the challenges posed by primary cementing, it is crucial to improve the characterization of the mud displacement in wellbores. Density difference and eccentricity have a significant effect on the displacement efficiency (**Figure 2.9**) (Vaughn, 1965; Iyoho and Azar, 1981; Crook et al., 1985; Chen et al., 1990; Hacıislamoglu and Langlinais, 1990; Tehrani et al., 1992; Zheng, 1995; Zhang et al., 1997; Gao et al., 2005; Sun et al., 2005; Ozbayoglu and Omurlu, 2006; Yang et al., 2008; Deng et al., 2011; Feng et al., 2011). Bu et al. (2016) presented a laminar flow theory of mud-cement displacement in the eccentric annulus. The displacement was assumed as a steady flow. No circumferential flow velocity, interfacial mixture, chemical reactions were considered in the model. Cement directly displaced the mud. Rheological behaviors of both fluids follow

the Herschelo-Bulkey model. The differential force equilibrium equation can be written as

Equation 1.

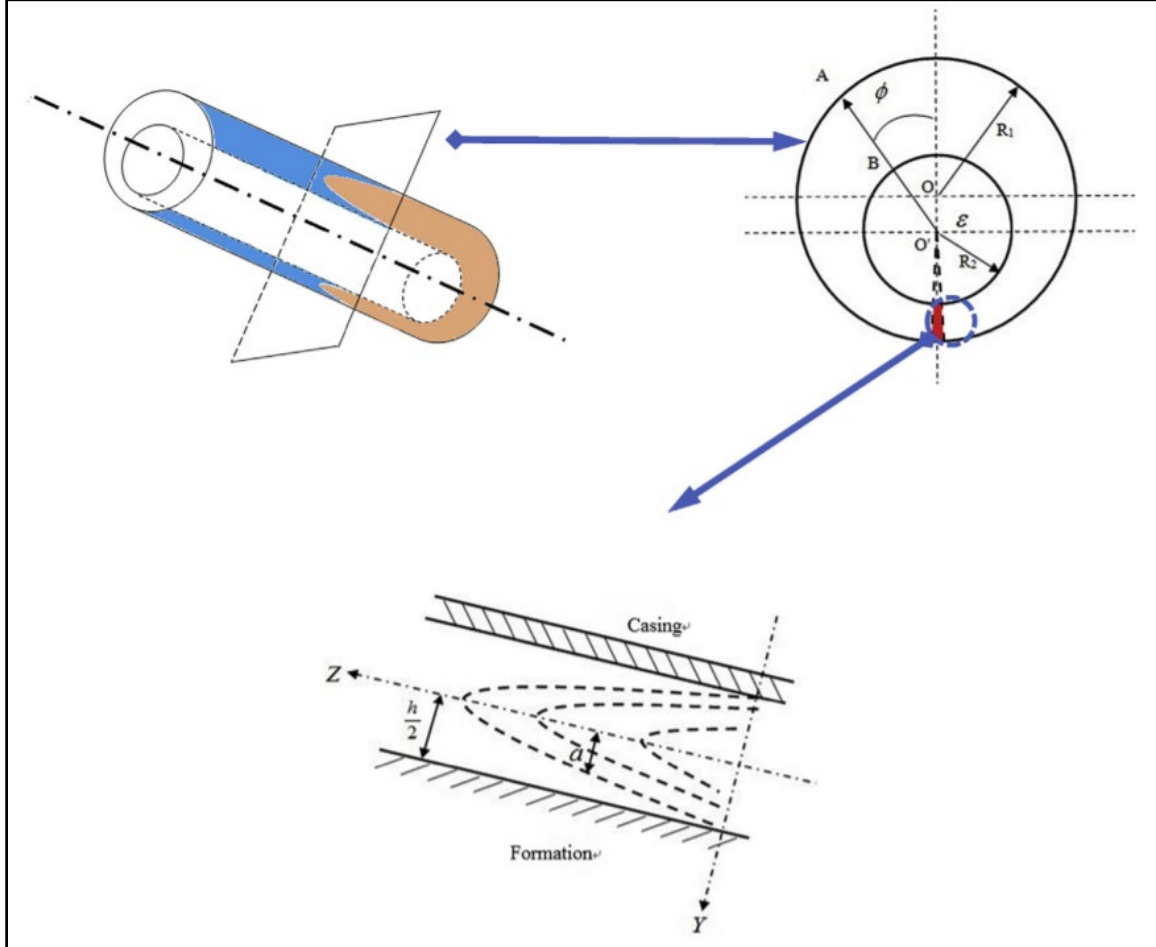


Figure 2.9 Drilling fluid displaced by cement slurry in the eccentric annulus. Casing eccentricity is calculated by $e = \frac{\varepsilon}{R_1 - R_2}$, where e is casing eccentricity, R1 and R2 are wellbore radius and casing radius.

$$\rho \left(\frac{\partial V_z}{\partial t} + V_r \frac{\partial V_z}{\partial r} + V_\phi \frac{\partial V_z}{r \partial \phi} + V_z \frac{\partial V_z}{\partial z} \right) = - \frac{\partial P}{\partial z} + \left[\frac{\partial(r\tau_{rz})}{r \partial r} + \frac{\partial \tau_{\phi z}}{r \partial \phi} + \frac{\partial \tau_{zz}}{\partial z} \right] - \rho g \cos \theta \quad (1)$$

Based on Liu et al. (1988) and Liao et al. (2003), the shear stress of cement and mud is expressed in **Equations 2** and **3**. Where τ_c and τ_m are shear stress of cement and mud in Pa. ρ_c and ρ_m indicate cement and mud density in kg/m^3 . $\frac{\partial P}{\partial z}$ is friction pressure

gradient in Pa/m. α is the distance between the interface and Z-axis. θ is inclination angle in $^\circ$.

$$\tau_c = \left(\frac{\partial P}{\partial z} + \rho_c g \cos \theta \right) y \quad (2)$$

$$\tau_m = \left(\frac{\partial P}{\partial z} + \rho_m g \cos \theta \right) y + (\rho_c - \rho_m) g a \cos \theta \quad (3)$$

Cement and mud rheological behavior follows the Herschel-Bulkley model (Herschel and Bulkley, 1926), represented in **Equations 4** and **5**, respectively. Where c and m in subscripts mean cement and mud. τ_c and τ_m are shear stress of cement and mud in Pa. τ_{oc} and τ_{om} are yield stress, respectively in Pa. K_c and K_m are consistency coefficient of cement and mud in $\text{Pa} \cdot \text{s}^n$. n_c and n_m are liquidity index of cement and mud (generally $n_c < n_m$). V_c and V_m are axial velocity of cement and mud in the eccentric annulus in m/s.

$$\begin{cases} \tau_c = \tau_{oc} & (\tau_c \leq \tau_{oc}) \\ \tau_c = \tau_{oc} + K_c \left(\left| \frac{dV_c}{dy} \right| \right)^{n_c} & (\tau_c \geq \tau_{oc}) \end{cases} \quad (4)$$

$$\begin{cases} \tau_m = \tau_{om} & (\tau_m \leq \tau_{om}) \\ \tau_m = \tau_{om} + K_m \left(\left| \frac{dV_m}{dy} \right| \right)^{n_m} & (\tau_m \geq \tau_{om}) \end{cases} \quad (5)$$

Substituting **Equations 4** and **5** into **Equations 2** and **3**:

$$\tau_{oc} + K_c \left(-\frac{dV_c}{dy} \right)^{n_c} = \left(\frac{\partial P}{\partial z} + \rho_c g \cos \theta \right) y \quad 0 \leq y < a \quad (6)$$

$$\tau_{om} + K_m \left(-\frac{dV_m}{dy} \right)^{n_m} = \left(\frac{\partial P}{\partial z} + \rho_m g \cos \theta \right) y + (\rho_c - \rho_m) g a \cos \theta \quad a \leq y < \frac{h}{2} \quad (7)$$

The boundary conditions are in **Equation 8**.

$$V_c|_{y=a} = V_m|_{y=a}, V_m|_{y=\frac{h}{2}} = 0 \quad (8)$$

Solving **Equations 6-8**, we can obtain the axial flow velocity distributions of cement slurry and drilling fluid, V_c and V_m in **Equations 9** and **10**. Where $A = \frac{1}{K_c} \left(\frac{\partial p}{\partial z} + \rho_c g \cos \theta \right)$, $B =$

$$\frac{1}{K_m} \left(\frac{\partial p}{\partial z} + \rho_m g \cos \theta \right), \text{ and } C = \frac{g a \cos \theta}{K_m (\rho_c - \rho_m)} - \frac{\tau_{om}}{K_m}.$$

$$V_c = \frac{n_c}{A(n_c + 1)} \cdot \left[\left(Aa - \frac{\tau_{oc}}{K_c} \right)^{\frac{n_c+1}{n_c}} - \left(Ay - \frac{\tau_{oc}}{K_c} \right)^{\frac{n_c+1}{n_c}} \right] + \frac{n_m}{A(n_m+1)} \cdot \left[\left(\frac{Bh}{2} + C \right)^{\frac{n_m+1}{n_m}} - (Ba + C)^{\frac{n_m+1}{n_m}} \right] \quad (9)$$

$$V_m = \frac{n_m}{B(n_m+1)} \cdot \left[\left(\frac{Bh}{2} + C \right)^{\frac{n_m+1}{n_m}} - (By + C)^{\frac{n_m+1}{n_m}} \right] \quad (10)$$

Thus, the flow rate of cement and mud with a circumferential angle can be calculated using **Equations 11** and **12**.

$$\begin{aligned} dQ_c &= \int_{-a}^a \left(R_2 + \frac{h}{2} + y \right) V_c dy = 2 \left(R_2 + \frac{h}{2} \right) \int_0^a V_c dy \\ &= 2 \left(R_2 + \frac{h}{2} \right) \cdot \left\{ \frac{n_c^2}{A^2(n_c+1)(2n_c+1)} \cdot \left[\left(-\frac{\tau_{oc}}{K_c} \right)^{\frac{2n_c+1}{n_c}} - \left(Aa - \frac{\tau_{oc}}{K_c} \right)^{\frac{2n_c+1}{n_c}} \right] + \frac{an_c}{A(n_c+1)} \cdot \left(Aa - \frac{\tau_{oc}}{K_c} \right)^{\frac{n_c+1}{n_c}} - \frac{an_m}{B(n_m+1)} \cdot \left\{ [Ba + C]^{\frac{n_m+1}{n_m}} - \left[\frac{Bh}{2} + C \right]^{\frac{n_m+1}{n_m}} \right\} \right\} \quad (11) \end{aligned}$$

$$\begin{aligned} dQ_m &= \int_{-a}^{\frac{h}{2}} \left(R_2 + \frac{h}{2} + y \right) V_m dy + \int_{\frac{h}{2}}^{-a} \left(R_2 + \frac{h}{2} + y \right) V_m dy = 2 \left(R_2 + \frac{h}{2} \right) \int_a^{\frac{h}{2}} V_m dy \\ &= 2 \left(R_2 + \frac{h}{2} \right) \cdot \left\{ \frac{n_m^2}{B^2(n_m+1)(2n_m+1)} \cdot \left\{ [Ba + C]^{\frac{2n_m+1}{n_m}} - \left[\frac{Bh}{2} + C \right]^{\frac{2n_m+1}{n_m}} \right\} + \frac{\left(\frac{h}{2} - a \right) n_m}{B(n_m+1)} \cdot \left[\frac{Bh}{2} + C \right]^{\frac{n_m+1}{n_m}} \right\} \quad (12) \end{aligned}$$

Foroushan et al. (2020) studied the displacement in a vertical annulus. The optimal density difference depended on the inclination and casing eccentricity of the wellbore. For the concentric annulus, the displacement efficiency decreased with an increment of the inclination when cement density was higher than mud. The higher density of the displacing fluids provided a stable interface with high displacement efficiency.

Kiran et al. (2019) mentioned the importance of the geometrical configuration of well on the displacement. The size of the borehole could be different from the drill-bit size due to breakout, washout, and collapse. The irregular wellbore shape may consequently affect cement fluid dynamics in the annulus, reducing the displacement efficiency (**Figure 2.10**). Etrati et al. (2020) studied the influence of enlarged length, pump rate, density difference, and viscosity ratio on cement performance. Increasing flow rate could aggravate potential contaminations. A large density difference enhanced the displacement, while viscosity differences had an insignificant effect. Renteria et al. (2019) focused on the impacts of irregularity in high deviated wells. In the horizontal sections, the cement slurry tended to flow at the bottom because of the density difference, while casing eccentricity led to the cement displaced more mud in the wide side of the annulus than the thin side. In the inclination sections, residual muds were left in the washout section during the displacement of high yield stress muds.

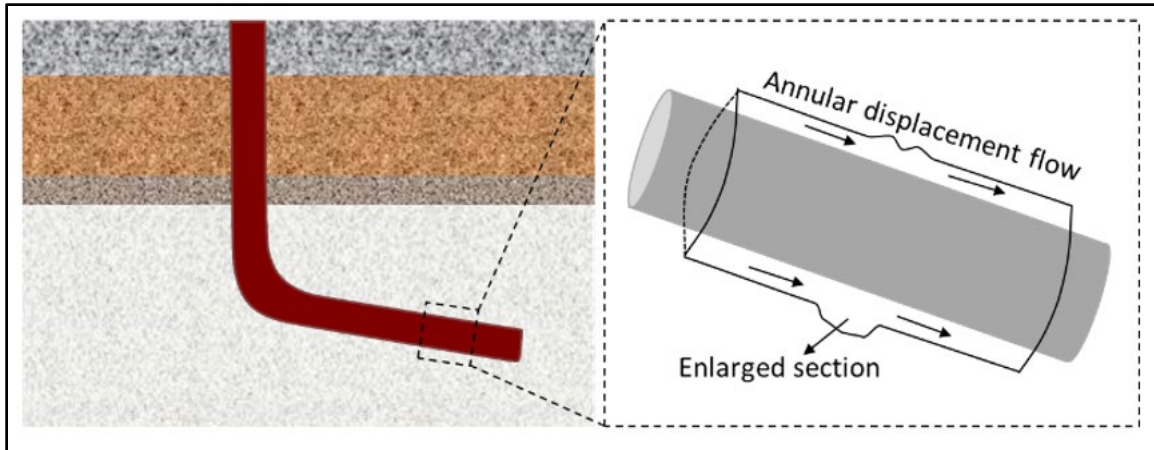


Figure 2.10 Mud displacement efficiency influenced by enlarged wellbore due to washout.

2.7.2. Mechanical Integrity Concerns

Mechanical integrity refers to structural degradation that occurs when the loadings exceed the limitation of cement. Wang and Taleghani (2014) presented six failure modes in the cement sheath – radial cracking, inner and outer debonding, incomplete cementing, shear cracking, and channelization (**Figure 2.11**). Cylindrical stress (i.e., hoop, radial, and axial stress) is an effective tool to determine failure. Radial stress is the normal stress acting toward or away from the central axis of a cylinder. Hoop stress is defined as normal stress in the tangential direction. Axial stress is a normal stress parallel to the axis of the cylinder. Based on the previous studies, the type of failure can be determined by the comparison between stress magnitude and mechanical strength (**Equation 13-16** and **Figure 2.12**). Regardless of in-situ stresses, radial cracking develops when the hoop stress exceeds the tensile strength of cement sheath (Garnier et al., 2010; Bustgaard and Nesheim, 2016; Patel et al., 2019). Compressive failure initiates when the hoop stress exceeds the compressive strength of cement (Lavrov and Torsæter, 2016). Debonding initiates when radial stress at the casing-cement or cement-formation interface exceeds the tensile strength of the cement

(Lavrov and Torsæter, 2016). When radial stress is compressive, and the magnitude exceeds the compressive strength of the cement, stress crushing occurs (Lavrov and Torsæter, 2016).

Following equations are shown the determination of cement failure (Garnier et al., 2010; Rahimi, 2014; Bustgaard and Nesheim, 2016; Patel et al., 2019; Lavrov and Torsæter, 2016):

$$\text{Radial cracking: } \sigma_{\theta} \geq T_0 \text{ (tension)} \quad (13)$$

$$\text{Compressive failure: } |\sigma_{\theta}| \geq C_0 \text{ (compression)} \quad (14)$$

Where σ_{θ} is the hoop stress. T_0 and C_0 are the tensile and compressive strength of the cement sheath, respectively.

$$\text{Radial debonding: } \sigma_r \geq T_0 \text{ (tension)} \quad (15)$$

$$\text{Compressive failure: } \sigma_r \geq C_0 \text{ (compression)} \quad (16)$$

Where σ_r is the radial stress.

Goodwin and Crook (1992) studied that increment of internal casing pressure is a major reason leading to radial cracks. Bios et al. (2012) considered the influence of cement-formation relationship in mechanics. When the cement was stiffer than the formation, radial cracks had a high possibility to occur. When the cement was softer than the formation, plastic deformation was observed. Small plastic deformations and radial cracks also exist when cement is under cyclical loading at downhole conditions (Shadravan et al., 2015). Nygaard et al. (2014) evaluated the effect of mechanical and thermal loading on cement failure by numerical simulation. ‘Based on the sensitivity analysis, at the same boundary conditions, the risk of radial fractures in cement was higher with higher Young’s modulus

cement and higher Poisson's ratio. However, radial stress was not sensitive to variable Young's modulus and Poisson's ratio. Moreover, it was shown that the pore pressure affecting effective stresses is crucial in consideration of cement failure. The simulation also quantified that under thermal cooling conditions, it would become easier to induce the failure of debonding by decreasing the compressive mechanical stresses near the wellbore.

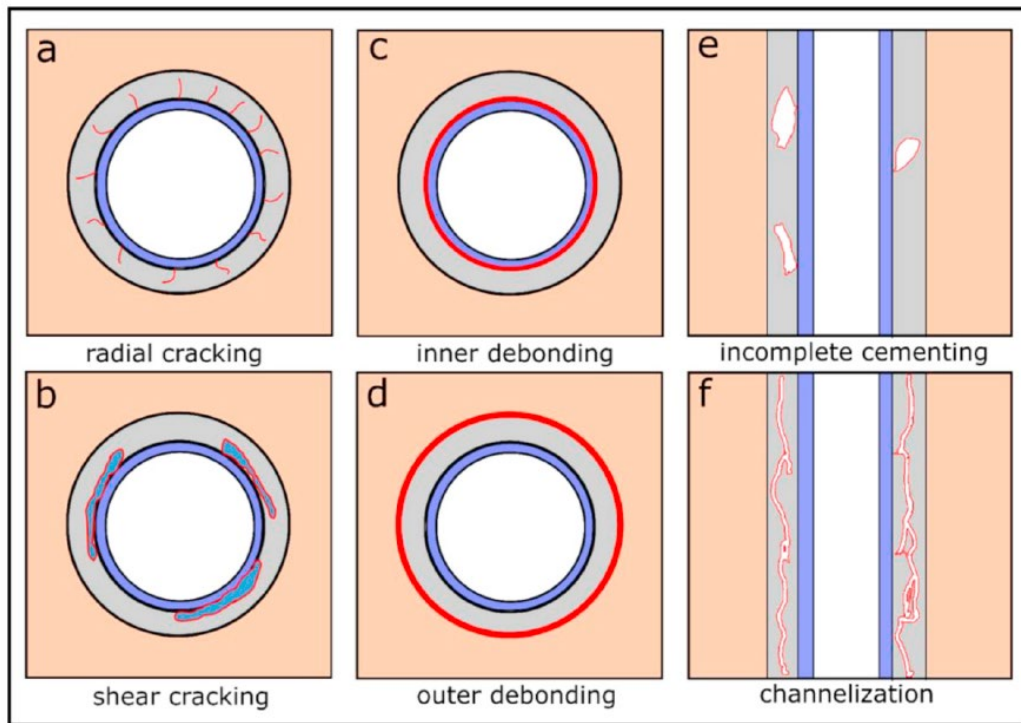


Figure 2.11 Schematic showing six typical cement failure modes. Casing, cement, and formation are represented by blue, gray, and orange colors. Red lines indicate the failure in each case (modified from Wang and Taleghani, 2014)

Nath et al. (2018) investigated cement-casing bonding by the DIC technique. DIC is a non-contact optical method to track the accurate strain distribution. A sample with outside steel casing and inside class H cement was tested under diametrically compressive load to evaluate the integrity of cement. Several conditions were studied: variable water-cement ratio, the effects of barite and bentonite, mud contamination, and mud cake. The results

showed that it is risky to apply the cement with a higher water-cement ratio. Additions, such as barite, would help to maintain the integrity by an increment of mechanical strength, while mud contamination would fail the cement-casing bonding.

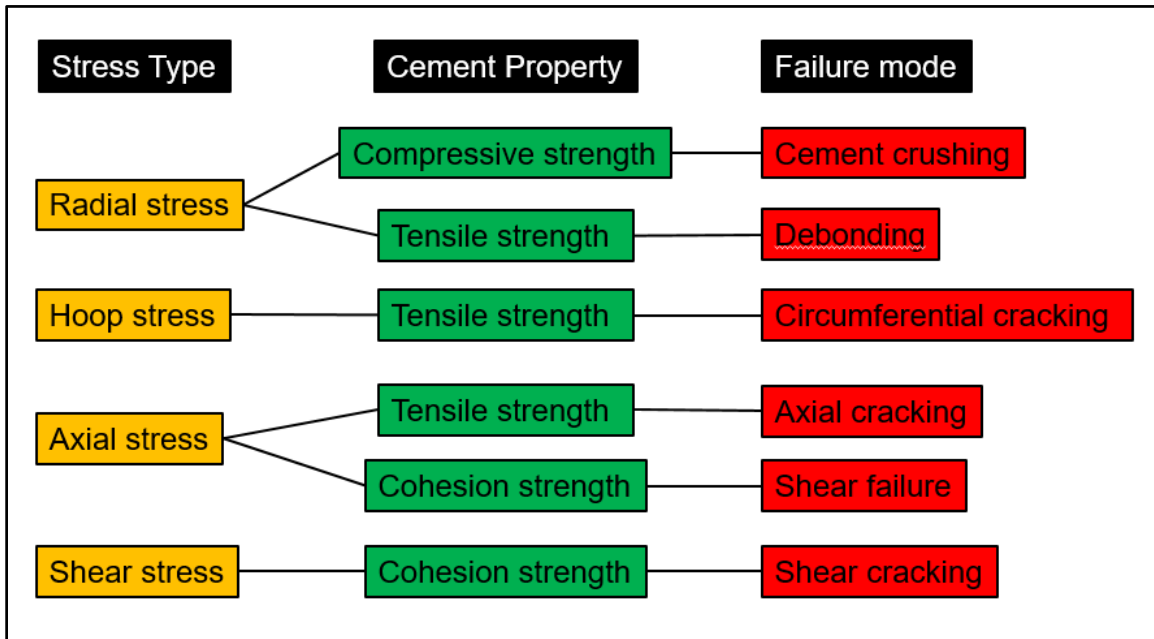


Figure 2.12 Failure criterion and its corresponding failure mode.

Well construction in high-temperature poses many other challenges in cement integrity. The range of temperature in high-temperature wells is typically above 150°C (NORSOK D-010, 2004). Different from oil and gas wells, geothermal well does not generate any revenue until the nearby facilities such as power plant and electric grid have been constructed. Thus the long-term integrity maintenance is significantly important. In high-temperature wells (i.e., geothermal wells), a failure of cement can be induced with high differential temperature in the system (Okech et al., 2015). The difference of temperature between casing and reservoir results in expansion or shrinkage of the cement, inducing differential stress in the system and consequently cause failure (Therond et al.

2016). Reddy et al. (2005) reported that compressive strength is variable with different curing temperatures.

Except for thermal properties, several other parameters contribute to the failure of cement sheath in high-temperature reservoirs, such as pressure differential in the system, tectonic stresses, mechanical properties, etc. Hossain and Amro (2010) reported that larger differential pressure increased the risk of cement failure. Differential pressure could come from the pressure difference between casing pressure and tectonic stresses. Bios et al. (2011 and 2012) investigated the effect of the relationship between stiffness of cement sheath and formation. In the case with decreasing temperature, the probability of casing-cement and cement-formation interfaces debonding was relatively high when the formation was stiffer than cement. The risk of casing-cement interface debonding was more severe when the cement coefficient of thermal dilation was small, and the cement was stiffer than the formation. For a decreasing pore pressure environment, casing-cement and cement formation bond failed when the formation was stiffer than cement. Casing-cement debonding occurred when low cement Poisson's coefficient was applied, and cement was stiffer than formation.

Thermal conductivities of six Mexican cementing systems are tested, and new empirical equations for correlating thermal conductivity with the temperature of geothermal cement were generated by Santoyo et al. (2001). Thermal expansion in the cement sheath induced by the expansion coefficient significantly affects the wellbore integrity as observed by Zhang and Wang (2017).

Thermal cycling is another main factor that triggers cement fatigue. De Andrade (2014) used a CT-Scan technique to monitor the development of fractures in the cement sheath. According to the observations, compressive failure was identified as the most common failure mechanism. Increment in the number of thermal cycling would be detrimental to the zonal isolation. Patel and Salehi (2019) presented a useful approach of developing sensitivity response curves to evaluate the short- and long-term integrity of cement sheath. The authors used an analytically validated 3D FEA model of cement sheath in liner-casing overlap for the study. The study presented the sensitivity of radial, hoop, shear, and interfacial stress to various design and operation parameters such as cement properties, cement sheath dimensions, wellbore pressure, annulus pressure, etc. Patel et al. (2019) presented an assessment of stresses in cement with expansion agents. Based on FEA modeling simulations using various expanding cement recipes, the authors indicated that expanding cement has a lower risk of structural failure compared to conventional non-expanding cement.

Li et al. (2010) published a 2D analytical model of cement sheath coupling effects of temperature and pressure in a non-uniform in-situ field. The model calculated radial and hoop stresses in a casing-cement-formation system. Maximum and minimum principal stresses were applied at a far distance away from the wellbore. The non-uniform applied loads (i.e., in-situ stresses, internal casing pressure, thermal loads) could be divided into two parts – (i) uniform inner and outer pressure with thermal effects and (ii) non-uniform outer pressure (see **Figure 2.6**). Details of the deviation are shown below (**Equations 17-37**):

For situation (i), because of the differential temperature between casing (T_i) and reservoir (T_f), the temperature distribution within the cement along the radial orientation (T) is:

$$T = T_i - (T_i - T_f) \frac{\ln \frac{r}{b}}{\ln \frac{c}{b}} \quad (17)$$

The radial (ε_r), hoop (ε_θ), and axial (ε_z) strain can be written as:

$$\begin{cases} \varepsilon_r = \frac{1}{E} [\sigma_r - \nu(\sigma_\theta + \sigma_z)] + \alpha T \\ \varepsilon_\theta = \frac{1}{E} [\sigma_\theta - \nu(\sigma_z + \sigma_r)] + \alpha T \\ \varepsilon_z = \frac{1}{E} [\sigma_z - \nu(\sigma_r + \sigma_\theta)] + \alpha T \end{cases} \quad (18)$$

Where E is Young's modulus, ν is Poisson's ratio, and α is thermal expansion coefficient. Because plane strain theory is applied in the model, ε_z is zero.

$$\sigma_z = \nu(\sigma_r + \sigma_\theta) - E\alpha T \quad (19)$$

Combine **Equation 19** with **Equation 18**:

$$\begin{cases} \varepsilon_r = \frac{1+\nu}{E} [(1-\nu)\sigma_r - \nu\sigma_\theta] + (1+\nu)\alpha T \\ \varepsilon_\theta = \frac{1+\nu}{E} [(1-\nu)\sigma_\theta - \nu\sigma_r] + (1+\nu)\alpha T \end{cases} \quad (20)$$

Then re-write **Equation 20** into **Equation 21**:

$$\begin{cases} \sigma_r = \frac{E}{(1+\nu)(1-2\nu)} [(1-\nu)\varepsilon_r + \nu\varepsilon_\theta - (1+\nu)\alpha T] \\ \sigma_\theta = \frac{E}{(1+\nu)(1-2\nu)} [(1-\nu)\varepsilon_\theta + \nu\varepsilon_r - (1+\nu)\alpha T] \end{cases} \quad (21)$$

Radial and hoop stresses need to satisfy the balance equation (**Equation 22**):

$$\frac{d\sigma_r}{dr} + \frac{\sigma_r - \sigma_\theta}{r} = 0 \quad (22)$$

Combine **Equations 20** and **22** together, the displacement (u) can be calculated by:

$$\frac{d}{dr} \left[\frac{1}{r} \frac{d(ru)}{dr} \right] = \alpha \frac{1+\nu}{1-\nu} \frac{dT}{dr} \quad (23)$$

Because of the strain-displacement relationship (**Equation 24**), strains can be written as:

$$\begin{cases} \varepsilon_r = \frac{du}{dr} = \alpha \frac{1+\nu}{1-\nu} \left(T - \frac{1}{r^2} \int_{r_i}^r T r dr \right) + R_1 - \frac{R_2}{r^2} \\ \varepsilon_\theta = \frac{u}{r} = \alpha \frac{1+\nu}{1-\nu} \frac{1}{r^2} \int_{r_i}^r T r dr + R_1 + \frac{R_2}{r^2} \end{cases} \quad (24)$$

According to **Equation 21**, **Equation 24** can be written as:

$$\begin{cases} \sigma_r = \frac{E}{1+\nu} \left[-\alpha \frac{1+\nu}{1-\nu} \frac{1}{r^2} \int_{r_i}^r T r dr + \frac{R_1}{1-2\nu} - \frac{R_2}{r^2} \right] \\ \sigma_\theta = \frac{E}{1+\nu} \left[\alpha \frac{1+\nu}{1-\nu} \frac{1}{r^2} \int_{r_i}^r T r dr + \frac{R_1}{1-2\nu} + \frac{R_2}{r^2} - \alpha \frac{1+\nu}{1-\nu} T \right] \end{cases} \quad (25)$$

In **Equations 24** and **25**, R_1 and R_2 are the integral constant. p_2 and p_3 are determined by the displacement boundary conditions (**Equation 26**).

$$\begin{cases} u_{rc}|_{r=b} = u_{pc}|_{r=b} + u_{Tc}|_{r=b} \\ u_r|_{r=b} = u_p|_{r=b} + u_T|_{r=b} \\ u_r|_{r=c} = u_p|_{r=c} + u_T|_{r=c} \\ u_{rf}|_{r=c} = u_{pf}|_{r=c} + u_{Tf}|_{r=c} \end{cases} \quad (26)$$

The cylindrical stresses near the wellbore in the casing-cement-formation system can be estimated using the following equations (**Equation 27**):

$$\begin{cases} \sigma_r = \frac{b^2 p_2 - c^2 p_3}{c^2 - b^2} - \frac{b^2 c^2 (p_2 - p_3)}{c^2 - b^2} \frac{1}{r^2} \\ \sigma_\theta = \frac{b^2 p_2 - c^2 p_3}{c^2 - b^2} + \frac{b^2 c^2 (p_2 - p_3)}{c^2 - b^2} \frac{1}{r^2} \end{cases} \quad (27)$$

For situation (ii), the stress induced by non-uniform pressure is analyzed. The Airy stress function (φ) is related to the stress tensor (σ) by:

$$\begin{cases} \sigma_r = \frac{1}{r} \frac{\partial \varphi}{\partial r} + \frac{1}{r^2} \frac{\partial^2 \varphi}{\partial \theta^2} \\ \sigma_\theta = \frac{\partial^2 \varphi}{\partial r^2} \\ \tau_{r\theta} = -\frac{\partial}{\partial r} \left(\frac{1}{r} \frac{\partial \varphi}{\partial \theta} \right) \end{cases} \quad (28)$$

The Airy stress function can be assumed as:

$$\varphi = \left(Jr^2 + Kr^4 + \frac{M}{r^2} + N \right) \cos 2\theta \quad (29)$$

Where J, K, M, and N are the unknown constants and required to be determined.

The stresses can be expressed by **Equations 28** and **29**:

$$\begin{cases} \sigma_r = -2 \left(J + \frac{3M}{r^4} + \frac{2N}{r^2} \right) \cos 2\theta \\ \sigma_\theta = 2 \left(J + 6Kr^2 + \frac{3M}{r^4} \right) \cos 2\theta \\ \tau_{r\theta} = 2 \left(J + 3Kr^2 - \frac{3M}{r^4} - \frac{N}{r^2} \right) \sin 2\theta \end{cases} \quad (30)$$

The strains are determined by:

$$\begin{cases} \varepsilon_r = \frac{1-\nu^2}{E} \left(\sigma_r - \frac{\nu}{1-\nu} \sigma_\theta \right) \\ \varepsilon_\theta = \frac{1-\nu^2}{E} \left(\sigma_\theta - \frac{\nu}{1-\nu} \sigma_r \right) \\ \varepsilon_{r\theta} = \frac{1+\nu}{E} \tau_{r\theta} \end{cases} \quad (31)$$

Combine **Equations 30** and **31** together:

$$\begin{cases} \varepsilon_r = -\frac{2(1+\nu)}{E} \left[J + 6Kr^2\nu + \frac{3M}{r^4} + \frac{2N}{r^2}(1-\nu) \right] \cos 2\theta \\ \varepsilon_\theta = \frac{2(1+\nu)}{E} \left[J + 6(1-\nu)Kr^2 + \frac{3M}{r^4} + \frac{2N}{r^2}\nu \right] \cos 2\theta \\ \varepsilon_{r\theta} = \frac{2(1+\nu)}{E} \left(J + 3Kr^2 - \frac{3M}{r^4} - \frac{N}{r^2} \right) \sin 2\theta \end{cases} \quad (32)$$

Because of the geometric equation, $\varepsilon_r = \frac{du}{dr}$ and $\varepsilon_\theta = \frac{u}{r}$, **Equation 32** can be written as:

$$\begin{cases} \varepsilon_r = \frac{\partial u_r}{\partial r} \\ \varepsilon_\theta = \frac{1}{r} \frac{\partial u_\theta}{\partial \theta} + \frac{u_\theta}{r} \\ \varepsilon_{r\theta} = \frac{1}{2} \left[\frac{1}{r} \frac{\partial u_r}{\partial \theta} + \frac{\partial u_\theta}{\partial r} - \frac{u_\theta}{r} \right] \end{cases} \quad (33)$$

So the radial and hoop displacements are derived by **Equation 34**:

$$\begin{cases} u_r = -\frac{2(1+\nu)}{E} \left[Jr + 2Kr^3\nu - \frac{M}{r^3} - \frac{2N}{r}(1-\nu) \right] \cos 2\theta + f(\theta) \\ u_\theta = \frac{2(1+\nu)}{E} \left[Jr + (3-2\nu)Kr^3 + \frac{M}{r^3} + \frac{N}{r}(2\nu-1) \right] \sin 2\theta - \int f(\theta) d\theta + g(r) \end{cases} \quad (34)$$

$f(\theta)$ and $g(r)$ are neglected because the formulations calculate the rigid body displacements which are not considered in this study. So the **Equation 34** is:

$$\begin{cases} u_r = -\frac{2(1+\nu)}{E} \left[Jr + 2Kr^3\nu - \frac{M}{r^3} - \frac{2N}{r}(1-\nu) \right] \cos 2\theta \\ u_\theta = \frac{2(1+\nu)}{E} \left[Jr + (3-2\nu)Kr^3 + \frac{M}{r^3} + \frac{N}{r}(2\nu-1) \right] \sin 2\theta \end{cases} \quad (35)$$

Based on the boundary conditions in **Equation 36**, 12 equations (**Equation 37**) are generated to solve $J_c, K_c, M_c, N_c, J, K, M, N, J_f, K_f, M_f,$ and N_f :

$$\begin{cases} \sigma_{rc}|_{r=a} = 0, \tau_{r\theta c}|_{r=a} = 0 \\ \sigma_{rc}|_{r=b} = \sigma_r, \tau_{r\theta c}|_{r=b} = \tau_{r\theta} \\ u_{rc}|_{r=b} = u_r, u_{\theta c}|_{r=b} = u_\theta \\ \sigma_{rf}|_{r=c} = \sigma_r, \tau_{r\theta f}|_{r=c} = \tau_{r\theta} \\ u_{rf}|_{r=c} = u_r, u_{\theta f}|_{r=c} = u_\theta \\ \sigma_{rf}|_{r=d} = -p'_f, \tau_{r\theta f}|_{r=d} = \tau_f \end{cases} \quad (36)$$

$$\left\{ \begin{array}{l}
J_c + \frac{3M_c}{a^4} + \frac{2N_c}{a^2} = 0 \\
J_c + 3K_c a^2 - \frac{3M_c}{a^4} - \frac{N_c}{a^2} = 0 \\
J_c + \frac{3M_c}{b^4} + \frac{2N_c}{b^2} = J + \frac{3M}{b^4} + \frac{2N}{b^2} \\
J_c + 3K_c b^2 - \frac{3M_c}{b^4} - \frac{N_c}{b^2} = J + 3K b^2 - \frac{3M}{b^4} - \frac{N}{b^2} \\
J_c b + 2K_c b^3 v_c - \frac{M_c}{b^3} - \frac{2N_c}{b} (1 - v_c) = \frac{E_c(1+v)}{E(1+v_c)} [J b + 2K b^3 v - \frac{M}{b^3} - \frac{2N}{b} (1 - v)] \\
J_c b + (3 - 2v_c) K_c b^3 + \frac{M_c}{b^3} + \frac{N_c}{b} (2v_c - 1) = \frac{E_c(1+v)}{E(1+v_c)} [J b + (3 - 2v) K b^3 + \frac{M}{b^3} + \frac{N}{b} (2v - 1)] \\
J_f + \frac{3M_f}{c^4} + \frac{2N_f}{c^2} = J + \frac{3M}{c^4} + \frac{2N}{c^2} \\
J_f + 3K_f c^2 - \frac{3M_f}{c^4} - \frac{N_f}{c^2} = J + 3K c^2 - \frac{3M}{c^4} - \frac{N}{c^2} \\
J_f c + 2K_f c^3 v_f - \frac{M_f}{c^3} - \frac{2N_f}{c} (1 - v_f) = \frac{E_f(1+v)}{E(1+v_f)} [J c + 2K c^3 v - \frac{M}{c^3} - \frac{2N}{c} (1 - v)] \\
J_f c + (3 - 2v_f) K_f c^3 + \frac{M_f}{c^3} + \frac{N_f}{c} (2v_f - 1) = \frac{E_f(1+v)}{E(1+v_f)} [J c + (3 - 2v) K c^3 + \frac{M}{c^3} + \frac{N}{c} (2v - 1)] \\
J_f + \frac{3M_f}{d^4} + \frac{2N_f}{d^2} = \frac{\sigma_H - \sigma_h}{2} (1 - \frac{a^2}{d^2}) (1 - 3 \frac{a^2}{d^2}) \\
J_f + 3K_f d^2 - \frac{3M_f}{d^4} - \frac{N_f}{d^2} = -\frac{\sigma_H - \sigma_h}{2} (1 - \frac{a^2}{d^2}) (1 + 3 \frac{a^2}{d^2})
\end{array} \right. \quad (37)$$

The total stress equals the sum of stresses in the situation (i) and (ii).

Chapter 3: Experimental and Numerical Investigation of Cement Mechanical Integrity

In this section, an investigation of cement integrity under diametric compressive loads is presented. DIC technique is used to measure the full-field strain and deformation distribution. Neat class H, nano-modified class H, and geopolymer cement are tested in a casing-cement-formation system under diametric compressive loads. This study helps to understand the bond strength of different cement systems. The result of neat class H cement is used to verify the numerical model for further advancing the investigation of the cement performance by simulating different properties. Failure location and mode are analyzed to identify the risky zone. Sensitivity analysis is conducted, and the effect of Young's modulus and Poisson's ratio is assessed by comparing the mechanical stress to the corresponding strength limitation. This work aims to understand the most influencing factor of cement bond strength.

3.1. Experimental Setup

DIC is a photogrammetry system to monitor the strain distribution on the surface by comparing the images after and before deformation. This technology is employed to record the strain pattern in the casing-cement-formation sample subjected to diametric load. Both strain distributions in the casing-cement and cement-formation interfaces are recorded. Class H cement is selected because it is a commonly used cement in US GoM (Eberhardt and Shine, 2004). API standard procedures of cement preparation are followed.

3.1.1. Sample Preparation

Table 3.1 presents the details of cement receipt for each scenario. Neat class H cement is referred to as a reference sample consisting of 859 g cement powder with 38% BWOC of water. Nano-graphite with 0.5% BWOC is mixed with the neat class H to generate nano-modified class H cement. The components of nano-synthetic graphite are shown in **Table 3.2**. Geopolymer cement system is made from 700 g precursor and 370 ml K-silicate solution. The total volume of final mixing cement slurries is kept at a constant of 600 ml. The mixing procedure is suggested by the API standard. Cement slurries are mixing in a 3.5 hp commercial blender with 4000 rpm for 15 seconds and 12000 rpm for 35 seconds. The mixing procedure provides the same energy to minimize the influence of stirring energy on cement properties, such as thickening time (Hibbert et al., 1995). A steel pipe with 0.6 in. (15.24 mm) of ID (inner diameter) and 0.85 in. (21.59 mm) of OD (outer diameter) was set concentrically in the Berea sandstone with 1.25 in. (31.75 mm) of ID and 2 in. (50.80 mm) of OD (**Figure 3.1**). The height of the sample is 1 inch (25.4 mm). The cement slurry is placed between a concentric casing and Brea sandstone formation curing for 24 hrs with a stable temperature of 158±9°F (70±5°F).

Table 3.1 Details of cement slurry design.

<i>Cement type</i>	<i>Component</i>	<i>Amount</i>
<i>Neat class H</i>	<i>Cement</i>	<i>859 g</i>
	<i>Water (38% BWOC)</i>	<i>326.4 g</i>
<i>Nano-modified class H</i>	<i>Cement</i>	<i>859 g</i>
	<i>Water (38% BWOC)</i>	<i>326.4 g</i>
	<i>Nano-graphite (0.5% BWOC)</i>	<i>4.3 g</i>
<i>Geopolymer</i>	<i>Precursor</i>	<i>700 g</i>
	<i>K-silicate solution</i>	<i>370 g</i>

Table 3.2 Components of nano-synthetic graphite.

<i>Property</i>	<i>Value</i>
<i>Carbon (%)</i>	99.94
<i>Sulfur (%)</i>	0.009
<i>pH</i>	6.05
<i>Surface area (m²/g)</i>	325-375
<i>Density (g/cc)</i>	2.16

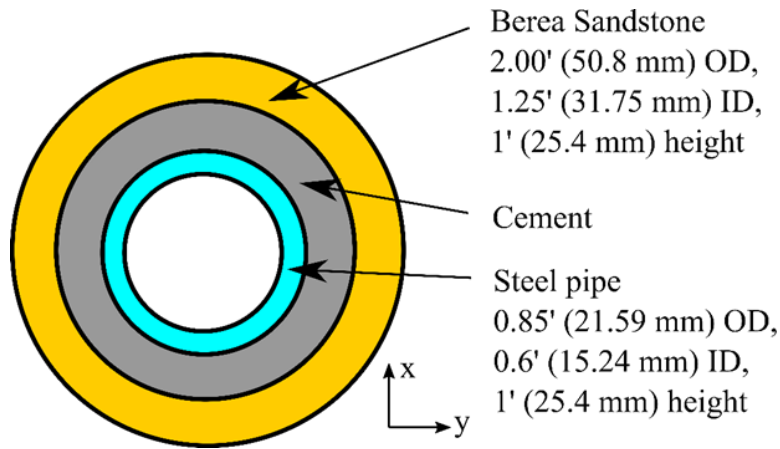


Figure 3.1 Dimension of the casing-cement-formation system used in diametric compression tests. Blue, gray, and yellow colors indicate steel casing, cement sheath, rock formation, respectively.

3.1.2. DIC and Diametric Compression Test Setup

Diametric compression test (also known as a modified tensile bond strength test) is recommended in this study since the occurrence of failure in cement sheath in the wellbore is more likely to be tensile in nature due to low tensile strength. To minimize the effect of stress concentration, curved loading platens are magnetically attached to the load frame (ASTM D3967-08, 2016). **Figure 3.2** shows the experimental setup. The samples are sprayed paint with a black-and-white speckled pattern. The high-speed camera records the displacement of the speckles due to diametric compression. Image acquisition and processing are made by DIC analysis software to calculate the strain distribution of the

sample. In this study, the camera is set as four (4) fps (frames per second) to minimize the time interval providing a more accurate strain distribution. The loading rate is kept at a constant of 0.1 mm/min, satisfying 6 min of the testing time upper limitation suggested by ASTM (ASTM D3967-08, 2016).

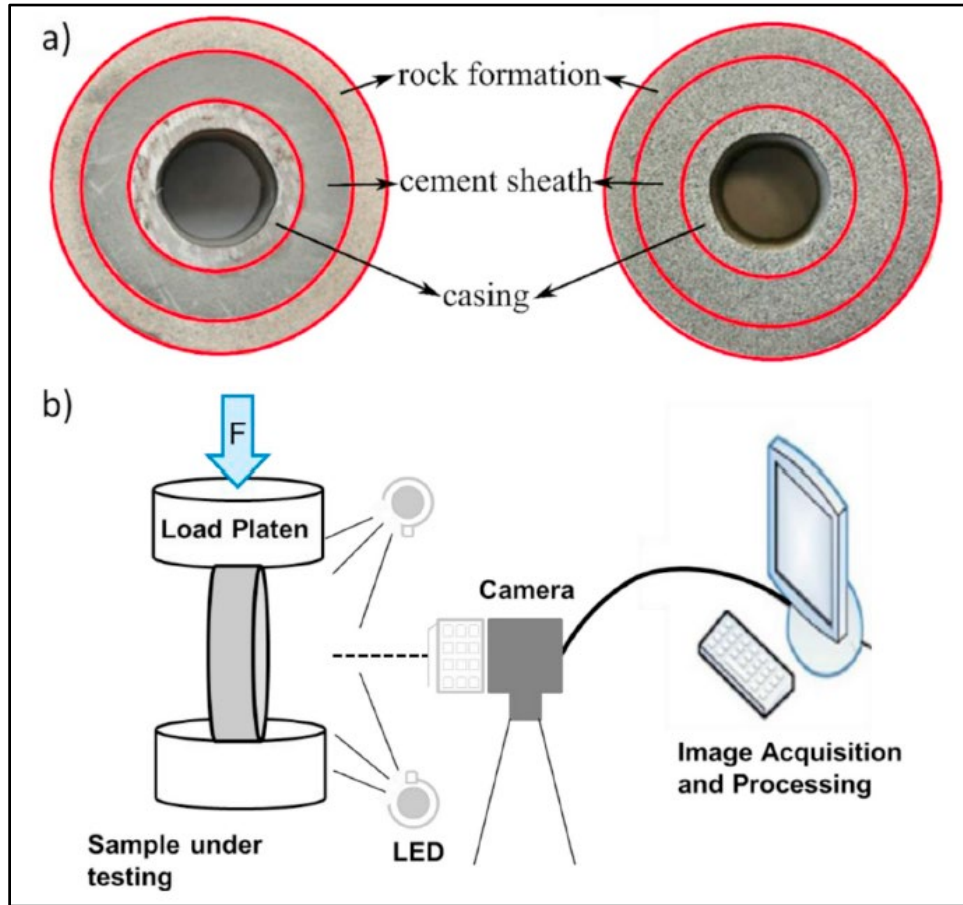


Figure 3.2 a) Casing-cement-formation system before and after painting; b) Graphically explanation of the measurement of full-field strain and deformation using DIC technique.

3.2. Numerical Model Setup

An FEA model is developed using a multiphysics engineering simulation software, ANSYS. The model assumed that casing-cement and cement formation interfaces are bonded. Because the nature of the cement sheath is an extremely low permeability material

(cement permeability recommended by API is below $200\mu\text{D}$) and the purpose of the study is to evaluate structural stresses, the cement sheath was modeled as a solid with linear elastic properties and treated as an impermeable material. For verification purposes, the base case indicates neat class H cement placed between the casing and Brea sandstone rock formation. The model is further extended to different cement Young's modulus and Poisson's ratio while casing and rock formation properties remain constant.

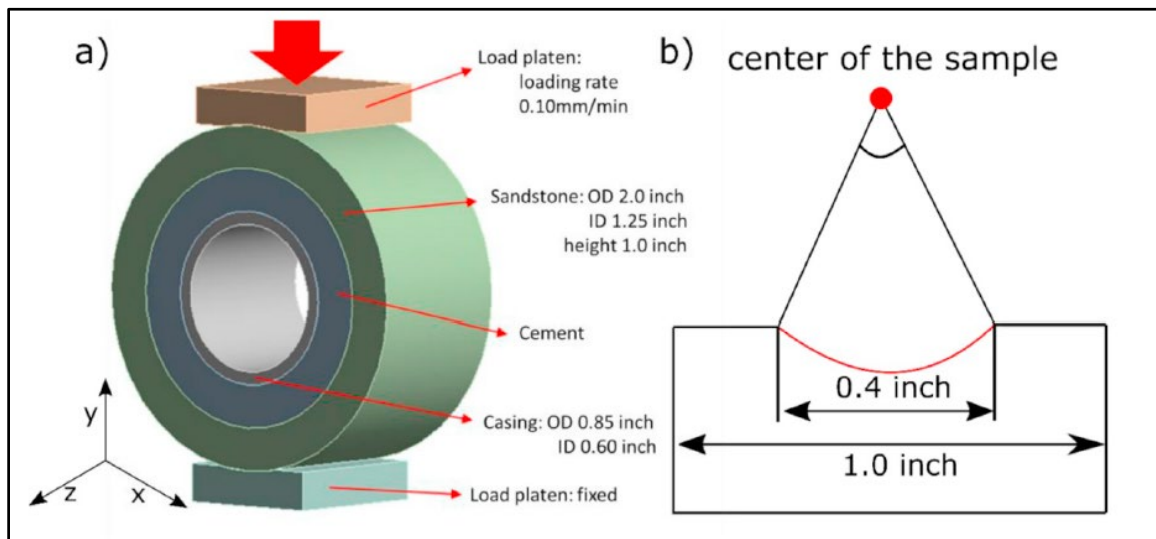


Figure 3.3 a) Geometry of the casing-cement-formation system compressing diametrically with a curved loading platen; b) Magnified sketch of load platen. The Red line represents the contact surface between load platen and sample. The contact angle is 23° .

Based on the failure propagation theory, the initiation and development of cement failure along both circumferential (x - y plane) and axial direction (z -direction) are not uniform (Feng et al., 2017). The 2D plane strain theory assumes that the state of strain in the z -direction is zero. It cannot be utilized to simulate the development of failure in real conditions. In order to overcome the limitations of the 2D plan strain, a 3D model was developed for a casing-cement-formation system (**Figure 3.3a**). The dimension is the completely same as the experimental setup. Garcia et al. (2017) studied the stress

distribution with different contact angles (the angle subtended from the center of the sample by the contact area) in the diametric compression test. No stress concentration is observed when the angle is larger than 12°. In this study, a curved loading platen with 23° of contact angle is attached to the sample for accurate results (**Figure 3.3b**).

Young’s modulus and Poisson’s ratio are utilized to define the casing, cement, and formation (**Table 3.3**). The interface between load platen and formation is followed the no-separation interfacial behaviors. Surfaces are allowed to slide while no gap is at the interface. A load is applied on the upper platen, and a fixed boundary condition is on the lower platen (**Figure 3.3a**). As mentioned in Chapter 3, the loading rate is 0.1 mm/min (or 0.00167 mm/second). The first failure is initiated at the time of 110 seconds. Because the model simulates the elastic performance before cement yielding, the equivalent boundary condition of 0.18 mm displacement is used to evaluate cement stresses at the time of failure.

Table 3.3 Material properties of the casing, cement, and formation in the base case.

<i>Mechanical properties</i>	<i>Casing</i>	<i>Cement</i>	<i>Formation</i>
<i>Young’s modulus (E)</i>	<i>200 GPa</i>	<i>9.7 GPa</i>	<i>10 GPa</i>
<i>Poisson’s ratio (ν)</i>	<i>0.30</i>	<i>0.20</i>	<i>0.30</i>
<i>Compressive strength (C_o)</i>	<i>-</i>	<i>25 MPa</i>	<i>-</i>
<i>Tensile strength (T_o)</i>	<i>-</i>	<i>1.40 MPa</i>	<i>-</i>

**Casing and formation properties are cited from Patel et al. (2019) and Molina et al. (2016), respectively. Cement properties are tested in the lab.*

In addition to the base case scenario, six other scenarios with variable cement properties are simulated. The purpose is to investigate the effect of cement Young’s modulus and Poisson’s ratio on the risk of failure. **Table 3.4** lists the properties for each of the scenarios. Elastic properties of formation are kept constant due to its uncontrollability nature. Typical casing properties with 200 GPa of Young’s modulus and 0.3 of Poisson’s

ratio are used in all scenarios. Scenario #1 is the base case, as discussed earlier, which uses the neat class H cement. Five scenarios (scenario #2–5) are created to cover the range of cement recipes from ductile to brittle. Values of material properties were selected such that the study encompasses various types of cement recipes.

Table 3.4 Young’s modulus and Poisson’s ratio of cement and formation used for evaluating the effect of elastic properties on cement performances.

<i>Scenario’s number</i>	<i>Cement</i>		<i>Formation</i>	
	<i>Young’s modulus (E_c)</i>	<i>Poisson’s ratio (ν_c)</i>	<i>Young’s modulus (E_f)</i>	<i>Poisson’s ratio (ν_f)</i>
#1	9.7 GPa	0.20	10	0.30
#2	5	0.20	10	0.30
#3	15	0.20	10	0.30
#4	25	0.20	10	0.30
#5	9.7	0.10	10	0.30
#6	9.7	0.30	10	0.30
#7	9.7	0.40	10	0.30

3.3. Diametric Compression Test Result

The strain distribution of cement in the casing-cement-formation system is tested under a diametric compressive load. Load-strain relationship plots are measured to digitally illustrate the bond failure. Three kinds of cement systems are tested – neat class H, nano-graphite H, and geopolymer cement.

3.3.1. Neat Class H and Nano-Modified Cement

Figure 3.4a illustrates the horizontal and vertical strain distributions of the neat class H case. At the beginning of diametric compression (i.e., 61 seconds), the maximum horizontal strain is in the casing-cement interface at 45° to the direction of the compressive load in tension, while the maximum vertical strain is at the same location in compression. As the magnitude of applied load increases, strain propagates through the cement to the

formation. Failure initiates at the casing-cement interface firstly between 73 to 110 seconds then propagates to the cement. The exact failure initiation time can be determined by a load-strain figure which will be described later. **Figure 3.4b** is the strain map of nano-modified class H cement. The high magnitude of strain is at the same location as neat class H. At 173-225 seconds, failure initiates in the casing-cement interface, then propagates to the formation. The interfacial bond of nano-modified cement fails later than neat class H cement, which means the former system has a stronger bond strength.

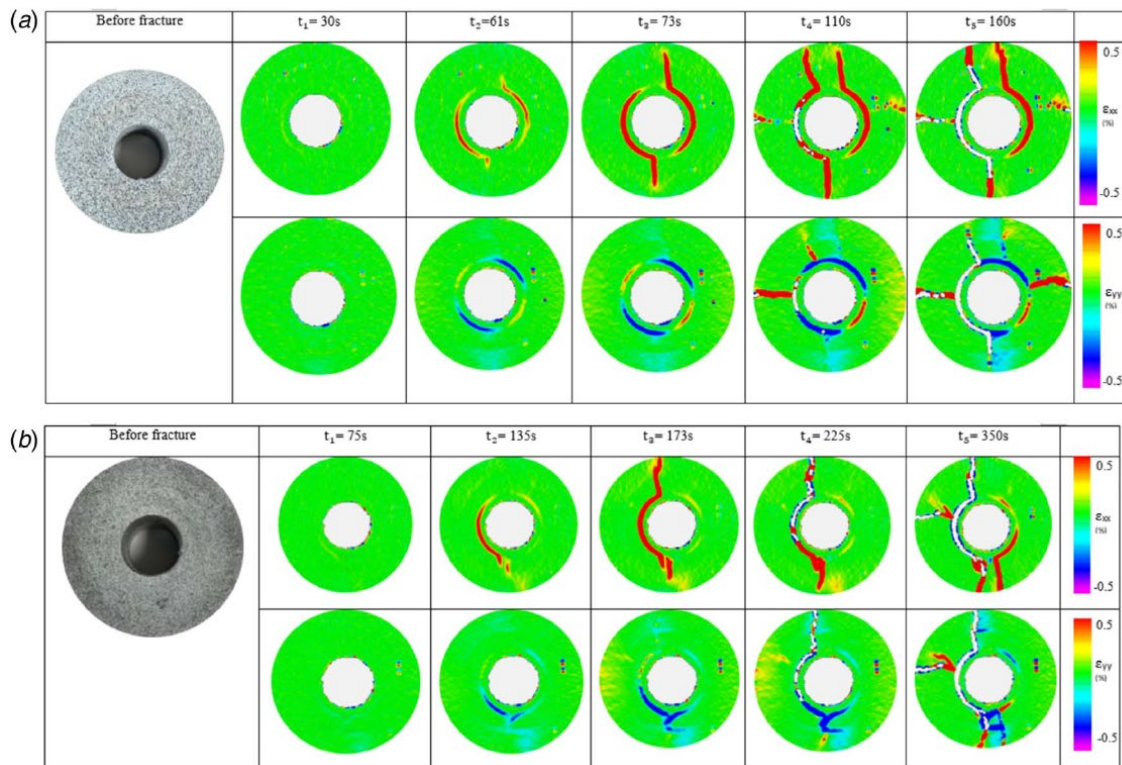


Figure 3.4 a) Strain distribution of the neat class H cement at different times; b) Strain distribution of the nano-modified class H cement at different times. The first row illustrates the horizontal strain distribution, while the second row is the vertical strain distribution.

The relationship between load and axial strain presents the comparison of two cement performance resisting diametric loads (**Figure 3.5**). For neat class H cement, a load

drops down is at 2000 lbf of load in 110 seconds with 0.003 axial strain. Then, the load and strain resume to increase until complete failure at 2750 lbf in 160 seconds with 0.0054 of strain. For nano-modified class H cement, the drop occurs at 510 lbf in 170 seconds with 0.0056 of strain. At 360 seconds, the nano-modified class H cement fails with 1500 lbf of load and 0.012 of strain. The last cement system has twice deformation and a half load before shearing compared with the other. The nano-modified class H cement has a better performance resisting more loads due to its higher ductility.

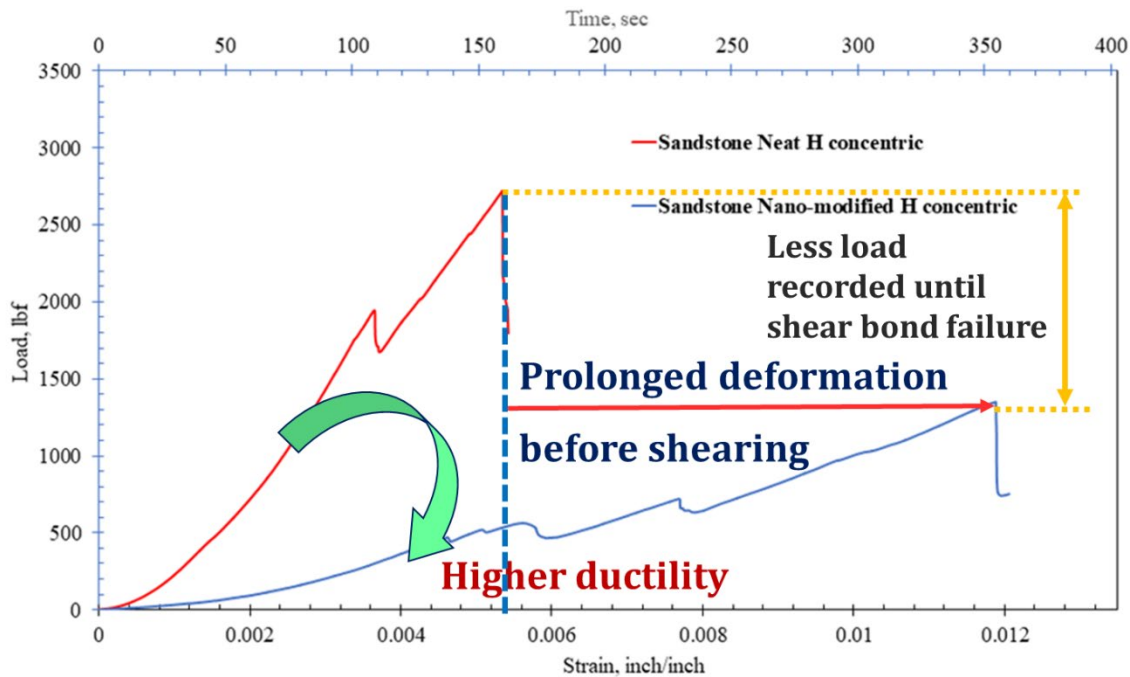


Figure 3.5 Comparison of the neat class H to nano-modified cement under diametric compression.

3.3.2. Neat Class H and Geopolymer Cement

Figure 3.6 shows the strain distribution of the geopolymer case. The maximum strain is at 45° to the load in the casing-cement interface. As the diametric compression increases, strain is generated in the casing-cement interface as well as within the cement

sheath. It is because of the extremely ductile nature of the geopolymer (**Figure 3.7**). When the applied load resulting in an axial strain larger than 0.0024, the corresponding load remains constant with the increasing strain. At 81-170 seconds, the figure shows a bond failure in the casing-cement interface. However, it may seem because of the surface shearing. DIC only records the surface deformation and has a limitation for structural deform detection. The further evaluation is presented in **Figure 3.7**. The bond remains intact until 250 seconds at 300 lbf of the corresponding load. In general, the geopolymer cement system has the best performance on the resistance of failure under a diametric compressive load.

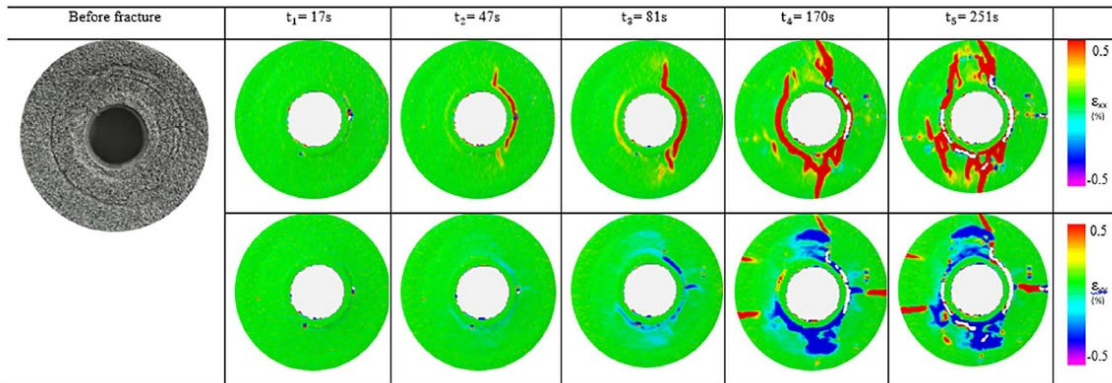


Figure 3.6 Strain distribution of the casing-geopolymer-formation at different times. The first row illustrates the horizontal strain distribution, while the second row is the vertical strain distribution.

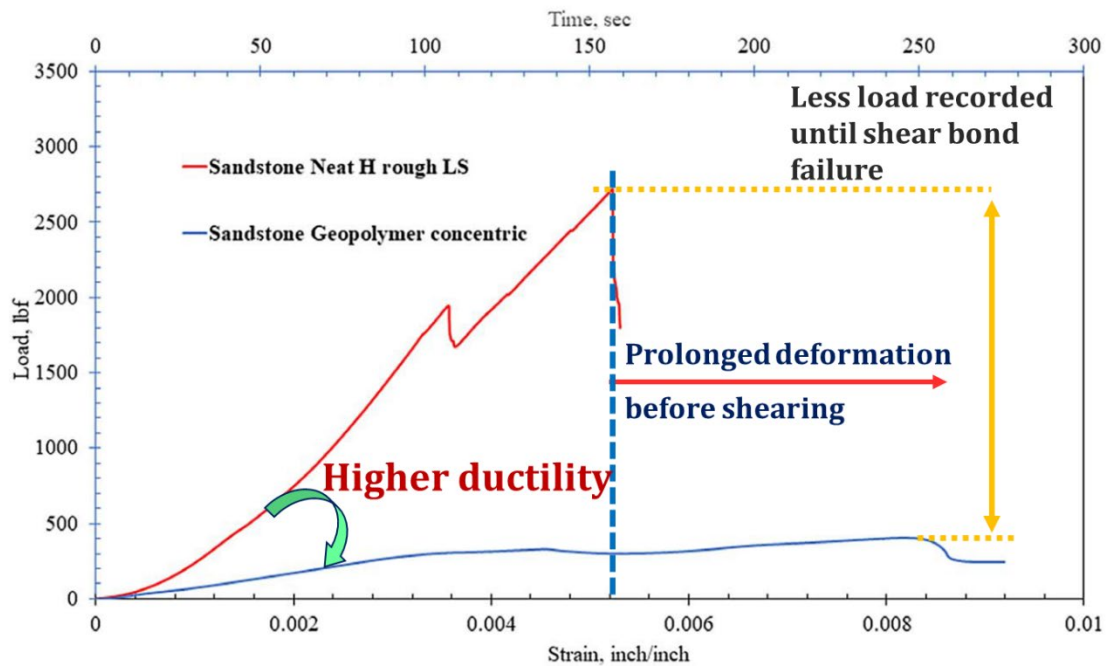


Figure 3.7 Comparison of the neat class H to geopolymer cement under diametric compression.

3.4. Numerical Simulation Verification

Comparison of the numerical solution to DIC diametric compression test results is shown in **Figure 3.8**. The experimental result shows three zones with different time-load relationships. At 0-110 seconds (yellow zone), the corresponding load continuously increases following elastic behaviors. At 110 seconds, the load drops 300 lbf, indicating the initiation of the cement failure. Then, the corresponding load resume to increase until 160 seconds (blue zone). This is because a part of sub-bonds is failed due to high stress. Some sub-bonds still remain intact (**Figure 2.10**). After 160 seconds, no increasing corresponding load is observed (green zone). Bond completely fails, and the residual resistance is coming from the interfacial friction.

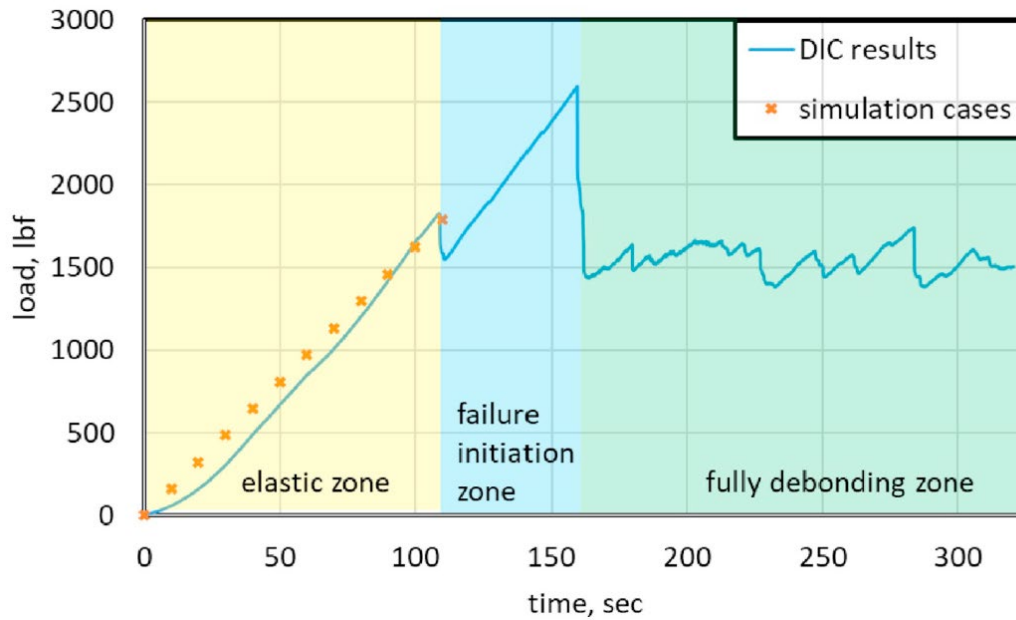


Figure 3.8 Comparison of the numerical solution to DIC diametric compression test results. Yellow, blue, and green mark out the elastic, failure initiation, and fully debonding zones, respectively.

The scope of the model is using linear elastic cement properties to simulate stress distribution before failure. Hence, for the purpose of the study, only the elastic zone before fracture initiation is considered (yellow zone in **Figure 3.8**). Load-strain verification results show that at the beginning of the elastic zone, the deviation between the model and the experimental load values is relatively apparent. For example, at 50 s, the load in the model is 800 lbf compared to 550 lbf in the experiment. The deviation is about 17.4%. With the increment of load, the error tends to decrease. In the experiment, the force at the end of the elastic zone, just before failure, is 1728 lbf, while in the model, the force is indicated at 1644 lbf. The deviation is about 5%. The deviation between experiment and model can be attributed to various factors such as heterogeneity in cement and sandstone (i.e., porosity, permeability, etc.), assumption of pure elastic material properties in the FEA model, lack

of accurate material properties, and strength limits, etc. This study focuses on the stress distribution at the failure point. Therefore, the error at the beginning of the compression will not have a significant influence on the accuracy of the model.

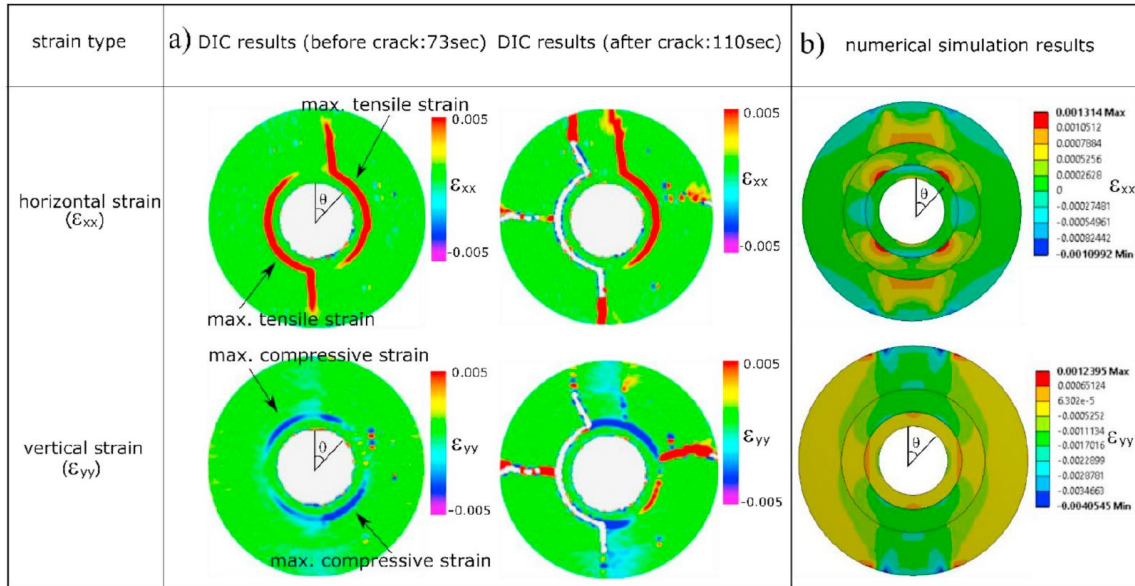


Figure 3.9 Comparison of the horizontal and vertical strain distribution obtained from a) DIC experiment and b) numerical simulation.

Figure 3.9 illustrates horizontal and vertical strain distribution generated from the DIC experiment and simulation. Both DIC and simulation results are in agreement with the maximum strain is at the casing-cement interface with 45° of the angle from the loading direction (θ in **Figure 3.9**). The maximum horizontal strain is in tension while it is compression for the maximum vertical strain. As the load increases, both results show that strain propagates through the cement to the formation. The strain distribution pattern from DIC and FEA are qualitatively similar in terms of locations of strain concentration. However, the strain values are different mainly since real cement and sandstone samples have heterogeneity. Porosity and permeability are not captured in the FEA model. In

general, based on the comparison in **Figure 3.8** and **3.9**, the model has a good match with few deviations.

3.5. Stress Distribution in The Base Scenario

For understanding the risk of cement failure in a finite element model, it is necessary to examine radial and hoop stresses around the configuration. Because of the symmetric nature of the problem, it is sufficient to examine stress distribution within one-quarter of the sample (i.e., 0° to 90°). **Figure 3.10a** and **3.10b** show hoop and radial stress distribution at the casing-cement and the cement-formation interfaces as a function of direction. Comparison of both figures demonstrates that in general, both stresses have a high magnitude in parallel (y-axis or $\theta = 0^\circ$) and perpendicular (x-axis or $\theta = 90^\circ$) direction. Hoop stress has a higher magnitude than radial stress. Particularly, hoop stress at the casing-cement interface is the dominant stress within the system. Both compressive ($\theta = 0^\circ$) and tensile ($\theta = 90^\circ$) hoop stresses at the casing-cement interface exceed limiting strengths of the cement, confirming failure. This observation also matches with the DIC results discussed in the previous section. The cement-formation interface, although not failing in this particular case, exhibits a high magnitude of stresses at $\theta = 45^\circ$ direction. Thus, in addition to the X and Y axis, stress distribution along $\theta = 45^\circ$ has been considered in upcoming results discussions.

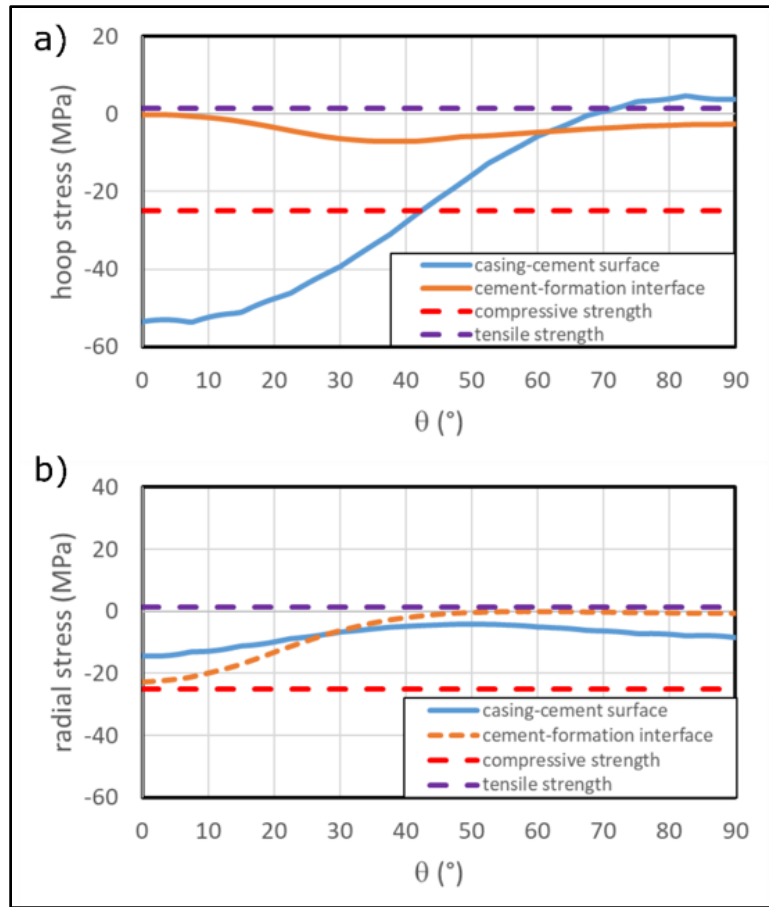


Figure 3.10 Radial and hoop stress distribution around the wellbore. Because of the symmetricity of the model, the stress in θ of 0° - 90° is shown. Blue and orange solid lines indicate stress in the casing-cement and cement-formation interfaces, respectively. Red and purple dash lines indicate compressive and tensile strengths.

Figure 3.11a and **3.11b** presents variation in hoop and radial stress along $\theta = 0^\circ$ (y-axis), 45° , and 90° (x-axis) respectively. For the hoop stress, both maximum compression and tension occur at the casing-cement interface. The maximum compression is observed at 0° , and the maximum tension is observed at 90° . The hoop stress in all three directions (0° , 45° , and 90°) does not have large changes in cement and formation (except interfaces). The range of the hoop stress within cement and formation is from -7MPa to 3MPa. Radial stress in the system is compressive for the most part. The maximum compressive stress of

about -22 MPa is observed at 0° in the formation. The phenomenon is expected because the compressive load is also applied along Y-axis. Although -22 MPa is close to the compressive strength limit, the casing-cement remains the first location of failure since hoop stresses have already exceeded both limiting strengths.

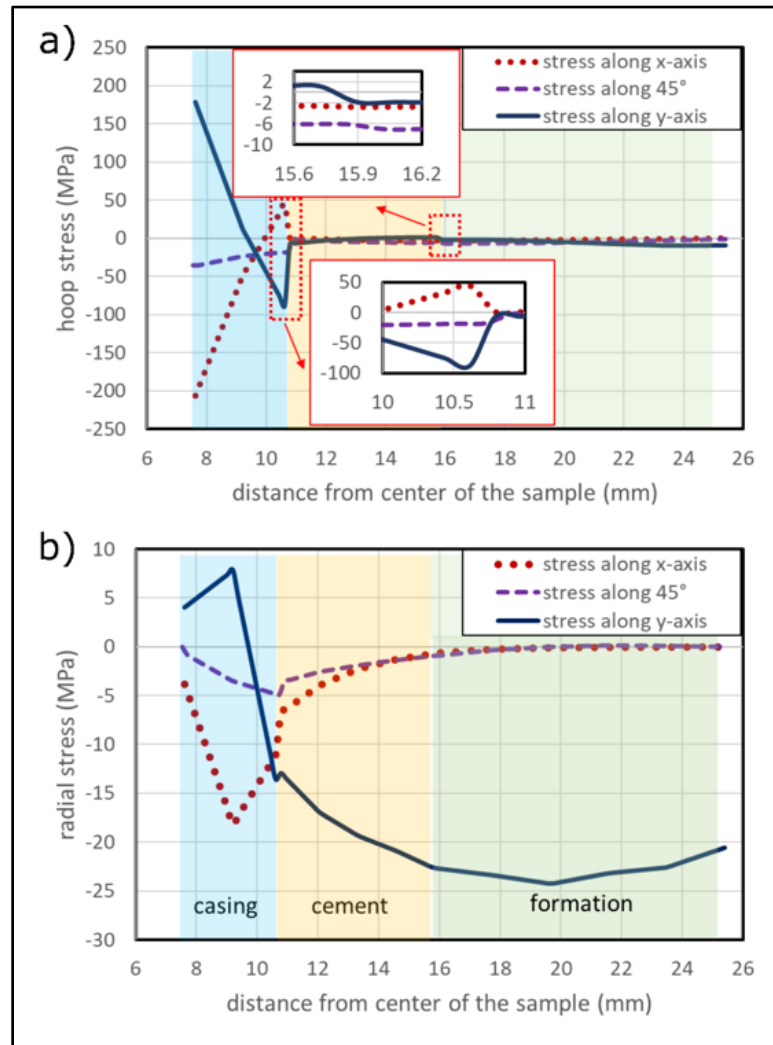


Figure 3.11 Radial and hoop stress distribution in different orientations. a) The comparison of hoop stress in 0° (y-axis), 45° , and 90° (x-axis); b) The comparison of radial stress in 0° (y-axis), 45° , and 90° (x-axis). The Blue area indicates the casing, the gray area is cement, and the red area is the formation.

In summary, **Figure 3.10** and **3.11** indicate that the casing-cement interface is the weakest region in the system being investigated. This matches with the observation in the DIC experiment. It can also be concluded based on simulated stress distribution, hoop stress is the primary cause of failure and the likely locations of failure initiation are 0° and 90° on the casing-cement interface.

3.6. Influence of Young's Modulus and Poisson's Ratio

By evaluation of the base case, the cylindrical stresses around the sample along 0° and 90° have the highest magnitude at the casing-cement interface. The stress distribution is affected by the mechanical properties. The mechanical properties worthy of reporting with reference to cement sheath are Young's modulus and Poisson's ratio (Patel et al. 2019a). It is critical to understanding the principles of failure in the cement sheath under imposed stresses. Previous studies on long-term well integrity risks showed that cement with lower E and higher ν reduces the risk of failures (Patel et al. 2019b; Patel and Salehi 2019). In this section, the effects of cement Young's modulus and Poisson's ratio on the failure of the cement sheath along variable orientations are evaluated (**Figure 3.12-4.8**). The compressive and tensile strength is assumed as 25MPa (Liu et al. 2015) and 1.4MPa (Nygaard et al. 2014).

Figure 3.12 shows the influences of cement Young's modulus (blue lines) and Poisson's ratio (red lines) along 0° (y-axis). According to the comparison of stresses at interfaces with variable Young's modulus, the highest compressive stress occurs at the casing-cement interface with high Young's modulus (**Figure 3.12b**) in the tangential orientation. The highest tension is at the cement-formation interface with low Young's

modulus (**Figure 3.12d**) in the tangential orientation. The results with variable Poisson's ratio show that compressive failure occurs at the casing-cement interface when low Poisson's ratio is applied (**Figure 3.12b**). The radial cracks may exist at the cement-formation interface when applying a low Poisson's ratio (**Figure 3.12d**).

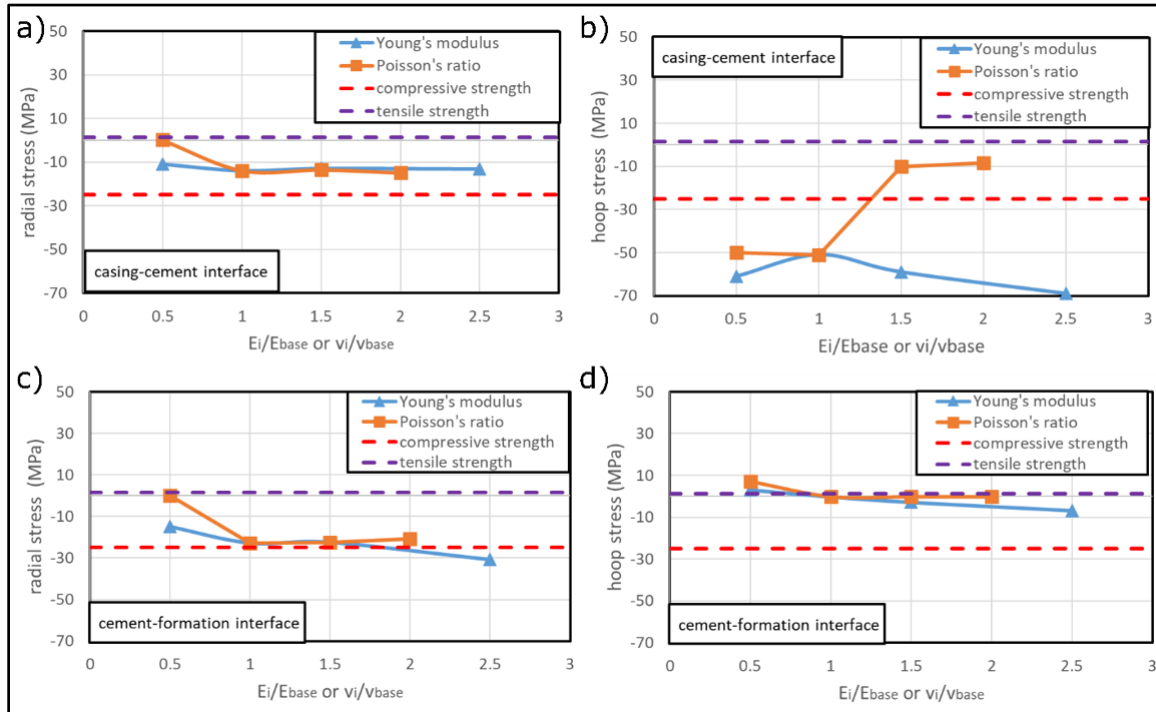


Figure 3.12 Effect of Young's modulus and Poisson's ratio along 0° on a). radial stress at the casing-cement interface, b). hoop stress at the casing-cement interface, c). radial stress at cement-formation interface, and d). hoop stress at cement-formation interface.

Figure 3.13 shows the influences of cement Young's modulus and Poisson's ratio along 45° . All cases show that with the increment of Young's modulus, the radial and hoop stresses increase compression to induce a high risk of compressive failures. The increment of Poisson's ratio results in decreasing compression in radial and hoop stress at casing-cement and cement-formation interfaces. The highest compression exists at the casing-

cement interface with a high Young's ratio or/and with a low Poisson's ratio (**Figure 3.13b**).

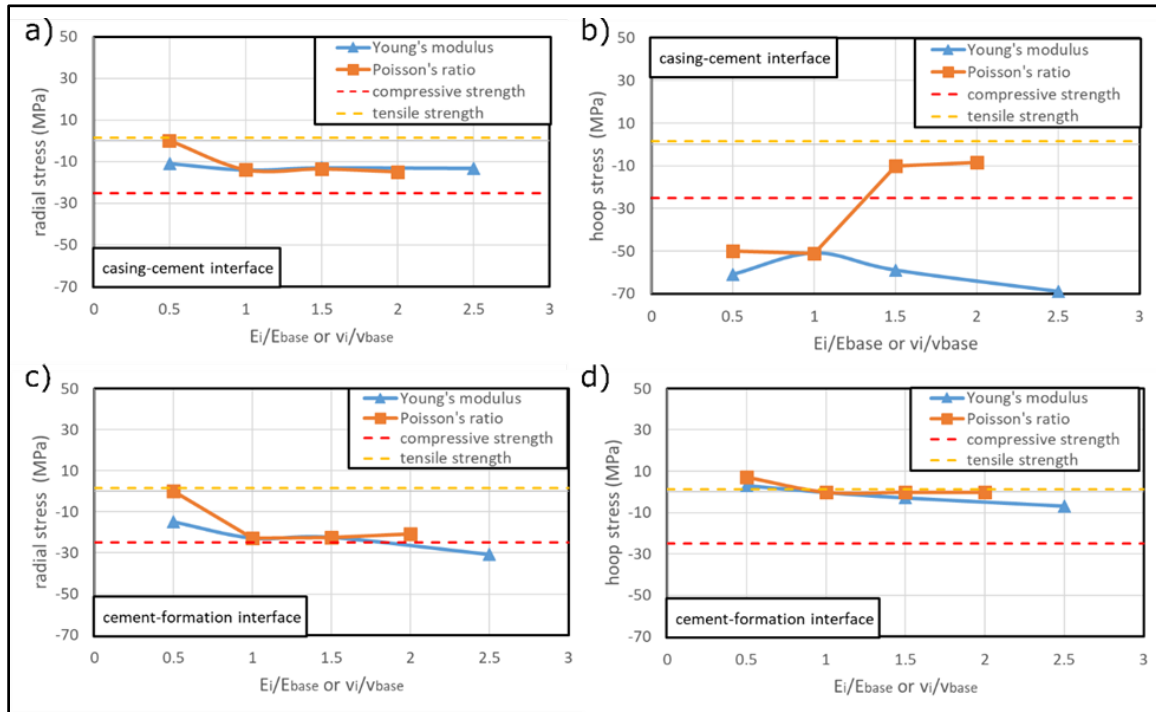


Figure 3.13 Effects of Young's modulus and Poisson's ratio along 45° on a). radial stress at the casing-cement interface, b). hoop stress at the casing-cement interface, c). radial stress at cement-formation interface, and d). hoop stress at cement-formation interface.

Figure 4.8 shows the influences of cement elastic properties along 90° (x-axis). For the effects of Young's modulus, the risk of radial cracks at the casing-cement interface with low Young's modulus or/and low Poisson's ratio (**Figure 3.14b**). The highest risk of compressive failure zone is at casing cement interface with high cement Young's modulus and low Poisson's ratio (**Figure 3.14a**).

It is clear from the results that the influence of cement material properties on radial stress at the casing interface is stronger than in hoop stress at the casing interface. It is the

opposite of the observations along the y-axis, where cement material properties exert a higher influence on hoop stress than radial stress.

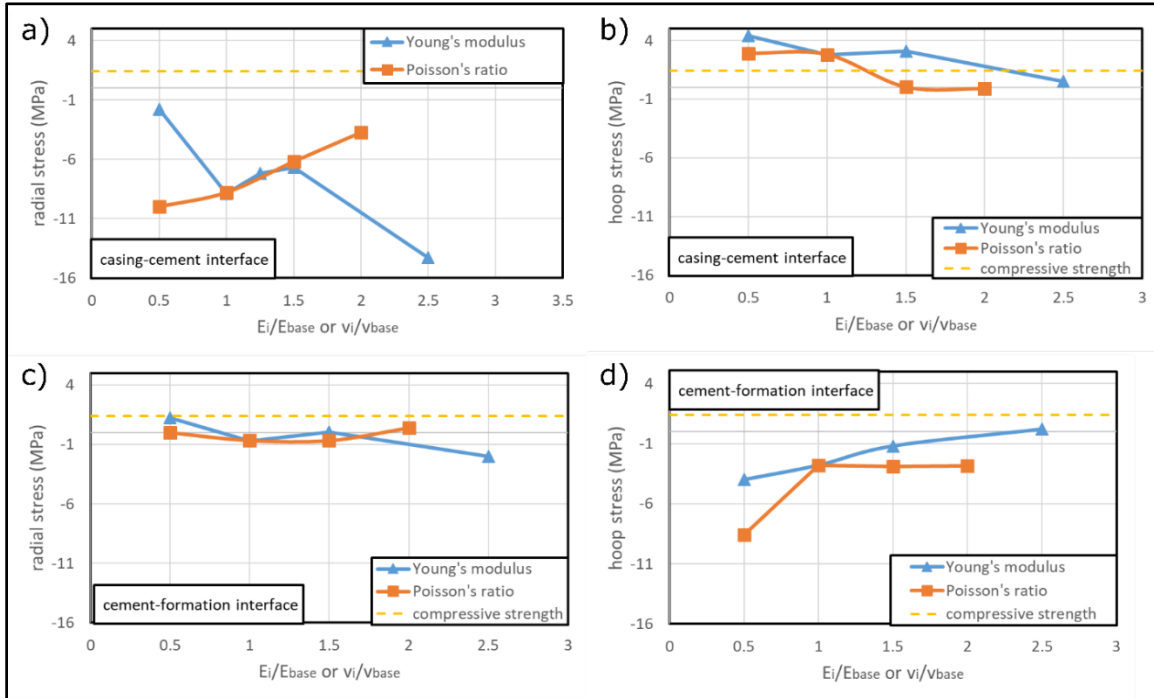


Figure 3.14 Effects of Young's modulus and Poisson's ratio along 90° on a). radial stress at the casing-cement interface, b). hoop stress at the casing-cement interface, c). radial stress at cement-formation interface, and d). hoop stress at cement-formation interface.

3.7. Chapter Summary

In this study, a diametric compression test investigating the bonding of oil well cement to subsurface formations and the casing is introduced. DIC analysis provides an insight into the cement bond integrity. The strain distribution and relationship between axial strain and applied diameter load are utilized to verify the 3D finite element model of the casing-cement-formation system. Various scenarios are simulated to study the effect of Young's modulus and Poisson's ratio on the integrity of casing-cement and cement-formation interfaces (**Figure 3.15**).

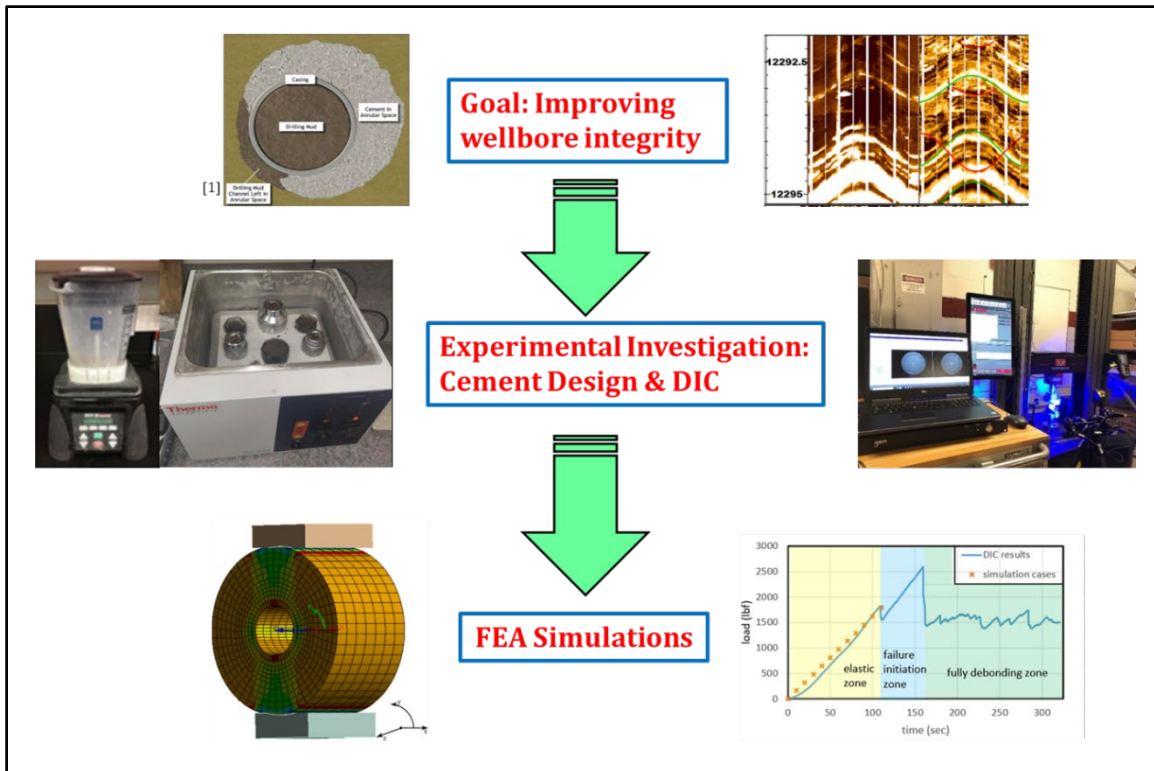


Figure 3.15 Flowchart of the extensive investigation of cement performance using a numerical approach.

The following points are concluded from the study that helps improve understanding of cement failure.

- According to the lab experiments, the maximum failure load is 63% lower than neat Class H cement. Geopolymer can support higher deformation because of its ductility.
- The experiments show less maximum failure load and high deformation for the nano-synthetic graphite cement system before sample failure.
- All scenarios fail at the casing-cement interface because of the development of mechanical interlocking bonds between cement and formation.

- A numerical simulation is conducted for the advanced investigation on the effect of cement Young's modulus and Poisson's ratio. A reasonable match is obtained between failure prediction from finite element model and experimental setup using DIC technique.
- Along with the casing-cement interface, failure is likely to initiate parallel to applied diametric load ($\theta=0^\circ$) followed by perpendicular orientation (90°).
- High hoop stress exceeding the limiting strength is observed to be the primary cause of failure of the casing-cement-formation system.
- Cement material properties (Young's modulus and Poisson's ratio) have a notable influence on cement integrity. Specifically, hoop stress has higher sensitivity to material properties than radial stress. In general, flexible cement with low Young's modulus and high Poisson's ratio exhibits a low risk of failure.

Chapter 4: Numerical Investigation of Temperature and Pressure Impacts on Cement Integrity (A Parametric Study)

Based on the previous studies, heat transformation of one direction is understood, either heat transfers from formation to pipe or heat transfer oppositely. The comparison of two differential temperature patterns was not understood. The specific objectives of this study are to: (i) compare the stress distribution in a casing-cement-formation system under both differential temperature patterns or heat flow directions, (ii) assess the influence of thermal parameters, other important material properties and operational factors that affect the performance of cement.

A 2D numerical model is performed based on the FEA method consisting of casing, cement sheath, and formation. It follows the plane strain theory. The boundary conditions such as tectonic stresses around the wellbore, casing pressure, and temperature are based on the Frontier Observatory for Research in Geothermal Energy (FORGE) geothermal wellbore in Utah shown in **Table 4.1**. The permeability and porosity are extremely low, so the poroelastic effect is not considered in this study (Moore et al., 2019). Because of the symmetric nature of the problem, it is sufficient to simulate one-quarter of the casing-cement-formation system (from 0° to 90°). Material properties are obtained from logging data and laboratory measurements. Sealability is quantitatively evaluated by the cylindrical stress distribution in the cement sheath.

Table 4.1 The properties of FORGE geothermal wellbore (from Moore et al. 2019).

<i>Depth</i>	<i>2300 m (7536 ft)</i>
<i>Maximum horizontal stress gradient</i>	<i>14.0 kPa/m (0.62 psi/ft)</i>
<i>Minimum horizontal stress gradient</i>	<i>17.4 kPa/m (0.77 psi/ft)</i>
<i>Bottom hole temperature</i>	<i>190 °C (375 °F)</i>

Parametric and sensitivity analyses are performed for both heat flow directions. The temperature effects on material properties are not considered in the study. Parameters assessed are thermal conductivity, expansion coefficient, differential temperature, internal casing pressure, Young's modulus, Poisson's ratio, and geo-mechanical stress ratio. In order to maintain the accuracy of the model, analytical equations are used to verify the FEA results.

4.1. Numerical Setup

The schematic of the 2D finite element model is shown in **Figure 4.1**. A cement sheath with an inner diameter (ID) of 7 inches (177.8 mm) and outer diameter (OD) of 8.75 inches (222.25 mm) is placed between casing and formation. Quadrilateral elements with an average size of 0.136 inches (3.45 mm), 0.29 inches (7.3 mm), 0.55 inches (14 mm) are used to mesh the casing, cement, and formation, respectively. Based on the Kirsch analytical solution, the formation dimension is over ten times larger than cement OD, 90 inches (2286 mm) to avoid any boundary effects (Jaeger et al., 2007, Wise et al., 2019). According to Kiran et al. (2017), tectonic stress is one of the variables affecting cement integrity significantly. Maximum and minimum horizontal in-situ stresses are applied. Casing pressure (P_i) and temperature (T_i) are applied to the internal surface of the casing. Tectonic stresses (i.e., maximum and minimum stresses) and formation temperature (T_f)

are subjected to the boundary of formation. θ is defined as the angle from maximum horizontal stress (σ_{h-max}). θ equals 0° when the direction is parallel to σ_{h-max} and 90° when perpendicular to the direction of σ_{h-max} (**Figure 4.1**).

The connecting surfaces of the casing-cement and cement-formation are assumed to be bonded. As API suggested (cement permeability recommended is below $200 \mu D$), cement is an extremely low permeability material, and the purpose of the study is to evaluate structural stresses. Hence, the cement sheath is modeled as a solid with linear elastic properties and treated as an impermeable material. **Table 4.2** shows the thermal and mechanical properties used in the model. The effects of differential temperature on cement mechanical properties are not considered.

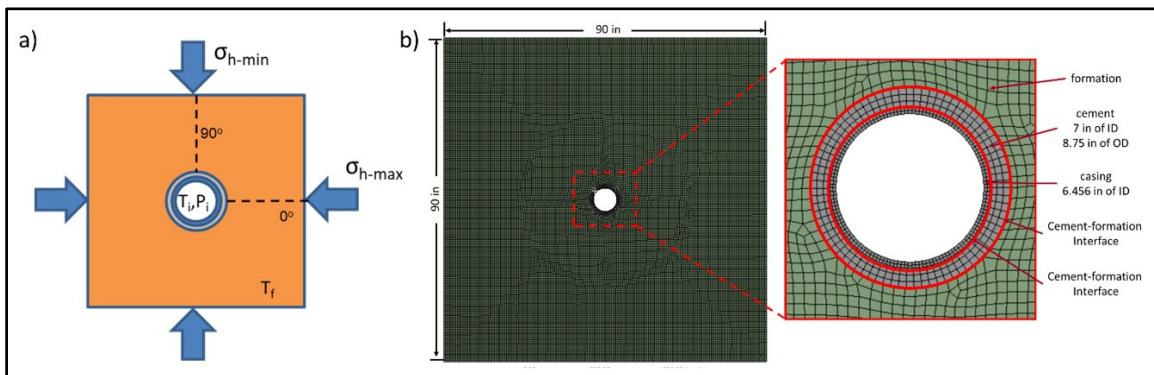


Figure 4.1 a) Schematic of the 2D numerical model with boundary conditions. b) Actual model with mesh elements (left) and the dimension of casing and cement (right).

To evaluate the structural integrity of the cement sheath, cylindrical stresses in and around the wellbore are useful. Theoretically, annular cement sheaths can be assumed as thick- or thin-walled cylinders for calculating mechanical stresses under variable loadings. Radial and hoop stress is compared with the strength to determine the failure risk. The details are presented in Chapter 2.

Table 4.2 Material properties of the casing, cement, and formation for the base case.

<i>Model component</i>	<i>Parameter</i>	<i>Base value</i>
<i>Steel casing</i>	<i>Young's modulus, E_s (GPa)</i>	<i>200</i>
	<i>Poisson's ratio, ν_s</i>	<i>0.30</i>
	<i>Thermal expansion coefficient, α_s ($10^{-6}/K$)</i>	<i>11.43</i>
	<i>Thermal conductivity, K_s (W/m•K)</i>	<i>45</i>
<i>Cement sheath</i>	<i>Young's modulus, E (GPa)</i>	<i>12.5</i>
	<i>Poisson's ratio, ν</i>	<i>0.34</i>
	<i>Thermal expansion coefficient, α ($10^{-6}/K$)</i>	<i>9.4</i>
	<i>Thermal conductivity, K (W/m•K)</i>	<i>0.30</i>
<i>Formation</i>	<i>Young's modulus, E_f (GPa)</i>	<i>68.9</i>
	<i>Poisson's ratio, ν_f</i>	<i>0.26</i>
	<i>Thermal expansion coefficient, α_f ($10^{-6}/K$)</i>	<i>8.0</i>
	<i>Thermal conductivity, K_f (W/m•K)</i>	<i>2.90</i>

4.2. Analytical Verification

In this study, the analytical validation is based on Li et al. (2010). The materials considered in the model, i.e., steel casing, cement sheath, and rock formation, are thermo-linear elastic. All of the interfacial connections (casing-cement and cement-formation) are bonded. There is no defect, and the system is axisymmetric.

The model couples thermal and non-uniform in-situ stress field together. It can be separated into two parts: the model imposed by (i) uniform inner and outer pressure with thermal effects and (ii) non-uniform outer pressure. The details of the derivation are shown in Chapter 2. This Chapter only shows the verification results.

For the model analytical verification, T_i and T_f are selected to be 75°C and 190°C, respectively. 10 MPa of casing pressure (P_i), 40 MPa of maximum horizontal stress, and 32 MPa of minimum horizontal stress are applied in the model as boundary conditions. The two horizontal stresses are calculated based on the gradient of in-situ stress in FORGE geothermal wellbore reports (Table 4.1). Table 4.2 presents the details of material

properties used in the validation. Analytical results are calculated and compared with simulated radial and hoop stresses in the cement sheath. The comparison is graphically presented in **Figure 4.2**.

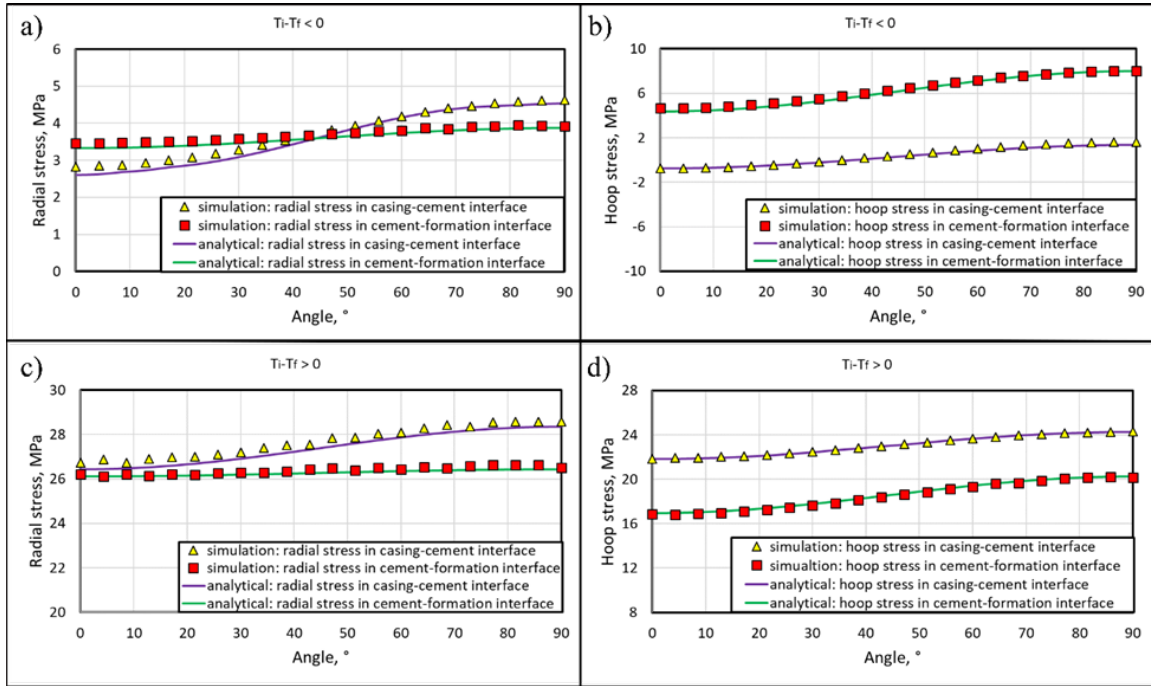


Figure 4.2 Comparison of radial and hoop stresses at casing-cement and cement-formation interface between analytical and simulating results: a) radial and b) hoop stress distribution when heat flow toward casing; c) radial and d) hoop stress distribution when heat flows away from the casing.

Simulated radial and hoop stresses in the cement sheath are compared with the analytical calculations. Results are graphically presented in **Figure 4.2a** (radial stress) and **Figure 4.2b** (hoop stress) when the casing temperature is lower than formation temperature ($T_i < T_f$). The deviation of FEA simulation from the analytical calculation is less than 7% when heat transfer is from the formation to casing. **Figure 4.2c** and **4.2d** represent the comparison in the opposite heat flow direction ($T_i > T_f$). The deviation is less than 4%. In

both cases, finite element model predictions match reasonably with the analytical calculations.

4.3. Failure Analysis of Two Heat Flow Directions

The effect of temperature on failures is shown by using validated FEA simulation. The variable temperature cases used in this study are provided in **Table 4.3**. The temperature range simulated is from 75°C to 190°C for casing and formation temperatures. The influence of temperature and heat flow is assessed by cylindrical stress distribution. In the simulation, only the temperature is applied as a variable parameter. In contrast, the other parameters (i.e., material properties, casing and formation pressures, and tectonic stress ratio) are the same value in model verification (**Table 4.2**).

Table 4.3 Casing and formation temperatures used in the sensitivity analysis.

<i>temperature pattern</i>	<i>Scenario #</i>	T_i	T_f	ΔT
$\Delta T < 0$	1	75	190	-115
	2	100	190	-90
	3	125	190	-65
	4	150	190	-40
	5	175	190	-15
$\Delta T \geq 0$	6	190	190	0
	7	190	175	15
	8	190	150	40
	9	190	125	65
	10	190	100	90
	11	190	75	115

* ΔT is the temperature difference between casing and formation. It is calculated by $\Delta T = T_i - T_f$.

Based on the radial and hoop stresses distribution across the casing, cement, and formation, it was observed that the maximum magnitude of stresses (tension and compression) occur at the casing-cement and cement-formation interfaces. **Figure 4.3** and **4.3b** show radial and hoop stress at the two interfaces in 0° and 90° directions. The stress is a function of variable differential temperatures. Positive values indicate compressive stress, while negative values indicate tensile stress. For the radial stress, the casing-cement interface at 90° exhibits consistently higher magnitude stress than other locations at all differential temperatures. When heat transfers from the casing to the formation ($\Delta T > 0$), stress increases and becomes more compressive with increasing differential temperature. Stresses at all four locations have approximately similar sensitivity to differential temperature. For the opposite heat flow direction ($\Delta T < 0$), an increase in differential temperature compensates for the compressive radial stress and makes it tensile.

For the hoop stress, at both heat flow modes ($\Delta T > 0$ and $\Delta T < 0$), stresses in the casing-cement interface (at both 0° and 90°) are more sensitive to differential temperatures than the cement-formation interface. Similar to radial stress, $\Delta T > 0$ further increases the compressive nature of the hoop stress while $\Delta T < 0$ direction tends to push hoop stress towards tensile nature. Location of highest magnitude stress depends on the direction of heat flow and magnitude of temperature difference. The maximum tensile hoop stress is observed in the casing-cement interface at 0° when heat transfers from the formation to the casing ($\Delta T < 0$). This tensile hoop stress increases the risk of casing-cement debonding. The maximum compressive hoop stress is found in the casing-cement interface at 90° when

heat transfers in the opposite direction ($\Delta T > 0$). In this case, cement crushing is likely to happen.

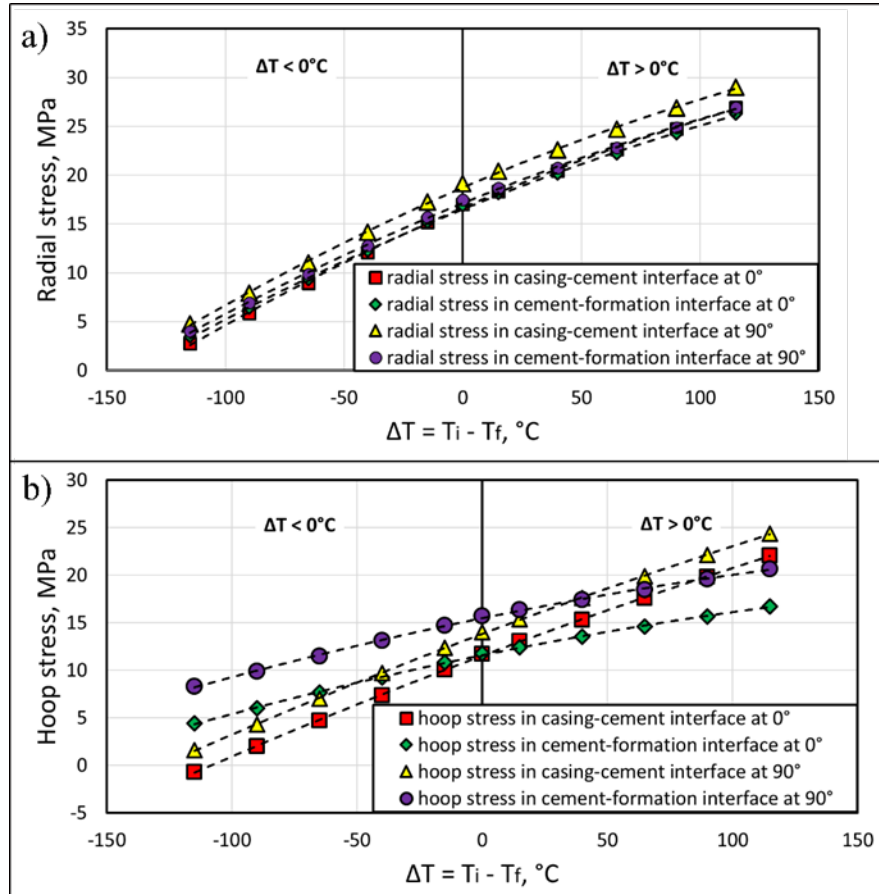


Figure 4.3 a) Radial stress and b) hoop stress in variable differential temperature (ΔT) in the casing-cement and cement-formation interfaces at 0° and 90° .

4.4. Sensitivity Analysis

Figure 4.3a and **4.3b** illustrate that a high differential temperature between casing and formation results in a higher risk of cement failure. A parametric study was conducted for both kinds of heat flow patterns ($\Delta T > 0$ and $\Delta T < 0$). The list of variables investigated is shown in **Table 4.4**. The sensitivity response curve is used to compare the impact of different parameters on the cylindrical stresses in a single plot (Patel and Salehi, 2019).

The analysis ignores the effects of temperature on material properties. Each variable was changed individually while keeping the other variables constant. To make the properties comparable, normalized parameter values are used. The normalized parameter is calculated by dividing the value of the parameter in each case by the base case value ($normalized\ parameter = \frac{parameter\ value}{base\ case\ value}$). The sensitivity response curves are expressed by the relationship between the outcome values (radial and hoop stresses) and normalized parameters.

There are three kinds of variables - thermal and mechanical properties of cement, internal casing pressure, and lithological properties involved in this study. For the thermal properties, thermal conductivity and thermal expansion coefficients are studied. Thermal conductivity represents the effects of temperature distribution on cement failure. Thermal expansion coefficients scale the thermal strain of material and the induced thermal stress if the thermal deformation is restraint (Zeng et al., 2012). Changing the coefficients results in different stress magnitudes and consequently different failure modes. The mechanical properties involve Young's modulus and Poisson's ratio to investigate the effects of cement recipe or material aging by temperature, corrosion, or other degrading environments. Internal casing pressure is one of the major loads in a wellbore. The increment of the internal casing pressure happens during positive pressure tests, formation integrity tests, increased mud weight, and hydraulic fracture. The reduction of casing pressure occurs in the event of loss circulation or influx of lighter formation fluid (Patel and Salehi, 2019). Lithological properties are represented in terms of tectonic stress ratio (N_R). Tectonic stress

ratios are dependent on lithology. Tectonic stress ratio is defined as the ratio of maximum and minimum horizontal stress ($horizontal\ stress\ ratio = \frac{\sigma_{h-max}}{\sigma_{h-min}}$).

Table 4.4 Studied parameters for the sensitivity response analysis.

<i>Parameter</i>	<i>Base Value</i>	<i>Sensitivity Analysis Value</i>
<i>Young's modulus (GPa)</i>	12.5	5 (0.4), 10 (0.8), 12.5 (1.0), 20 (1.6), 35 (2.8)
<i>Poisson's ratio</i>	0.34	0.20 (0.59), 0.25 (0.74), 0.34 (1.0), 0.45 (1.32)
<i>Horizontal stress ratio</i>	1.25	1.00 (0.80), 1.25 (1.0), 2.00 (1.60), 2.50 (2.0)
<i>Thermal conductivity of cement (W/m•K)</i>	0.3	0.2 (0.67), 0.3 (1.0), 0.5 (1.67), 1.0 (3.33)
<i>Expansion coefficient of cement (10⁻⁶/K)</i>	9.4	7.0 (0.74), 8.0 (0.85), 9.4 (1.0), 11.0 (1.17), 12.0 (1.28)
<i>Differential temperature (°C)</i>	115	0 (0), 40 (0.35), 65 (0.57), 90 (0.78), 115 (1.0), 140 (1.22)
<i>Casing pressure (MPa)</i>	10	0 (0), 5 (0.5), 10 (1.0), 15 (1.5), 20 (2)

* The temperature difference (ΔT) for conductivity, expansion coefficient, Young's modulus, Poisson's ratio, stress ratio and casing pressure cases is 115°C.

** Numbers inside parenthesis are normalized values of parameters.

An illustration of the radial and hoop stress in 0° and 90° as applying different parametric study cases is presented. The results show that the highest magnitude of stresses and consequently a high risk of integrity loss is at the cement-casing interface of the cement sheath. Therefore, in order to simplify the comparison, sensitivity response analysis is only presented at the casing-cement interface.

4.4.1. Heat Flow from Formation to Casing ($\Delta T < 0$)

Heat flow transfer from the formation to casing is representative of injection wells. Especially in the geothermal wellbore, cold fluid is injected in the high-temperature

reservoir, with increasing depth, the temperature difference tends to be higher than shallow depth. **Figure 4.4a** to **4.4d** illustrate the cylindrical stresses in the casing-cement interface at both 0° and 90° when $\Delta T < 0$.

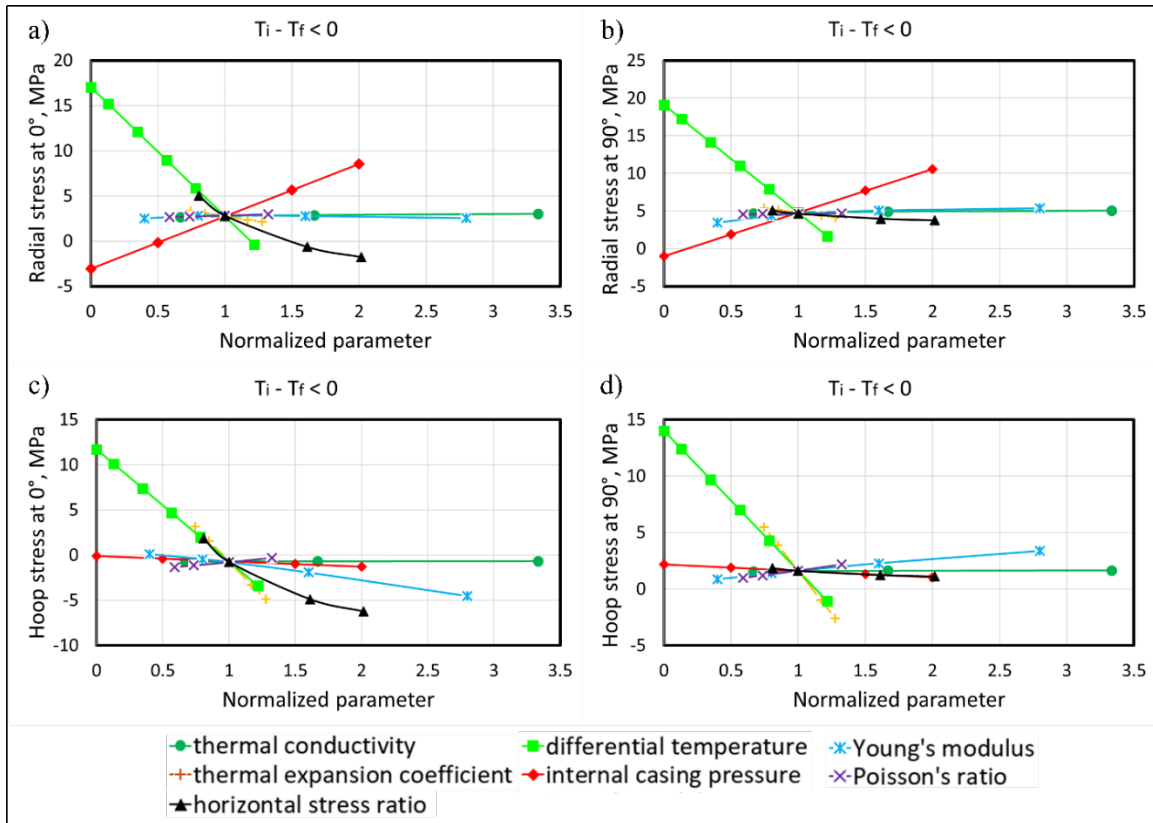


Figure 4.4 Radial stress in the casing-cement interface when heat transfers from the formation to casing ($\Delta T < 0$) a) at 0° and b) at 90° ; hoop stress in the casing-cement interface c) at 0° and d) at 90° .

For the radial stresses in 0° and 90° (**Figure 4.4a** and **4.4b**), the differential temperature is the most sensitive parameter, followed by internal casing pressure and horizontal stress ratio (**Table 4.5**). The other parameters such as thermal conductivity, expansion coefficient, Young's modulus, and Poisson's ratio do not exert notable influence on the radial and hoop stress. An increase in casing pressure increases the compressive nature and magnitude of radial and hoop stresses. On the other hand, an increase in

differential temperature and horizontal stress ratio reduces radial and hoop stresses and makes them more tensile. The tensile stress at 0° (**Figure 4.4a**) is larger than at 90° (**Figure 4.4b**).

The thermal expansion coefficient is the most critical parameter for the hoop stresses (**Figure 4.4c** and **4.4d**), followed by differential temperature, horizontal stress ratio, and Young's modulus (**Table 4.5**). An increase in temperature difference, horizontal stress ratio, and thermal expansion coefficient tend to reduce the hoop stress and make it more tensile. In general, hoop stress at 90° direction has a higher magnitude than along 0° .

The comparison shows that the debonding and radial fracture at the casing-cement interface in 0° is the most probable failure mode. For both cylindrical stresses (radial and hoop), differential temperature and horizontal in-situ stress are the critical parameters. For hoop stress, the thermal expansion coefficient is also a highly influential variable.

4.4.2. Heat Flow from Formation to Casing ($\Delta T > 0$)

Casing temperature larger than formation temperature is likely in production wells wherein high-temperature geothermal fluid is produced. Especially against shallow depth, where formation temperature is low. **Figure 4.5a** to **4.5d** illustrate the cylindrical stress in the casing-cement interface at both 0° and 90° when $\Delta T > 0$. The stresses are predominantly compressive.

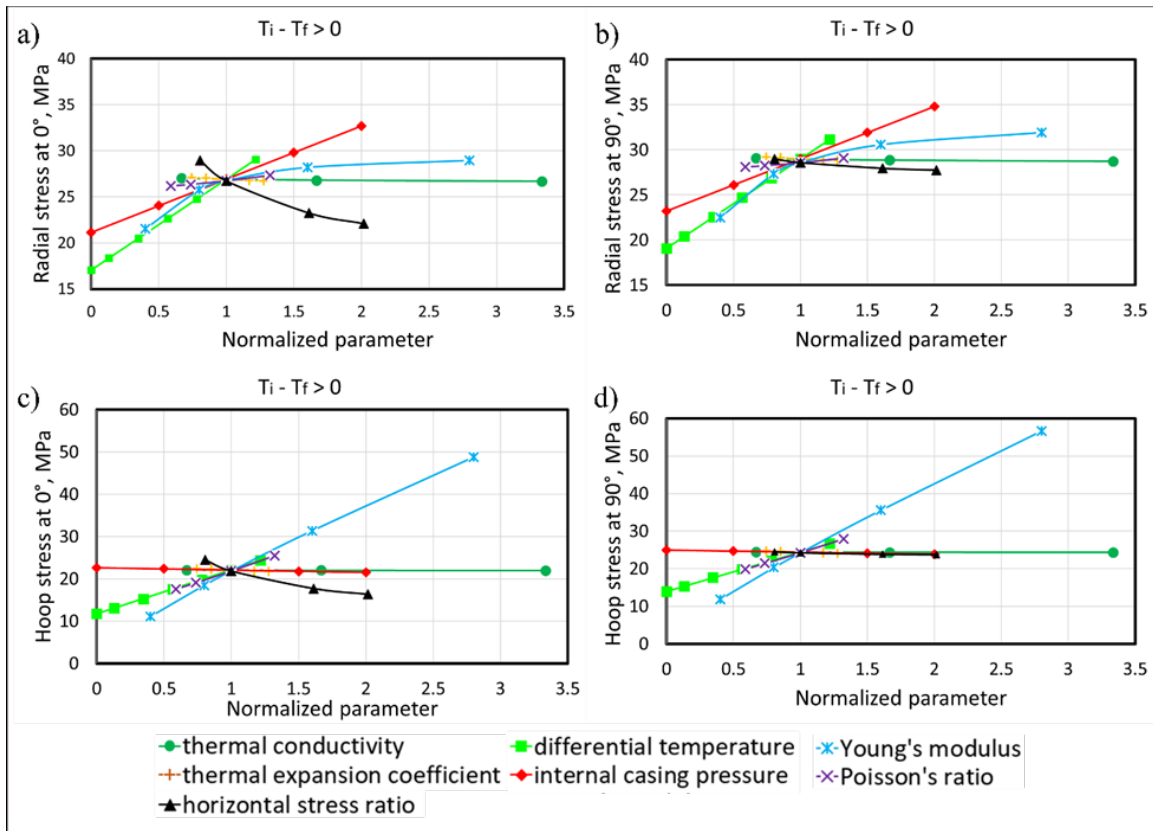


Figure 4.5 Radial stress in the casing-cement interface when heat transfers from the casing to the formation ($\Delta T > 0$) a) at 0° and b) at 90° ; hoop stress in the casing-cement interface c) at 0° and d) at 90° .

For the radial stress (**Figure 4.5a and 4.5b**), the effects of the variables in parallel and perpendicular directions are similar. The magnitudes of compression in the perpendicular direction (i.e., 90°) are larger than parallel (i.e., 0°). The most sensitive parameter to the radial stress is the differential temperature followed by internal casing pressure, Young's modulus, and stress ratio (**Table 4.5**). Young's modulus and stress ratio are more sensitive at low magnitudes compared to higher magnitudes. High differential temperature, casing pressure, Young's modulus, and low-stress ratio results in sufficient compressive stress to exceed the limitation of cement strength. It would increase the risk of cement crushing.

For the hoop stress (**Figure 4.5c and 4.5d**), stress has the largest sensitivity to change in Young's modulus. The other parameters, such as Poisson's ratio, differential temperature, and stress ratio induce notable change (**Table 4.5**). Same as radial stress, the compressive stress in the perpendicular direction is slightly larger than parallel. An increase of Young's modulus, differential temperature, and Poisson's ratio results in higher compressive hoop stress. Contrary to this, increases in stress ratio reduce the compressive nature of hoop stress and push it towards tensile.

The comparison of two directions under the condition of $\Delta T > 0$ shows that cement crushing (compressive failure) in the casing-cement interface at 90° is the most likely failure mode compared to tensile failures.

Table 4.5 Summary of mechanical stress sensitivity to different parameters.

<i>Direction</i>	<i>Radial stress (σ_r)</i>	<i>Hoop stress (σ_θ)</i>
<i>$\Delta T < 0$</i>		
0°	$\Delta T > P_i > N_R$ ($\alpha, K, E,$ and ν are not sensitive)	$\alpha > \Delta T > N_R > E$ ($K, \nu,$ and P_i are not sensitive)
90°	$\Delta T > P_i > N_R$ ($\alpha, K, E,$ and ν are not sensitive)	$\alpha > \Delta T > N_R > E$ ($K, \nu,$ and P_i are not sensitive)
<i>$\Delta T > 0$</i>		
0°	$\Delta T > P_i > E > N_R$ ($K, \alpha,$ and ν are not sensitive)	$E > \nu > \Delta T > N_R$ ($K, P_i,$ and α are not sensitive)
90°	$\Delta T > P_i > E > N_R$ ($K, \alpha,$ and ν are not sensitive)	$E > \nu > \Delta T > N_R$ ($K, P_i,$ and α are not sensitive)

4.5. Chapter Summary

This study investigates the integrity of cement bonds between casing and formation under the influence of thermal stresses. An analytical model is used to generate theoretical values of stresses to verify the 2D finite element model of the casing-cement-formation system. Finite element simulations show a good match with the analytical model of radial and hoop stresses. The deviation between FEA and analytical calculations for both heat flow directions ($\Delta T > 0$ and $\Delta T < 0$) is less than 7%. Various scenarios are simulated to study the influence of temperature difference, thermal conductivity, and thermal expansion coefficients on stresses in cement. Sensitivity analysis has been presented to show the influence of thermal factors relative to other important parameters like casing pressure, cement material properties, and in-situ geomechanical stresses. The following points are concluded from the study that helps to improve understanding of cement failure.

- Based on the comparison of two kinds of temperature patterns, it can be concluded that under in-situ tectonic stresses, when heat transfers from the formation to the casing ($\Delta T < 0$) and differential temperature is high, the risk of radial fracture in the casing-cement interface at 0° is high.
- When heat transfer from the casing to the formation ($\Delta T > 0$) with large temperature difference, the risk of cement crushing near casing-cement interface at 90° is the likely failure mode in the cement.
- Stress distributions in wellbore were investigated for various simulation cases. It was observed that the magnitude of radial and hoop stresses and consequently the risk of failure is higher at the cement-casing interface compared to other locations

within the wellbore. The risk of failure is high in directions parallel (0°) and perpendicular (90°) to maximum horizontal in-situ stress along with the casing-cement interface.

- Sensitivity of radial and hoop stresses to temperature difference when heat transfer is from the formation to the casing ($T_i < T_f$) is higher compared to the opposite scenario ($T_i > T_f$).
- For the range of parameters investigated, scenarios with heat transfer away from the wellbore exhibited a higher magnitude of stresses than cases with heat transfer towards the wellbore.
- Sensitivity analysis indicates that regardless of the direction of heat transfer, radial and hoop stresses in cement have a higher sensitivity to temperature changes compared to pressure load.
- Regardless of the direction of heat transfer, radial stress in cement has a high sensitivity to both temperature difference and pressure load. Thermal conductivity and expansion coefficient has no significant influences.
- For hoop stress, temperature difference has a high impact, but pressure load does not strongly influence it. Thermal conductivity is not important, and the thermal expansion coefficient is influential only for heat transfer direction towards the wellbore.

Chapter 5: Numerical Investigation of Cement Hydraulic Integrity Impacted by Displacement Factors

As mentioned in Chapter 2, an excellent cement design should satisfy mechanical and hydraulic well integrity requirements. In this Chapter, the performance of drilling fluid displaced by cement slurry is simulated using a 3D numerical model via a computational fluid dynamics (CFD) approach. The effects of WBM contamination, cement injection rate, density difference on displacement efficiency are studied. The novel information of this study is to improve the design of the mud displacement procedure and consequently improve the wellbore integrity and secure zonal isolation.

5.1. CFD Simulation Setup

A 3D CFD model is developed using ANSYS FLUENT to simulate the displacement efficiency with different cement recipes and wellbore conditions. Cement slurries directly displace drilling fluid. No spacer or other fluids are considered. Neat class G cement and geopolymer are compared in this study for the investigation of the displacement performance in the enlarged annulus between casing and formation. The geometry of the annulus depicts based on well logging data from the Tuscaloosa Marine Shale (TMS), whose enlarged section is common due to washout on the weak formation. Effects of density ratio, cement injection rate, and WBM contamination are also evaluated for finding the influenced parameter (**Figure 5.1**).

The CFD model is based on the multiphase finite volume method. Pressure-velocity is coupled using the pressure implicit method with the splitting of operators (PISO). The well is assumed horizontal. Drilling mud is removed by cement slurry in the casing-

formation annulus calculated based on laminar flow theory. The inner diameter is 10 inches (254 mm). Although casing eccentricity would have a remarkable influence on the displacement, this investigation aims to explore the optimized fluid selection and operational factor. The eccentric effect is not discussed. The casing is assumed concentric. The outer diameter is generated based on the one well in the TMS. According to the caliper log, the well depth from 12020.5 ft (3663.85 m) to 12032.5 ft (3667.51 m) is simulated due to the existence of an enlarged zone (**Figure 5.2**). A Mesh size of 5 mm is applied to provide enough accuracy of the results.

Table 5.1 shows the flow properties of cement slurries and WBM used in this study. The properties are collected from laboratory tests. The rheology is described by the Herschel-Bulkley model. The cement slurry is injected with a flow rate of 0.2 m/s for 1200 sec. The total injected cement slurry is 2.16 m³ (13.586 bbl). The flow is assumed as a laminar flow based on calculations of Equation 38. The boundary condition of the outlet is defined as no pressure. Non-slip stationary walls are applied in the interfaces of casing and formation (inner and outer surfaces of the annulus).

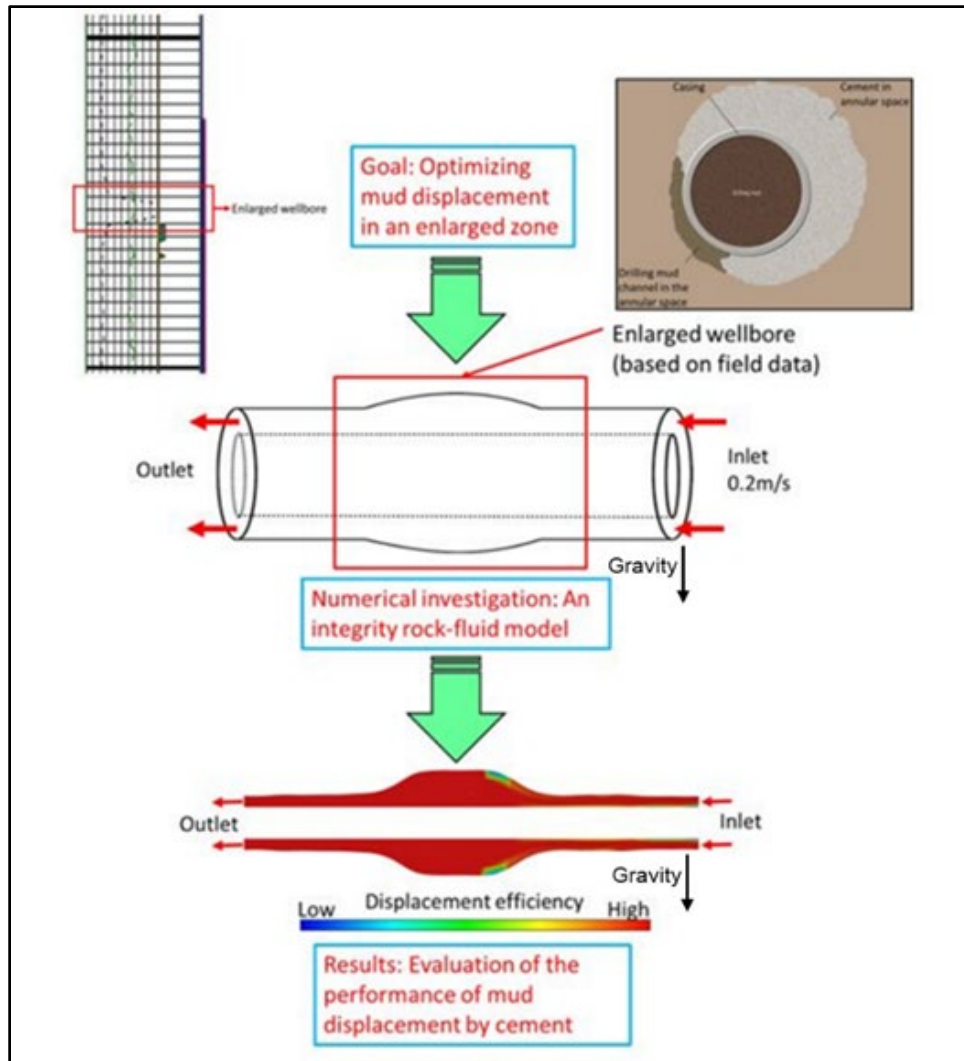


Figure 5.1 Flowchart of using an integrated rock-fluid model to investigate the mud displacement characterization in enlarged wellbores (Caliper log of TMS is used for the develop annulus geometry).

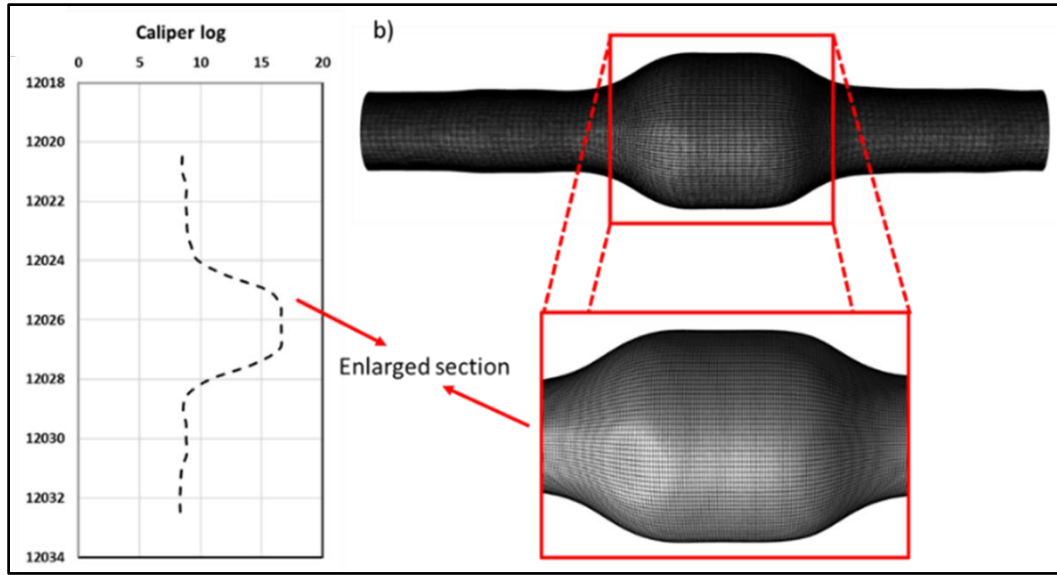


Figure 5.2 a) Caliper log of one well in TMS from 12020.5 ft to 12032.5 ft; b) Verified fine mesh used in the model.

$$N_{Re} = \left[\frac{2(3n+1)}{n} \right] \times \left\{ \frac{\rho v_p^{(2-n)} \left(\frac{dp}{2} \right)^n}{\tau_0 \left(\frac{dp}{2v_p} \right)^n + k \left[\frac{(3n+1)}{nC_c} \right]^n} \right\} \quad (38)$$

Table 5.1 Properties of cement slurries and drilling muds used in the model.

Properties	Water based mud	Neat class G cement	Neat Geopolymer
Density (kg/m ³)	1234.25	2160.00	1970.00
Yield shear stress (Pa)	0.85	0.149	0.6705
Consistency coefficient (Pa•s ⁿ)	1.5	3.2101	0.3649
Liquidity index	7.5	0.5867	0.8694

5.2. Result and discussion

The study compares different performances of neat class G cement and geopolymer by considering cement volume fraction. The cement volume fraction is calculated by dividing the volume of cement slurry by the total fluids volume showing in **Equation 39**. The lower cement volume fraction in the annulus results in an incomplete mud removal,

leading high risk of debonding (Renteria et al., 2019). Additionally, the effects of density ratio, cement injection rate, and cement contamination are assessed to optimize the pumping process for better, higher-quality mud removal. Throughout the investigation, the presented snapshots of the displacement results are based on the same volume of the injected cement slurry (cement slurry of 2.16 m³ is injected).

$$\text{cement volume fraction} = \frac{\text{volume of cement slurry}}{\text{total fluids volume}} \quad (39)$$

5.2.1. WBM Displaced by Neat Class G and Geopolymer

The cement volume fraction of the cross-section in the cement-formation annulus is studied. Neat class G cement and geopolymer have a good performance in the lower annulus. No residual mud and mud contamination issues are observed in the lower annulus (**Figure 5.3c**). For the upper annulus, cement has a good displacement performance near the casing. At the enlarged section of the wellbore, it is a high risk of having an incomplete drilling fluid removal issue (**Figure 5.3a**). Thus, the cement volume fraction of the middle enlarged section (black arrows in **Figure 5.3a** present measured location and direction) is shown to evaluate the displacement performance of neat class G and geopolymer (**Figure 5.3b**). Both cement slurries completely remove WBM within 0.1m away of the casing. As the distance is far from the casing, the displacement performance lowers down. Compared with geopolymer, neat class G has a lower displacement efficiency resulting in a severe mud contamination issue. At the formation interface, neat class G cement and geopolymer concentrations are zero, indicating a high risk of incomplete displacement induced debonding. Thus, for the enlarged wellbore, two kinds of cement lost well integrity at the

formation interface of the upper annulus. Compared with neat class G cement, geopolymer can remove more drilling fluid at the same location of the annulus.

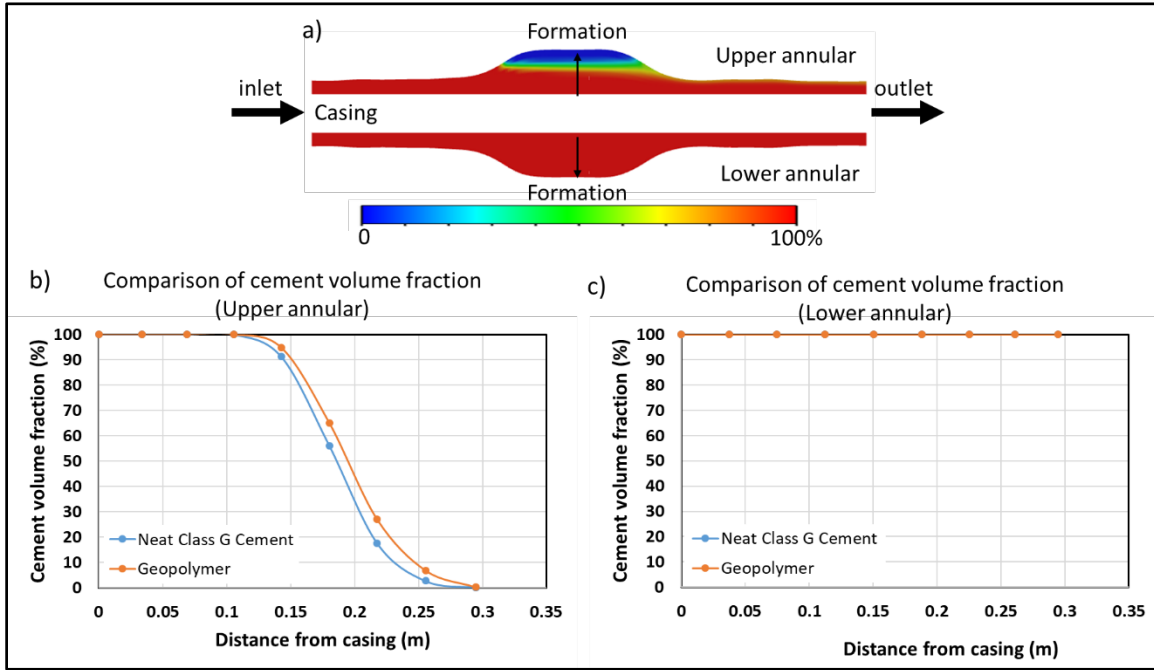


Figure 5.3 a) Snapshot of a class G cement-WBM displacement in the annulus. Comparison of cement volume fraction after displacement between neat class G and Geopolymer b) in the upper and c) lower annulus.

5.2.2. Effect of Density Ratio

As presented in **Figure 5.3**, geopolymer has a better displacement capability than neat class G cement. The influence of the density ratio between cement slurry and drilling fluid is studied to understand the difference. The density ratio is calculated by cement density divided by mud showing in **Equation 40**. **Figure 5.4** illustrates the comparison of cement concentration with different density ratios displacing WBM. The cement slurry density is variable, and other cement properties are the same as neat class G cement.

$$\text{density ratio} = \frac{\text{cement density}}{\text{mud density}} \quad (40)$$

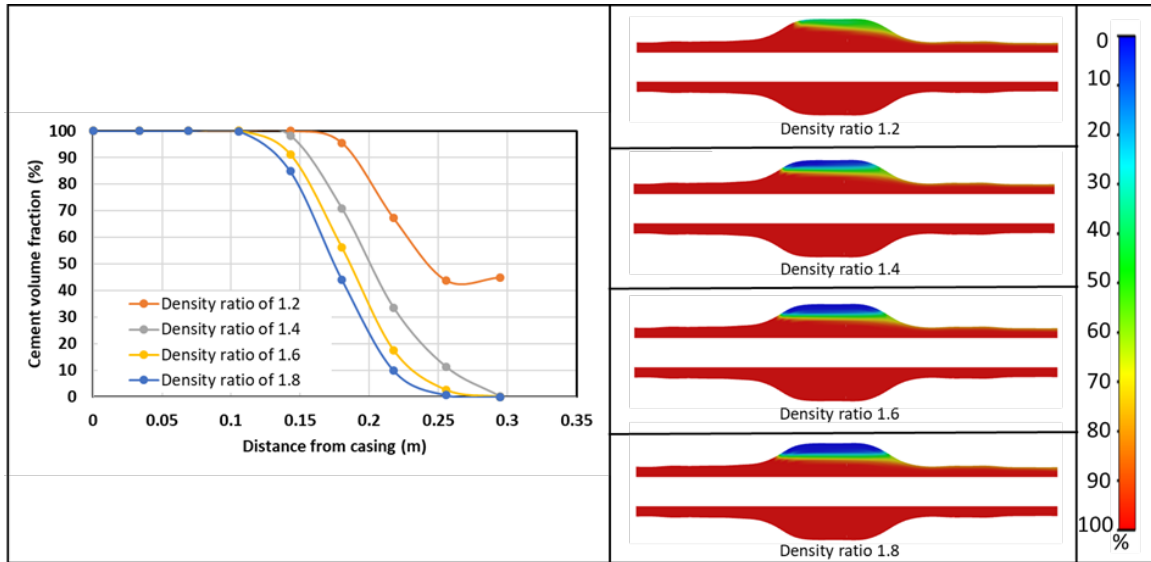


Figure 5.4 a) Comparison of cement volume fraction of the middle of the enlarged section in the upper annulus with different density ratios. b) Snapshots of mud displaced by the cement slurries with 1.2, 1.4, 1.6, and 1.8 of density ratios (from top to bottom) after displacement.

The lower annulus of all scenarios completely removes the drilling fluid. Mud contamination and residual model issues are in the enlarged section of the upper annulus (**Figure 5.4-right**). The cement slurry concentration is lower as the distance from the casing increases. When a cement slurry with high density displacing WBM because of buoyancy induced by mud-cement density difference, the cement tends to fill from the bottom. The drilling fluid is remaining at the top of the enlarged section. As the density increases, more residual mud is observed in the upper annulus. For the cases with a density ratio of 1.2 and 1.4, mud contamination happens, while for the density ratio of 1.6 and 1.8, no cement is near the formation interface resulting in an incomplete removal problem (**Figure 5.4-left**).

5.2.3. Effect of Cement Injection Rate

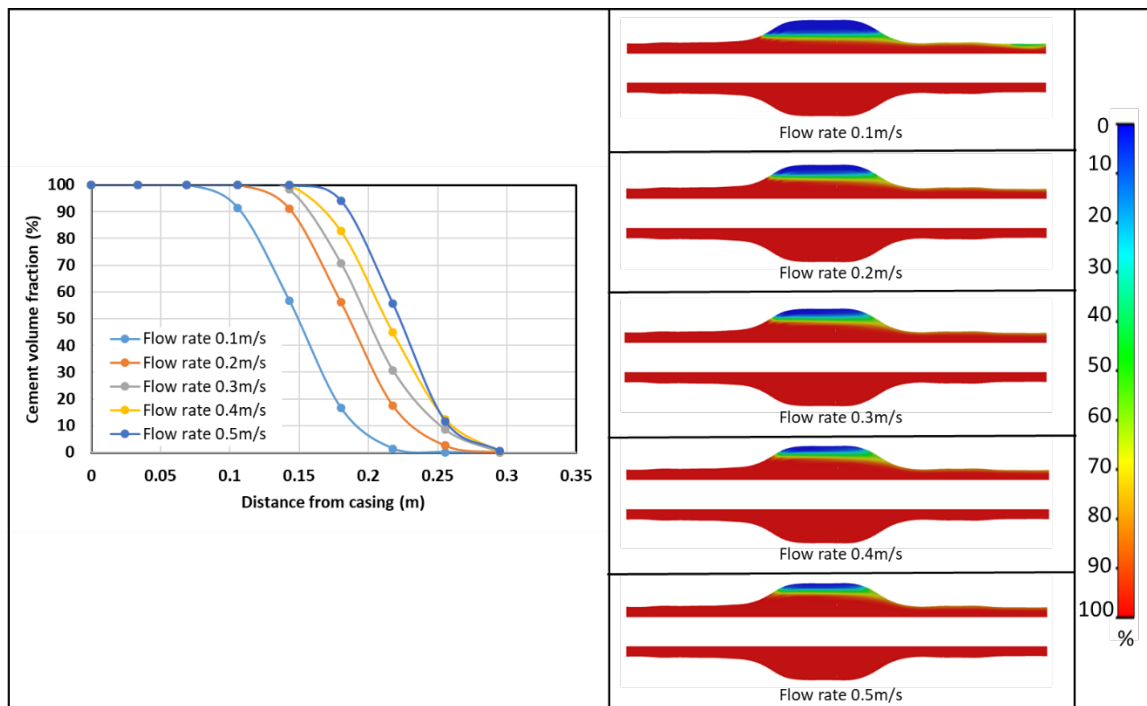


Figure 5.5 a) Comparison of cement volume fraction of the middle of the enlarged section in the upper annulus with different flow rates. b) Snapshots of mud displaced by the cement slurries with 0.1, 0.2, 0.3, 0.4, and 0.5m/s of flow rate (from top to bottom) after displacement.

As mentioned before, flow rates are a controlling parameter in the regular annulus. To extend the research into an enlarged annulus, cement with an injection rate of 0.1, 0.2, 0.3, 0.4, and 0.5 m/s are tested. Mud is completely removed within the 0.06, 0.11, 0.14, 0.15, and 0.17 m from the casing surface with increasing flow rates, respectively. A high risk of debonding is in the scenario with a low flow rate (**Figure 5.5-left**). Snapshots (**Figure 5.5-right**) show that for the lower flow rate (i.e., cement injected with the rate of 0.1 and 0.2 m/s), the enlarged section and near-outlet of annulus have mud contamination issues. The increasing injection rates (i.e., cement injected with the rate of 0.3, 0.4, and 0.5 m/s) improves the mud displacement due to a better sweep efficiency (Wu, 2016).

5.2.4. Effect of Mud Contamination

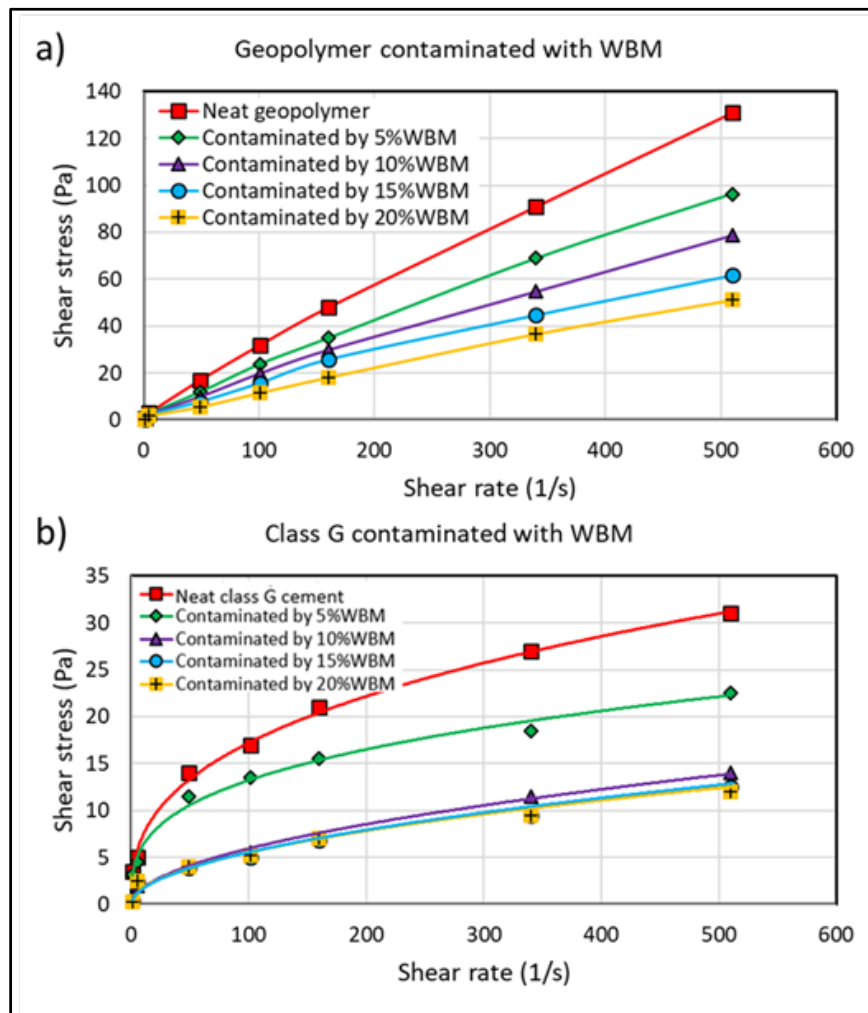


Figure 5.6 Relationship between shear stress and shear rate for a) geopolymer and b) class G cement contaminated with different amounts of WBM.

Previous studies showed that the circulating and residual mud might act as a source of contamination for when cement passes later, lowering the displacement efficiency. In this section, different amounts of WBM contaminated cement are assessed. The model is simulated based on flow properties measured in lab experiments. **Figure 5.6** illustrates the rheology testing results of neat geopolymer, class G cement, and contaminated with WBM. All the samples show a non-Newtonian shear thinning behavior as their viscosity decreases

with an escalation in shear rate due to the length of oligomers formed during conditioning of the slurry. An increasing amount of WBM contamination of both cement systems results in a reducing slurry's viscosity. Both types of cement and contaminated slurries are simulated based on the Herschel-Bulkley non-Newtonian rheological model.

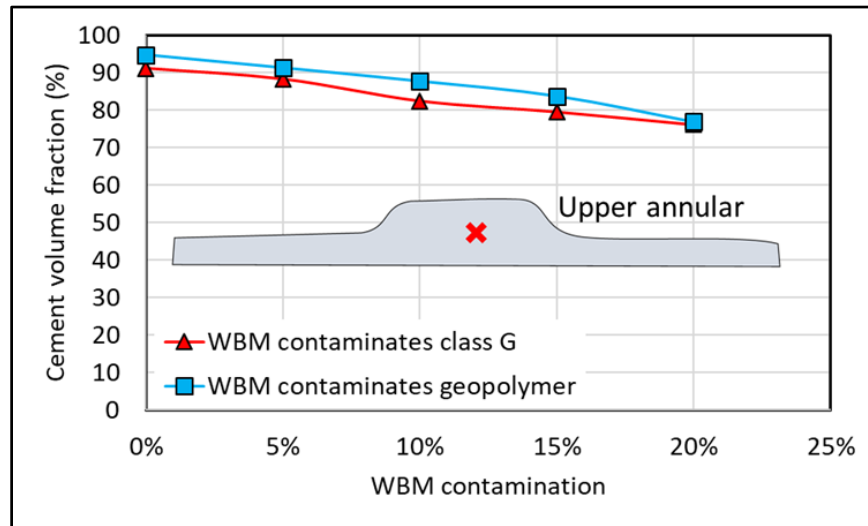


Figure 5.7 Cement volume fraction of middle point in the enlarged section (red “X” mark) of geopolymer and class G cement contaminated with different amounts of WBM.

To evaluate the effect of mud contamination, cement slurry contaminated with different amounts of WBM is investigated. **Figure 5.7** presents the cement volume fraction of the middle point in the enlarged section (red “X” mark) of the upper annulus due to the high risk of lack of cement integrity shown in the last section. The results show a better performance of geopolymer non-contaminated and contaminated cement. For the geopolymer, the cement volume fraction is from 95%, 91%, 87%, 84%, and 77% as 0%, 5%, 10%, 15%, and 20% of WBM contaminations. For the class G cement, the concentration of cement is 90%, 88%, 81%, 79%, and 76%, as the same range of WBM contaminations are applied. WBM contamination has less influence in geopolymer than

class G cement. The observation is in agreement with the previous studies investigating regular annuli (Sun et al., 2019).

5.3. Chapter Summary

This study investigated the characterization of the mud displacement in an enlarged wellbore. A 3D computational fluid dynamics model was used to generate theoretical values of cement concentration to evaluate the displacement qualification. The performances of neat class G cement and geopolymer were compared. Various scenarios were simulated to study the influence of density ratio, cement injection rate, and mud contamination on the displacement efficiency. Following are the major conclusions:

- This study utilized real well-logging data from the Tuscaloosa Marine Shale area to investigate mud displacement in an enlarged horizontal wellbore. The magnitudes of geopolymer and neat class G cement concentration are presented for the evaluation of removal efficiency. Both types of cement have a good performance in the lower annulus, while due to incomplete mud removal, debonding has a high possibility to occur near the formation surface of the upper annulus.
- For the same amount of cement slurry injection, the comparison between geopolymer and neat class G cement shows that the former cement has a high cement volume fraction resulting in a lower risk of cement failure.
- Parametric study of the density ratio presents that regardless of the changing of mud density, the cement volume fraction has a significant influence on the cement

slurry's density. The reducing density ratio causes few residual drilling fluids in the annulus due to buoyancy effects.

- Neat class G cement with different injection rates is used to test the influence of flow conditions. For the testing range, a high rate leads to a better displacement efficiency. Compared with the density ratio, the flow rate has a lower sensitivity on the cement volume fraction.
- Mud contamination is studied based on the rheological properties of WBM generated from lab experiments. WBM contaminations decrease the quality of geopolymer and class G cement. With the same amount of WBM contamination, geopolymer has a better performance.

Chapter 6: Conclusion, Recommendations, And Future Work

This dissertation studies the effect of cement recipe, wellbore conditions, applied stimulation on the cement performance. Structural failure of cement is evaluated by analyzing mechanical stresses around the wellbore to satisfy the requirement of mechanical integrity considerations. For the hydraulic integrity concerns, mud-cement displacement is investigated. Two kinds of FEA models are developed to study mechanical degradation (or structural degradation). One is based on diametric compression tests. The model is verified by the experimental results. It provides a novel method for a more accurate failure evaluation. The other solves wellbore integrity concerns in field-scale HTHP conditions. Analytical solutions are used to validate the model. The novel information of this work is first to show the direction of heat flow pattern on the cement integrity considerations, which is vital in geothermal wells. For hydraulic integrity concerns, a CFD model is developed based on the rheology and geometry properties generated from real conditions. In this investigation, the displacement efficiency in an enlarged horizontal well is studied. Following are the major summary, conclusions, and recommendations from this dissertation:

6.1. Summary

Mechanical integrity models:

- The interfacial bond strength of geopolymer and nano-graphite class H cement was investigated under diametric compression using the DIC technique.
- A validated FEA model was proposed to simulate the casing-cement-formation system based on the diametric compression results.

- A non-uniform stress model was developed to estimate the mechanical stresses in the cement.
- The effect of temperature and casing pressure was investigated.

Hydraulic integrity models:

- The hydraulic model estimated cement distribution in the annulus between the casing and formation.
- Two cement systems were compared using the CFD model.
- The effect of different parameters on cement displacement was evaluated.

6.2. Conclusions

Mechanical degradation models:

- The diametric compression test indicates that cement sheath is likely to fail at the casing interface before the formation interface. along with the casing-cement interface, failure would initiate at the location parallel to the applied load direction
- Heat flow directions are crucial in the analysis of the stress distribution of cement. For the same differential temperature between the casing and the formation, heat flow direction away from the wellbore ($\Delta T > 0$) generates approximately 65% higher magnitude of radial and hoop stresses in the cement compared to heat flow direction toward the wellbore ($\Delta T < 0$).
- The sensitivity of radial and hoop stresses to temperature difference when heat transfers from the formation to the casing ($T_i < T_f$) is higher than in the opposite direction ($T_i > T_f$).

- Compared with internal pressure, radial and hoop stresses within cement have a higher sensitivity to temperature if the direction of heat flow is not considered.
- The sensitivity analysis of each parameter under a specific heat flow direction is shown in **Table 5.5**. This table provides an important reference when designing the cement for different wellbore conditions/types.

Hydraulic degradation models:

- The comparison between geopolymer and neat class G shows that the volume fraction of the former slurry is 20% higher than the other, indicating that geopolymer has a low risk of interfacial debonding.
- In the range of studies, a high flow rate of cement slurry leads to high-quality cement. The cement slurry pumped into a wellbore with 0.1, 0.2, 0.3, 0.4, and 0.5 m/s of injection rate leads to mud removal at 0.06, 0.11, 0.14, 0.15, and 0.17 m from the casing surface with increasing flow rates, respectively.
- Geopolymer and class G cement contaminated with 5%, 10%, 15%, and 20% of WBM are simulated to evaluate the influence of mud contamination on the displacement of different cement types. A high contaminated cement has lower displacement efficiency. At the top of the annulus, the volume fraction of geopolymer is 10% higher than class G cement.

6.3. Recommendations

- The study presents a novel method to test cement bond strength. The test further advances the research by examining a more realistic condition of the wellbore, a casing-cement-formation system. In this novel study, a DIC validated FEA model

is developed. The approach of using the DIC technique to verify the numerical model with the experimental setup can be translated to other loading scenarios as well. An experimentally verified FEA model can be used to estimate the risk of failure in the cement sheath at different operating conditions. Moreover, the operating curves generated in this work can be used to estimate the performance of different cement recipes under diametric compression load. If elastic properties and limiting the strength of the cement are known, then it could be input into the curves to estimate whether failure would occur or not. Effect of curing temperature and time can also be assessed indirectly if cement material properties are known at those conditions. Overall, this paper adds novel information that could help engineers improve the design of the cement and consequently improve the wellbore integrity and secure zonal isolation.

- A field-scale FEA simulation is used to investigate stress distribution within cement in geothermal wells under various thermal scenarios. An analytical model was used to generate theoretical values of stresses to verify the 2D finite element model. The results show that although thermal factors, casing pressure, cement elastic properties, and in-situ geomechanical stresses have a closed relationship to the cement failure evaluation, heat flow cannot be negligible. The stress distribution of cement in production and injection wells is different. Especially for geothermal wells (i.e., Enhanced geothermal system, EGS, and Direct-use geothermal energy, DGE), two types of well are in one system. The influence of heat flow direction should be considered.

- Mud displacement is assessed using a CFD model. A real caliper log and rheological data are applied to the model to ensure accuracy. Cement design and operational constraints are required to be optimized. The proper design should have a high density difference, high flow rate, and high ability to resist mud contamination.
- Since the displacement model presents that mud contamination and cement voids issues are hard to mitigate by optimizing cement properties and increasing flow rate, other treatment, such as casing rotation, is required.

6.4. Future Work

- Dynamic influence – This dissertation uses a mechanical analysis to evaluate the cement integrity by comparing stress magnitude to cement’s strength. The stress is generated under stable in-situ conditions. The dynamic loads, such as the effect of pressure and thermal cycling, are not considered. However, dynamic loads are common in production and injection wells. To extend the scope of the study, the cycling effect should be investigated.
- Dewatering influence – During dewatering (or dehydration), cement tends to shrink. The deformation can result in tensile stress at the interfaces. Tensile stress is recognized as one of the major reasons for debonding. Therefore, the effect of dewatering on cement integrity is required for future research.
- Aging test – Based on the literature, aging wells have a high possibility for cement failure due to a low strength induced by degradation. This dissertation develops a model to evaluate stress with different elastic properties. However, the link between

elastic properties and aging is not established. Thus, the construction of a data library to measure the aging-properties relationship can enhance the well integrity study.

- All of the models show the total stress distribution. The model is assumed as an impermeable and nonporous material. Pore pressure is not considered. Realistically, pore pressure influences stress. Therefore, updating the model to show effective stress is believed can be an important improvement.
- CFD model verification – Although the input data for the mud displacement model is based on the real data, the model is not validated. Either analytical solutions or experimental results are required to improve the reliability of the model.

Nomenclature

Acronyms

2/3D	:	2/3 dimension
ACP	:	Annular casing pressure
API	:	American Petroleum Institute
ASTM	:	American Society for Testing and Materials
BOEMRE	:	Bureau of Ocean Energy Management, Regulation, and Enforcement
BOP	:	Blowout preventer
BWOC	:	By weight of cement
CCR	:	Central Contractor Registration
CFD	:	Computational fluid dynamics
DGE	:	Direct-use geothermal energy
DHSG	:	Deepwater Horizon Study Group in UC Berkeley
DIC	:	Digital image correlation
EGS	:	Enhanced geothermal system
FEA	:	Finite element analysis
FIT	:	Formation integrity test
FORGE	:	Frontier Observatory for Research in Geothermal Energy
fps	:	Frames per second
GoM	:	Gulf of Mexico
HTHP	:	High-temperature and high-pressure

ID	:	Inner diameter
ISO	:	International Organization for Standardization
LOT	:	Leak-off test
LOWC	:	Loss of well control
NORSOK	:	Norsk Søkkel Konkuranseposisjon (Standards by Norwegian Petroleum Industry)
OBM	:	Oil base mud
OD	:	Outer diameter
P&A	:	Plugging and abandonment
PISO	:	Pressure implicit method with splitting of operators
SCP	:	Sustained casing pressure
SCVF	:	Surface casing vent flow
TMS	:	Tuscaloosa Marine Shale
WBM	:	Water base mud

Symbols:

C_o	:	Compressive strength
T_o	:	Tensile strength
p'_f	:	Non-uniform pressure of the formation
a	:	Inner diameter of casing
b	:	Outer diameter of casing
c	:	Inner diameter of formation
d	:	outer diameter of formation

E_s, E, E_f	:	Young's modulus of casing, cement, and formation respectively
J, M, K	:	Constant to calculate radial, hoop, and shear stress under non-uniform formation pressure
K_s, K, K_f	:	Thermal conductivity of casing, cement, and formation respectively
N_R	:	Tectonic stress ratio
p_2	:	Casing-cement interfacial pressure
p_3	:	Cement-formation interfacial pressure
P_i	:	Casing pressure
r	:	Radial distance from the center of the wellbore
T_f	:	Formation temperature
T_i	:	Casing temperature
u_{pc}, u_p, u_{pf}	:	Radial displacement induced by uniform pressure in casing, cement, and formation respectively
u_{rc}, u_r, u_{rf}	:	Total radial displacement in casing, cement, and formation respectively
u_{Tc}, u_T, u_{Tf}	:	Radial displacement induced by temperature in casing, cement, and formation respectively
ΔT	:	Differential temperature between casing and formation

Greek Letter:

σ_{h-max}	:	Maximum horizontal stress
σ_{h-min}	:	Minimum horizontal stress
$\sigma_{rc}, \sigma_r, \sigma_{rf}$:	Radial stresses in casing, cement, and formation respectively

$\tau_{rc}, \tau_r, \tau_{rf}$:	Shear stresses in casing, cement, and formation respectively
ν_s, ν, ν_f	:	Poisson's ratio of casing, cement, and formation respectively
$\alpha_s, \alpha, \alpha_f$:	Thermal expansion coefficient of casing, cement, and formation respectively
ϵ_{xx}	:	Horizontal strain
ϵ_{yy}	:	Vertical strain
σ_r	:	Radial stress
σ_z	:	Axial stress
σ_θ	:	Hoop stress
$\tau_{interface}$:	Interfacial bond strength
ν_c	:	Poisson's ratio of cement sheath
ν_f	:	Poisson's ratio of formation
θ	:	Angle to the maximum horizontal stress
ξ	:	Cohesion strength
σ_r	:	Radial stress
σ_θ	:	Hoop stress

Reference

- Ahmed, S., Salehi, S., And Ezeakacha, C., 2020. Review of Gas Migration and Wellbore Leakage in Liner Hanger Dual Barrier System: Challenges and Implications for Industry. *Journal of Natural Gas Science and Engineering* 78: 103284. <https://doi.org/10.1016/j.jngse.2020.103284>
- Akgun, F., Shedid, S.A., and Al-Ghadban, H.H., 2004. Simulation Investigation of Casing Eccentricity Estimation for Different Inclination Angles and Tensile Forces Using Finite Element Method. Paper presented at the SPE International Petroleum Conference in Mexico, Puebla Pue., Mexico, November 2004. SPE-91811-MS. <https://doi.org/10.2118/91811-MS>
- API RP 65-2, Isolating Potential Flow Zones During Well Construction. 2nd Edition, 2010. Washington, DC: API.
- API RP 90, Annular Casing Pressure Management for Offshore Wells. 1st Edition, 2012. Washington, DC: API.
- API RP 90-2, Annular Casing Pressure Management for Onshore Wells. 1st Edition, 2016. Washington, DC: API.
- API RP 96, Deepwater Well Design and Construction. 1st Edition, 2011. Washington, DC: API.
- API Spec 10D. Casing Bow-Spring Centralizers and Centralizer Subs. 9th Edition, 2019. Washington, DC: API.
- ASTM International, 2016. ASTM D3967-8 Standard Test Method for Splitting Tensile Strength of Intact Rock Core Specimens.

- Bachu, S., 2017. Analysis of Gas Leakage Occurrence Along Wells in Alberta, Canada, From GHG Perspective—Gas Migration Outside Well Casing. *International Journal of Greenhouse Gas Control* 61: 146–154. <https://doi.org/10.1016/j.ijggc.2017.04.003>
- Bai, M., Sun, J., Song, K., Li, L., And Qiao, Z., 2015. Well Completion and Integrity Evaluation for CO2 Injection Wells. *Renewable and Sustainable Energy Reviews* 45: 556-564. <https://doi.org/10.1016/j.rser.2015.02.022>
- Bai, M., Zhang, Z., and Fu, X., 2016. A Review On Well Integrity Issues for CO2 Geological Storage and Enhanced Gas Recovery. *Renewable and Sustainable Energy Reviews* 59: 920-926. <https://doi.org/10.1016/j.rser.2016.01.043>
- Bair, S.E., Freeman, D.C., and Senko, J.M., 2010. Expert Panel Report: Bainbridge Township Subsurface Gas Invasion (Tech. Rep.). Ohio Department of Natural Resources Division of Mineral Resources Management.
- Bios, A.P., Garnier, A., Galdiolo, G., and Laudet, J.B., 2012. Use of A Mechanistic Model to Forecast Cement-Sheath Integrity. *SPE Drilling & Completion* 27 (2): 303–314. SPE-139668-PA. <https://doi.org/10.2118/139668-PA>
- Bios, A.P., Garnier, A., Rodot, F., Saint-Marc, J., Almard, N., 2011. How to Prevent Loss of Zonal Isolation Through a Comprehensive Analysis of Microannulus Formation. *SPE Drilling & Completion* 26 (1): 13–31. SPE-124719-PA. <https://doi.org/10.2118/124719-PA>

- BOEMRE, 2011. Report Regarding the Causes of the April 20, 2010 Macondo Well Blowout. The Bureau of Ocean Energy Management, Regulation and Enforcement. <https://www.bsee.gov/sites/bsee.gov/files/reports/safety/dwhfinal.pdf>
- Bois, A.P., Garnier, A., Galdiolo, G., And Laudet, J.B., 2012. Use of A Mechanistic Model to Forecast Cement-Sheath Integrity. SPE Drilling & Completion 27 (2): 303-314. <https://doi.org/10.2118/139668-PA>
- BP, 2010. Deepwater Horizon Accident Investigation Report. BP. <https://www.nytimes.com/interactive/projects/documents/bps-deepwater-horizon-accident-investigation-report>
- Brandl, A., Cutler, J., Seholm, A., Sansil, M., and Braun, G., 2011. Cementing Solutions for Corrosive Well Environments. SPE Drilling & Completion 26 (2): 208-219. SPE-132228-PA. <https://doi.org/10.2118/132228-PA>
- Broni-Bediako, E. and Amarin, R., 2019. Experimental Study On the Effects of Cement Contamination in A Water Based Mud. Advances in Geo-Energy Research 3 (3): 314-319.
- Brufato, C., Cochran, J., Power, L.C.D., El-Zeghaty, S.Z.A.A., Fraboulet, B., Griffin, T., Munk, S., Justus, F., Levine, J., Montgomery, C., Murphy, D., Pfeiffer, J., Pornpoch, T., Rishmani, L., 2003. From Mud to Cement – Building Gas Wells. Oilfield Review 15 (3): 62-76. https://marcellus-wv.com/online-courses/fracturing/msds/waste/marcellus-issues-in-west-virginia-an-introduction-2/well_construction/marcellus-issues-in-west-virginia-an-introduction-1/marcellus-issues-in-west-virginia-an-introduction/p62_76.pdf

- Brufato, C., Cochran, J., Power, L.C.D., El-Zeghaty, S.Z.A.A., Fraboulet, B., Griffin, T., Munk, S., Justus, F., Levine, J., Montgomery, C., Murphy, D., Pfeiffer, J., Pornpoch, T., Rishmani, L., 2003. From Mud to Cement – Building Gas Wells. *Oilfield Review* 15 (3): 62-76. https://marcellus-wv.com/online-courses/fracturing/msds/waste/marcellus-issues-in-west-virginia-an-introduction-2/well_construction/marcellus-issues-in-west-virginia-an-introduction-1/marcellus-issues-in-west-virginia-an-introduction/p62_76.pdf
- Bu, Y., Li, Z., Wan, C., and Li, H.A., 2016. Determination of optimal density difference for improving cement displacement efficiency in deviated wells. *Journal of Natural Gas Science and Engineering* 31: 119-128. <https://doi.org/10.1016/j.jngse.2016.03.008>
- Burton, K. 2005. Well structural integrity an increasing issue, *Offshore Magazine*, 2005, <http://ogj.pennnet.com/>
- Busahmin, B., Saeid, N.H., Alusta, G., And Zahran, E.S.M.M., 2017. Review On Hole Cleaning for Horizontal Wells. *ARNP Journal of Engineering and Applied Sciences* 12 (16): 4697-4708.
- Bustgaard, M., Nesheim, M.H., 2016. Model for Prediction of Cement Sheath Failure. Thesis, Norwegian University of Science and Technology, Norway.
- Calosa, W.J., Sadarta, B., And Ronaldi, R., 2010. Well Integrity Issues in Malacca Strait Contract Area. Paper presented at the SPE Oil and Gas India Conference and Exhibition, Mumbai, India, January 2010. SPE-129083-MS. <https://doi.org/10.2118/129083-MS>

- Carey, J.W., Svec, R., Grigg, R., Zhang, J., and Crow, W., 2010. Experimental Investigation of Wellbore Integrity and CO₂ – Brine Flow Along the Casing-Cement Microannulus. *International Journal of Greenhouse Gas Control* 4 (2): 272-282. <https://doi.org/10.1016/j.ijggc.2009.09.018>
- Carroll, S., Carey, J.W., Dzombak, D., Huerta, N.J., Li, L., Richard, T., Um, W., Walsh, S.D.C., and Zhang, L., 2016. Review: Role of Chemistry, Mechanics, And Transport On Well Integrity in CO₂storage Environments. *International Journal of Greenhouse Gas Control* 49: 149-160. <https://doi.org/10.1016/j.ijggc.2016.01.010>
- CCR, 2011. Macondo – The Gulf Oil Disaster. National Commission on the BP Deepwater Oil Spill and Offshore Drilling. Chief Counsel’s Report. http://www.wellintegrity.net/Documents/CCR_Macondo_Disaster.pdf
- Celia, M.A., Bachu, S., Nordbotten, J.M., Gasda, S.E., And Dahle, H.K., X. Quantitative Estimation of CO₂ Leakage from Geological Storage: Analytical Models, Numerical Models, And Data Needs. *Greenhouse Gas Control Technologies* 7: 663-671. <https://doi.org/10.1016/B978-008044704-9/50067-7>
- Chen, J., Huang, K., and Liu, Y., 1990. Displacement Efficiency of Cementing in Directional Wells. *China Petroleum* 11 (3): 98-105 (in Chinese).
- Chilingar, G.V. and Endres, B., 2005. Environmental hazards posed by the Los Angeles Basin urban oilfields: an historical perspective of lessons learned. *Environmental geology* 47: 302-317. <https://doi.org/10.1007/s00254-004-1159-0>
- Choi, M., Scherer, G.W., And Prudhomme, R.K., 2018. Novel Methodology to Evaluate Displacement Efficiency of Drilling Mud Using Fluorescence in Primary

- Cementing. *Journal of Petroleum Science and Engineering* 165: 647-654.
<https://doi.org/10.1016/j.petrol.2018.03.008>
- Colmenares, F.J., Padron, A., and Bennaceur, K., 1997. Evaluation of Treatments for Control of Fines Migration in the Ceuta Field in Venezuela. Paper presented at the SPE Annual Technical Conference and Exhibition, San Antonio, Texas, October. SPE-38596-MS. <https://doi.org/10.2118/38596-MS>
- Conley, S., Franco, G., Faloon, I., Blake, D., Peischl, J., and Ryerson, T., 2016. Methane Emissions from The 2015 Aliso Canyon Blowout in Los Angeles, CA. *Science* 351: 1317–1320. <https://doi.org/10.1126/science.aaf2348>
- Considine, T.J., Watson, R.W., Considine, N.B., and Martin, J.P., 2013. Environmental Regulation and Compliance of Marcellus Shale Gas Drilling. *Environmental Geosciences* 20 (1): 1-16. <https://doi.org/10.1306/eg.09131212006>
- Crook, R.J., Keller, S.R., and Wilson, M.A., 1985. Solutions to Problems Associated with Deviated Wellbore Cementing. Paper presented at the SPE's 60th Annual Technical Conference and Exhibition, Las Vegas, NV.
- Davies, R.J., Almond, S., Ward, R.S., Jackson, R.B., Adams, C., Worrall, F., Herringshaw, L.G., Gluyas, J.G., and Whitehead, M.A., 2014. Oil and Gas Wells and Their Integrity: Implications for Shale and Unconventional Resource Exploitation. *Marine and Petroleum Geology* 56: 239-254.
<https://doi.org/10.1016/j.marpetgeo.2014.03.001>

- De Andrade, J., Sangesland, S., 2016. Cement Sheath Failure Mechanisms: Numerical Estimates to Design for Long-Term Well Integrity. *Journal of Petroleum Science Engineering* 147: 682–698. <https://doi.org/10.1016/j.petrol.2016.08.032>
- De Andrade, Torsaeter, M., Todorovic, J., et al., 2014. Influence of Casing Centralization On Cement Sheath Integrity During Thermal Cycling. Paper presented at the IADC/SPE Drilling Conference and Exhibition, Fort Worth, Texas, USA, March 2014. SPE-168012-MS. <https://doi.org/10.2118/168012-MS>
- Deng, J., Wang, Y., and Jia, X., 2011. Method to Calculate Cementing Fluids' Density and Rheological Parameters. *Petroleum Drilling Technology* 39 (5): 45-48 (in Chinese).
- DHSG, 2011. Final Report on the Investigation of Macondo Well Blowout. Deepwater Horizon Study Group. <http://large.stanford.edu/courses/2011/ph240/mina1/docs/DHSGFinalReport-March2011-tag.pdf>
- Eberhardt, J.T. and Shine, J., 2004. Gulf of Mexico Cement Packer Completions Using Liquid Cement Premix. Paper presented at the SPE Annual Technical Conference and Exhibition, Houston, Texas, September 2004. SPE-90841-MS. <https://doi.org/10.2118/90841-MS>
- Eid, E., Tranggono, H., Khalifeh, M., Salehi, S., and Saasen, A., 2021. Impact of Mud Contamination On Performance of Rock-Based Geopolymers. Paper presented at the SPE Oklahoma City Oil and Gas Symposium, Oklahoma City, Oklahoma, USA.
- Ermila, M., Eustes, A.W., Mokhtari, M., 2013. Improving Cement Placement in Horizontal Wells of Unconventional Reservoirs Using Magneto-Rheological Fluids. Paper

- presented at the SPE/AAPG/SEG Unconventional Resources Technology Conference, Denver, Colorado, USA, August. URTEC-1619212-MS. <https://doi.org/10.1190/urtec2013-270>
- Erno, B. And Schmitz, R., 1996. Measurements of Soil Gas Migration Around Oil and Gas Wells in The Lloydminster Area. *Journal of Canadian Petroleum Technology* 35 (7): 37-16. <https://doi.org/10.2118/96-07-05>
- Etrati, A., Roustaei, A., and Frigaard, I.A., 2020. Strategies for Mud-Removal from Washouts During Cementing of Vertical Surface Casing. *Journal of Petroleum Science and Engineering* 195: 107454. <https://doi.org/10.1016/j.petrol.2020.107454>
- Feng, F., Ai, C., and Yu, F., 2011. Effect of Casing Eccentricity On Displacement in Horizontal Wells. *Oil Drilling Production Technology* 33 (3): 13-16 (in Chinese).
- Feng, Y., Li, X. and Gray, K. E. 2017. Development of a 3D Numerical Model for Quantifying Fluid-Driven Interface Debonding of an Injector Well. *International Journal of Greenhouse Gas Control* 62: 76-90. <http://dx.doi.org/10.1016/j.ijggc.2017.04.008>
- Fink, J., 2015. *Petroleum Engineer's Guide to Oil Field Chemical and Fluids*. 2nd Edition. Gulf Professional Publishing. Oxford. UK.
- Fleckenstein, W.W., Eustes III, A.W., And Miller, M.G., 2001. Burst-Induced Stresses in Cemented Wellbores. *SPE Drilling & Completion* 16 (2): 74-82. <https://doi.org/10.2118/62596-MS>

- Foroushan, H.K., Ozbayoglu, E.M., Gomes, P.J., and Yu, M., 2020. Mud/Cement Displacement in Vertical Eccentric Annuli. *SPE Drilling & Completion* 35 (2): 297-316. SPE-189646-PA. <https://doi.org/10.2118/189646-PA>
- Gao, Y., Sun, B., and Liu, D., 2005. Numerical Simulation On Stability of Cement Displacement Interface in Annulus. *Acta Petrolei Sinica* 26 (5): 119-122 (in Chinese).
- Garcia, V. J., Marquez, C. O., Zuniga-Suarez, A., Zuniga-Torres, B.C., Villalta-Granda, L.J., 2017. Brazilian Test of Concrete Specimens Subjected to Different Loading Geometries: Review and New Insights. *International Journal of Concrete Structures and Materials*, 11 (2): 343-363. <http://dx.doi.org/10.1007/s40069-017-0194-7>
- Garnier, A., Saint-Marc, J., Bois, A.P., Kemanach, Y., 2010. An Innovative Methodology for Designing Cement-Sheath Integrity Exposed to Steam Stimulation. *SPE Drilling and Completion* 25 (1), 58–69. <https://doi.org/10.2118/117709-PA>
- Goodwin, K.J., Crook, R.J., 1992. Cement Sheath Stress Failure. *SPE Drilling Engineering* 7 (4): 291–296. SPE-20453-PA. <https://doi.org/10.2118/20453-PA>
- Haciislamoglu, M. and Langlinais, J., 1990. Non-Newtonian Flow in Eccentric Annuli. *Journal of Energy Resource Technology* 112 (3): 163-169. <https://doi.org/10.1115/1.2905753>
- Harrison, S. S., 1983. Evaluating System for Groundwater Contamination Hazards Due to Gas-Well Drilling On the Glaciated Appalachian Plateau. *Groundwater* 21(6): 689–700. <https://doi.org/10.1111/j.1745-6584.1983.tb01940.x>

- Harrison, S. S., 1985. Contamination of Aquifers by Overpressuring the Annulus of Oil and Gas Wells. *Groundwater* 23(3): 317–324. <https://doi.org/10.1111/j.1745-6584.1985.tb00775.x>
- Herschel, W.H. and Bulkley, R., 1926. Measurement of Consistency as Applied to Rubber-Benzene Solutions. *Am. Soc. Test Proc.* 26 (2): 621-633.
- Hibbert, A.P., Kellingray, D.J. and Vidick, B., 1995. Effect of Mixing Energy Levels During Batch Mixing of Cement Slurries. *SPE Drilling & Completions* 10 (1): 49-52. SPE-25147-PA. <https://doi.org/10.2118/25147-PA>
- Holand, P. 2017. Loss of Well Control Occurrence and Size Estimators, Phase I and II. Report prepared for Bureau of Safety and Environmental Enforcement. <https://www.bsee.gov/sites/bsee.gov/files/tap-technical-assessment-program/765aa.pdf>
- Hossain, M.M. and Amro, M., 2010. Drilling and Completion Challenges and Remedies of CO₂ Injected Wells with Emphasis to Mitigate Well Integrity Issues. Paper presented at the SPE Asia Pacific Oil and Gas Conference and Exhibition, Brisbane, Queensland, Australia, October 2010. SPE-133830-MS. <https://doi.org/10.2118/133830-MS>
- Ingraffea, A.R., Wells, M.T., Santoro, R.L., and Shonkoff, S.B.C., 2014. Assessment and Risk Analysis of Casing and Cement Impairment in Oil and Gas Wells in Pennsylvania, 2000–2012. *Proceedings of the National Academy of Sciences of the United States of America* 111 (30): 10955-10960. <https://doi.org/10.1073/pnas.1323422111>

- IPCC, 2005. Special Report On Carbon Dioxide Capture and Storage. ECN Policy Studies: 195-277.
- ISO 10427-1. Petroleum and Natural Gas Industries – Equipment for Well Cementing – Part 1: Casing Bow-Spring Centralizers. 8th Edition, 2017. Geneva, Switzerland: ISO.
- ISO 16530-1, Well Integrity – Part 1: Lifecycle Governance Manual. 1st Edition, 2017. Geneva, Switzerland: ISO.
- Iyoho, A.W. and Azar, J.J., 1981. An Accurate Slot-Flow Model for Non-Newtonian Fluid Flow Through Eccentric Annuli. SPE Journal 21 (5): 565-572. SPE-9447-PA. <https://doi.org/10.2118/9447-PA>
- Jaeger, J.C., Cook, N.G.W., and Zimmerman, R.W., 2007. Fundamentals of Rock Mechanics. 4th edition. Malden, MA: Blackwell Publish.
- Jafariesfad, N., Khalifeh, M., Skalle, P., and Geiker, M.R., 2017. Nanorubber-Modified Cement System for Oil and Gas Well Cementing Application. Journal of Natural Gas Science and Engineering 47: 91-100. <https://doi.org/10.1016/j.jngse.2017.10.002>
- Jandhyala, S., Barhate, Y.R., Anjos, J., Fonseca, C.E., Petrobras, F., And Ravi, K., 2013. Cement Sheath Integrity in Fast Creeping Salts: Effect of Well Operations. Paper presented at the SPE Offshore Europe Oil and Gas Conference and Exhibition, Aberdeen, UK, September 2013. SPE-166622-MS. <https://doi.org/10.2118/166622-MS>

- Kamali, M., Khalifeh, M., Saasen, A., and Delabroy, L., 2020. Materials for Well Integrity – Short-Term Mechanical Properties of Cement Systems. Paper presented at the SPE Norway Subsurface Conference, Virtual, November. SPE-200739-MS. <https://doi.org/10.2118/200739-MS>
- Khalifeh, M. and Saasen, A., 2020. Introduction to Permanent Plug and Abandonment of Wells. Springer Nature publication. <http://library.oapen.org/handle/20.500.12657/23318>
- Khalifeh, M., Hodne, H., Saasen, A., Integrity, O., And Eduok, E.I., 2016. Usability of Geopolymers for Oil Well Cementing Applications: Reaction Mechanisms, Pumpability, And Properties. Paper presented at the SPE Asia Pacific Oil & Gas Conference and Exhibition, Perth, Australia, October. SPE-182354-MS. <https://doi.org/10.2118/182354-MS>
- Kimanzi, R., Wu, Y., Salehi, S., Mokhtari, M., and Khalifeh, M., 2020. Experimental Evaluation of Geopolymer, Nano-Modified, And Neat Class H Cement by Using Diametrically Compressive Tests. *Journal of Energy Resources Technology* 142 (9): 092101. <https://doi.org/10.1115/1.4046702>
- King, G.E., And King, D.E., 2013. Environmental Risk Arising from Well-Construction Failure—Differences Between Barrier and Well Failure and Estimates of Failure Frequency Across Common Well Types, Locations and Well Age, *SPE Production & Operations* 28 (4): 323-344. <https://doi.org/10.2118/166142-PA>
- Kiran, R., Salehi, S., Mokhtari, M., and Kumar, A., 2019. Effect of Irregular shape and Wellbore Breakout on Fluid Dynamics and Wellbore Stability. Paper presented at

- the 53rd U.S. Rock Mechanics/Geomechanics Symposium, New York City, New York, June 2019. ARMA-2019-2058.
- Kiran, R., Teodoriu, C., Dadmohammadi, Y., Nygaard, R., Wood, D., Mokhtari, M., and Salehi, S., 2017. Identification and Evaluation of Well Integrity and Causes of Failure of Well Integrity Barriers (A Review). *Journal of Natural Gas Science and Engineering* 45: 511-526. <https://doi.org/10.1016/j.jngse.2017.05.009>
- Lackey, G. and Rajaram, H., 2019. Modeling Gas Migration, Sustained Casing Pressure, and Surface Casing Vent Flow in Onshore Oil and Gas Wells. *AGU Publications: Water Resources Research* 55 (01): 298-323. <https://doi.org/10.1029/2018WR024066>
- Lackey, G., Rajaram, H., Sherwood, O.A., Burke, T.L., and Ryan, J.N., 2017. Surface Casing Pressure as an Indicator of Well Integrity Loss and Stray Gas Migration in The Wattenberg Field, Colorado. *Environmental Science and Technology* 51(6): 3567–3574. <https://doi.org/10.1021/acs.est.6b06071>
- Lan, Z., Xia, Y., And Zhang, C., 2000. The Repairing Technology of Driving Channel On Small Drifting-Diameter's Casing Damage in Daqing Oilfield. Paper presented at the International Oil and Gas Conference and Exhibition in China, Beijing, China, November 2000. SPE-65099-MS. <https://doi.org/10.2118/65099-MS>
- Lavrov, A., Torsæter, M., 2016. *Physics and Mechanics of Primary Well Cementing*, first ed. Springer, New York. <https://doi.org/10.1007/978-3-319-43165-9>
- Li, Y., Liu, S., Wang, Z., Yuan, J., And Qi, F., 2010. Analysis of Cement Sheath Coupling Effects of Temperature and Pressure in Non-Uniform In-Situ Field. Paper presented

- at the International Oil and Gas Conference and Exhibition in China, Beijing, China, June 2010. SPE-131878-MS. <https://doi.org/10.2118/131878-MS>
- Liao, H., Li, G., and Zhang, S., 2003. Theoretical Analysis of Cementing Displacement Mechanics of Laminar Flow for Slimhole. *Petroleum Drilling Technology* 31 (6): 30-32 (in Chinese).
- Liu, X., Nair, S.D., Cowan, M., van Oort, E., 2015. A novel method to evaluate cement-shale bond strength. Paper presented at the SPE International Symposium on Oilfield Chemistry, The Woodlands, Texas, USA, April 2015. SPE-173802-MS. <https://doi.org/10.2118/173802-MS>
- Liu, Y., Jiang, S., and Huang, K., 1988. One Dimensional Two Phase Flow of Cement Slurry Displacing Mud in an Eccentric Annulus. *Journal of Daqing Petroleum Institute* 12 (3): 35-43 (in Chinese).
- Ma, S. and Kawashima, S., 2019. A Rheological Approach to Study the Early-Age Hydration of Oil Well Cement: Effect of Temperature, Pressure and Nanoclay. *Construction and Building Materials* 215: 119-127. <https://doi.org/10.1016/j.conbuildmat.2019.04.177>
- Marlow, R.S., 1989. Cement Bonding Characteristics in Gas Wells. *Journal of Petroleum Technology* 41 (11): 1146-1153. <https://doi.org/10.2118/17121-PA>
- Molina, O., Vilarrasa, V. and Zeidouni, M. 2016. Geologic Carbon Storage for Shale Gas Recovery. *Energy Procedia* 114: 5748-5760. <https://doi.org/10.1016/j.egypro.2017.03.1713>

- Moore, J., McLennan, J., Allis, R., Pankow, K., Simmons, S., Podgorney, R., Wannamaker, P., Bartley, J., Jones, C., and Rickard, W., 2019. The Utah Frontier Observatory for Research in Geothermal Energy (FORGE): An International Laboratory for Enhanced Geothermal System Technology Development. Paper presented at the 44th Workshop on Geothermal Reservoir Engineering, 11-13 February, Stanford, California.
- Nath, F., Kimanzi, R.J., Mokhtari, M., and Salehi, S., 2018. A Novel Method to Investigate Cement-Casing Bonding Using Digital Image Correlation. *Journal of Petroleum Science and Engineering* 166: 482-489. <https://doi.org/10.1016/j.petrol.2018.03.068>
- NORSOK Standard D-010., 2013. Well Integrity in Drilling and Well Operations, rev. 4, Lysaker, Norway: Standards Norway.
- Norwegian Oil & Gas 117, Recommended Guidelines for Well Integrity. 6th Edition, 2017. Stavanger, Norway: Norwegian Oil & Gas.
- Nowamooz, A., Lemieux, J.M., Molson, J., And Therrien, R., 2015. Numerical Investigation of Methane and Formation Fluid Leakage Along the Casing of a Decommissioned Shale Gas Well. AGU Publication: *Water Resources Research* 51 (6): 4592-4622. <https://doi.org/10.1002/2014WR016146>
- Nygaard, R., Salehi, S., Weideman, B., And Lavoie, R., 2014. Effect of Dynamic Loading on Wellbore Leakage for The Wabamun Area CO₂-Sequestration Project. *Journal of Canadian Petroleum Technology* 53 (1): 69-82. <https://doi.org/10.2118/146640-PA>

- Oil & Gas iQ, 2018. High Pressure High Temperature, High Costs, High Stakes?
<https://www.oilandgasiq.com/content-auto-download/5b04c1b543dfd0385d3c7c22>. (Accessed October 4th, 2018).
- Okech, R.R., Liu, X., Falcone, G., and Teodoriu, C., 2015. Unconventional Completion Design for Deep Geothermal Wells. Paper presented at the SPE Latin American and Caribbean Petroleum Engineering Conference, Quito, Ecuador, November 2015. SPE-177228-MS. <https://doi.org/10.2118/177228-MS>
- Ozbayoglu, M.E. and Omurlu, C., 2006. Analysis of the Effect of Eccentricity on the Flow Characteristics of Annular Flow of Non-Newtonian Fluids Using Finite-Element Method. Paper presented at the SPE/ICoTA Coiled Tubing Conference & Exhibition, The Woodlands, Texas, USA, April 2006. SPE-100147-MS. <https://doi.org/10.2118/100147-MS>
- Patel, H., Salehi, S., 2019. Development of an Advanced Finite Element Model and Parametric Study to Evaluate Cement Sheath Barrier. *Journal of Energy Resource Technology* 141 (9): 1–8. <https://doi.org/10.1115/1.4043137>
- Patel, H., Salehi, S., Ahmed, R., Teodoriu, C., 2019. Review of Elastomer Seal Assemblies in Oil & Gas Wells: Performance Evaluation, Failure Mechanisms, And Gaps in Industry Standards. *Journal of Petroleum Science and Engineering* 179: 1046–1062. <https://doi.org/10.1016/j.petrol.2019.05.019>
- Patel, H., Salehi, S., Teodoriu, C., 2019. Assessing Mechanical Integrity of Expanding Cement. Paper presented at the SPE Oklahoma City Oil and Gas Symposium,

- Oklahoma City, Oklahoma, USA, April, 2019. SPE-195225-MS.
<https://doi.org/10.2118/195225-MS>
- Peng, S., Fu, J., And Zhang, J., 2007. Borehole Casing Failure Analysis in Unconsolidated Formations: A Case Study. *Journal of Petroleum Science and Engineering* 59 (3): 226-238. <https://doi.org/10.1016/j.petrol.2007.04.010>
- Radonjic, M. and Oyibo, A.E., 2014. Comparative Experimental Evaluation of Drilling Fluid Contamination On Shear Bond Strength at Wellbore Cement Interfaces. *World Journal of Engineering* 11 (6): 597-604. <https://doi.org/10.1260/1708-5284.11.6.597>
- Rahimi, R., 2014. The Effect of Using Different Rock Failure Criteria in Wellbore Stability Analysis. M.S. thesis. Missouri University of Science and Technology, Rolla, MO.
- Ramadan, M.A., Salehi, S., Ezeakacha, C., And Teodoriu, C., 2019. Analytical and Experimental Investigation of the Critical Length in Casing-Liner Overlap. *MDPI: Sustainability* 11: 6861. <https://doi.org/10.3390/su11236861>
- Randhol, P. And Carlsen, I.M., 2007. Presentation Assessment of Sustained Well Integrity On the Norwegian Continental Shelf. SINTEF Petroleum Research. <http://www.Co2captureandstorage.Info/Docs/Wellbore/Wellbore%20Presentations/4th%20Mtg/01.Pdf> (Accessed November 6th, 2020).
- Reddy, B.R., Santra, A.K., McMechan, D.E., Gray, D.W., Brenneis, C., and Dunn, R., 2005. Cement Mechanical Property Measurements Under Wellbore Conditions. Paper presented at the SPE Annual Technical Conference and Exhibition, Dallas, Texas, October 2005. SPE-95921-MS. <https://doi.org/10.2118/95921-MS>

- Renteria, A., Maleki, A., Frigaard, I.A., Lund, B., Taghipour, A., Ytrehus, J.D., 2019. Effects of Irregularity On Displacement Flows in Primary Cementing of Highly Deviated Wells. *Journal of Petroleum Science and Engineering* 172: 662-680. <https://doi.org/10.1016/j.petrol.2018.08.045>
- Roustaei, A., Goseelin, A., And Frigaard, I.A., 2015. Residual Drilling Mud During Conditioning of Uneven Boreholes in Primary Cementing. Part 1: Rheology and Geometry Effects in Non-Inertial Flows. *Journal of Non-Newtonian Fluid Mechanics* 220: 87-98. <https://doi.org/10.1016/j.jnnfm.2014.09.019>
- Roy, N., Molson, J., Lemieux, J.M., Van Stempvoort, D., and Nowamooz, A., 2016. Three-Dimensional Numerical Simulations of Methane Gas Migration from Decommissioned Hydrocarbon Production Wells into Shallow Aquifer. *AGU Publications: Water Resources research* 52 (07): 5598-5618. <https://doi.org/10.1002/2016WR018686>
- Santoyo, E., Garcia, A., Morales, J.M., Contreras, E., Espinosa-Paredes, G., 2001. Effective Thermal Conductivity of Mexican Geothermal Cementing Systems in The Temperature Range from 28°C to 200°C. *Applied Thermal Engineering* 21 (17): 1799-1812. [https://doi.org/10.1016/S1359-4311\(01\)00048-5](https://doi.org/10.1016/S1359-4311(01)00048-5)
- Schreppers, G., 2015. A Framework for Wellbore Cement Integrity Analysis. Paper presented at the 49th U.S. Rock Mechanics/Geomechanics Symposium, San Francisco, California, June 2015. ARMA-2015-349.
- Shadravan, A. and Amani, M., 2014. A Decade of Self-Sealing Cement Technology Application to Ensure Long-Term Well Integrity. Paper presented at the SPE

- Kuwait Oil and Gas Show and Conference, Mishref, Kuwait, October 2015. SPE-175237-MS. <https://doi.org/10.2118/175237-MS>
- Shadravan, A., Kias, E., Lew, R., and Maharidge, R., 2015b. Utilizing the Evolving Cement Mechanical Properties under Fatigue to Predict Cement Sheath Integrity. Paper presented at the SPE Kuwait Oil and Gas Show and Conference, Mishref, Kuwait, October 2015. SPE-175231-MS. <https://doi.org/10.2118/175231-MS>
- Shadravan, A., Narvaez, G., Alegria, A., Carman, P., Perez, C., and Erger, R., 2015c. Engineering the Mud-Spacer-Cement Rheological Hierarchy Improves Wellbore Integrity. Paper presented at the SPE E&P Health, Safety, Security and Environmental Conference-Americas, Denver, Colorado, USA, March 2015. SPE-173534-MS. <https://doi.org/10.2118/173534-MS>
- Shadravan, A., Schubert, J., Amani, M., And Teodoriu, C., 2015a. Using Fatigue-Failure Envelope for Cement-Sheath-Integrity Evaluation. SPE Drilling & Completion 30 (01): 68-75. <https://doi.org/10.2118/168321-PA>
- Shahriar, A. and Behdi, M.L., 2012. Optimization of Rheological Properties of Oil Well Cement Slurries Using Experimental Design. Materials and Structures 49 (9): 1403-1423. <https://doi.org/10.1617/s11527-012-9841-2>
- Shahriar, A., 2011. Investigation on Rheology of Oil Well Cement Slurries. PhD Dissertation. University of Western Ontario.
- Sherwood, O. A., Rogers, J. D., Lackey, G., Burke, T. L., Osborn, S. G., and Ryan, J. N., 2016. Groundwater Methane in Relation to Oil and Gas Development and Shallow Coal Seams in The Denver-Julesburg Basin of Colorado. National Academy of

- Sciences of the United States of America 113 (30): 8391–8396.
<https://doi.org/10.1073/pnas.1523267113>
- Sivakumar, V.C.B. And Janahi, I.A., 2004. Salvage of Casing Leak Wells On Artificial Lift in A Mature Oil Field. Paper presented at the Abu Dhabi International Conference and Exhibition, Abu Dhabi, United Arab Emirates, October 2004. SPE-88749-MS. <https://doi.org/10.2118/88749-MS>
- Sklet, S., 2005. Safety Barriers on Oil and Gas Platforms Means to Prevent Hydrocarbon Releases. Doctoral Thesis. The Norwegian University of Science and Technology (NTNU). <https://core.ac.uk/download/pdf/52100784.pdf>
- Sun, L., Huang, X., and Xiang, X., 2005. Status Quo of Domestic Horizontal Cementing Drilling Technology. Drilling Production Technology 28 (5): 23-25 (in Chinese).
- Sun, X., Wu, Q., Zhang, J., Qing, Y., Wu, Y., and Lee, S., 2017. Rheology, Curing Temperature and Mechanical Performance of Oil Well Cement: Combined Effect of Cellulose Nanofibers and Graphene Nano-Platelets. Materials and Design 114: 92-101. <https://doi.org/10.1016/j.matdes.2016.10.050>
- Tehrani, A., Ferguson, J., and Bittleston, S.H., 1992. Laminar Displacement in Annuli: A Combined Experimental and Theoretical Study. Paper presented at the SPE Annual Technical Conference and Exhibition, Washington, D.C., October 1992. SPE-24569-MS. <https://doi.org/10.2118/24569-MS>
- Teodoriu, C. and Bello, O., 2020. A Review of Cement Testing Apparatus and Methods Under CO2 Environment and Their Impact On Well Integrity Prediction – Where

- Do We Stand? *Journal of Petroleum and Engineering* 187: 106736.
<https://doi.org/10.1016/j.petrol.2019.106736>
- Therond, E., Bois, A.P., Whaley, K., and Murillo, R., 2016. Large-Scale Testing and Modeling for Cement Zonal Isolation in Water-Injection Wells. *SPE Drilling & Completion* 32 (4): 290–300. SPE-181428-PA. <https://doi.org/10.2118/181428-PA>
- Thomas, B.S., Gupta, R.C., Kalla, P., and Cseteneyi, L., 2014. Strength, Abrasion and Permeation Characteristics of Cement Concrete Containing Discarded Rubber Fine Aggregates. *Construction and Building Materials* 59: 204-212.
<https://doi.org/10.1016/j.conbuildmat.2014.01.074>
- Tvergaard, V., 2011. Resistance Curves for Mixed Mode Interface Crack Growth Between Dissimilar Elastic-Plastic Solids. *Journal of The Mechanics and Physics of Solids* 49 (11): 2689-2703. [https://doi.org/10.1016/S0022-5096\(01\)00074-6](https://doi.org/10.1016/S0022-5096(01)00074-6)
- Ugwu, I.O., 2008. Cement Fatigue and HPHT Well Integrity with Application to Life of Well Prediction. M.S. Thesis. Texas A&M University.
- Van Kleef, R.P.A.R., van Vliet, J.P.M., 1993. Improving The Reliability of Cement-Setting Time Test by Talking into Account the Influence of Shear. *SPE Drilling and Completion* 8 (1): 51–56. SPE-20926-PA. <https://doi.org/10.2118/20926-PA>
- Vaughn, R.D. and Grace, W.R., 1965. Axial Laminar Flow of Non-Newtonian Fluids in Narrow Eccentric Annuli. *SPE Journal* 5 (4): 277-280. SPE-1138-PA.
<https://doi.org/10.2118/1138-PA>

- Vidic, R.D., Brantley, S.L., Vandenbossche, J.M., Yoxtheimer, D., Abad, J.D., 2013. Impact of Shale Gas Development On Regional Water Quality. *Science* 340 (6134): 1235009. <https://doi.org/10.1126/science.1235009>
- Vignes, B. and Aadnoy, B.S., 2008. Well-Integrity Issues Offshore Norway. *SPE Production & Operations* 25 (2): 145-150. <https://doi.org/10.2118/112535-MS>
- Vignes, B., 2011. Contribution to Well Integrity and Increased Focus On Well Barriers from A Life Cycle Aspect. Phd Thesis. University of Stavanger.
- Vipulanandan, C. and Mohammed, A., 2015. Smart Cement Rheological and Piezoresistive Behavior for Oil Well Applications. *Journal of Petroleum and Engineering* 135: 50-58. <https://doi.org/10.1016/j.petrol.2015.08.015>
- Vivas, C., Salehi, S., Tuttle, J.D., and Rickard, B., 2020. Challenges and Opportunities of Geothermal Drilling for Renewable Energy Generation. *GRC Transactions* 44: 904-918.
- Vralstad, T., Skorpa, R., Opedal, N., and De Andrade, J., 2015. Effect of Thermal Cycling on Cement Sheath Integrity: Realistic Experimental Tests and Simulation of Resulting Leakages. Paper presented at the SPE Thermal Well Integrity and Design Symposium, Banff, Alberta, Canada, November 2015. SPE-178467-MS. <https://doi.org/10.2118/178467-MS>
- Walsh, S.D.C., Frane, W.L.D., Mason, H.E., and Carroll, S.A., 2013. Permeability of Wellbore-Cement Fractures Following Degradation by Carbonated Brine. *Rock Mechanics and Rock Engineering* 46 (3): 455-464. <https://doi.org/10.1007/s00603-012-0336-9>

- Wang, S. And Hu, S., 2019. Experimental Study of Crack Propagation in Cracked Concrete. MDPI: Energies 12 (20): 3854. <https://doi.org/10.3390/en12203854>
- Wang, W. And Taleghani, A.D., 2014. Three-Dimensional Analysis of Cement Sheath Integrity Around Wellbores. Journal of Petroleum Science and Engineering 121: 38-51. <https://doi.org/10.1016/j.petrol.2014.05.024>
- Watson, T.L. And Bachu, S., 2009. Evaluation of The Potential for Gas and CO2 Leakage Along Wellbore. SPE Drilling & Completion 24 (1): 115-126. <https://doi.org/10.2118/106817-PA>
- Watson, T.L. And Bachu, S., 2009. Evaluation of The Potential for Gas and CO2 Leakage Along Wellbore. SPE Drilling & Completion 24 (1): 115-126. <https://doi.org/10.2118/106817-PA>
- Williams, H., Khatri, D., Keese, R., Le Roy-Delage, S., Roye, J., Leach, D., Rottler, P., Porcherie, O., and Rodriguez, J., 2011. Flexible, Expanding Cement System (FECS) Successfully Provides Zonal Isolation Across Marcellus Shale Gas Trends. Paper presented at the Canadian Unconventional Resources Conference, Calgary, Alberta, Canada, November 2011. SPE-149440-MS. <https://doi.org/10.2118/149440-MS>
- Wilson, D.C., Eustes, A.W., and Fleckenstein, W.W., 2018. Lab testing cement-steel bonding at shallow temperature and pressure conditions. Paper presented at the SPE Western Regional Meeting, Garden Grove, California, USA, April 2018. SPE-190031-MS. <https://doi.org/10.2118/190031-MS>
- Wise, J., Nygaard, R., and Hareland, G., 2019. Numerical Analysis of Wellbore Integrity and Cement Sheath Debonding for Wells in the Eugene Island OPD, Gulf of

- Mexico. Paper presented at the 53rd U.S. Rock Mechanics/Geomechanics Symposium, 23-26 June, New York City, New York. ARMA-2019-0439
- Wu, Y., Patel, H., and Salehi, S., 2020. Effect of Pressure Cycling On the Development of Micro-Annulus in Cement Sheath. Paper presented at the SPE/AAPG/SEG Unconventional Resources Technology Conference, Virtual, July 2020. URTEC-2020-2583-MS. <https://doi.org/10.15530/urtec-2020-2583>
- Wu, Y., Patel, H., And Salehi, S., 2020. Parametric Study of Mechanical Stresses Within Cement Sheath in Geothermal Wells. *Geothermics* 90: 102000. <https://doi.org/10.1016/j.geothermics.2020.102000>
- Wu, Y., Patel, H., And Salehi, S., 2020. Thermal Considerations of Cement Integrity in Geothermal Wells. Paper presented at the 45th Stanford Geothermal Reservoir Engineering Workshop, 10-12 February, Stanford, California.
- Wu, Y., Patel, H., Salehi, S., And Mokhtari, M., 2020. Experimental and Finite Element Modelling Evaluation of Cement Integrity Under Diametric Compression. *Journal of Petroleum Science and Engineering* 188: 106844. <https://doi.org/10.1016/j.petrol.2019.106844>
- Xu, H., Zhang, Z., Shi, T., And Xiong, J., 2015. Influence of The WHCP On Cement Sheath Stress and Integrity in HTHP Gas Well. *Journal of Petroleum Science and Engineering* 126: 174-180. <https://doi.org/10.1016/j.petrol.2014.11.028>
- Yang, J., Deng, J., and Feng, Y., 2008. Numerical Simulation On Effect of Density Difference On Displacement Efficiency at Low Cement-Slurry Velocity. *Petroleum Drilling Technology* 36 (5): 62-65 (in Chinese).

- Yuan, Z., Schubert, J., Chantose, P., And Teodoriu, C., 2013. Casing Failure Mechanism and Characterization Under HPHT Conditions in South Texas. Paper presented at the International Petroleum Technology Conference, Beijing, China, March 2013. IPTC-16704-MS. <https://doi.org/10.3997/2214-4609-pdb.350.iptc16704>
- Yuan, Z., Schubert, J., Teodoriu, C., And Gardoni, P., 2012. HPHT Gas Well Cementing Complications and Its Effect On Casing Collapse Resistance. Paper presented at the SPE Oil and Gas India Conference and Exhibition, Mumbai, India, March 2012. SPE-153986-MS. <https://doi.org/10.2118/153986-MS>
- Yuan, Z., Teodoriu, C., And Schubert, J., 2013. Low Cycle Cement Fatigue Experimental Study and The Effect On HPHT Well Integrity. *Journal of Petroleum Science and Engineering* 105: 84-90. <https://doi.org/10.1016/j.petrol.2013.03.006>
- Zeng, Q., Li, K., Fen-Chong, T., and Dangla, P., 2012. Effect of Porosity On Thermal Expansion Coefficient of Cement Pastes and Mortars. *Construction and Building Materials* 28 (1): 468-475. <https://doi.org/10.1016/j.conbuildmat.2011.09.010>
- Zhang, Y., Li, B., and Liu, Y., 1997. Theory and Application for Helical Flow of Drilling Fluid in The Annuli of Directional Wells. *SPE Advanced Technology Series* 5 (1): 146–155. SPE-30824-PA. <https://doi.org/10.2118/30824-PA>
- Zhang, Z. and Wang, H., 2017. Effect of Thermal Expansion Annulus Pressure On Cement Sheath Mechanical Integrity in HPHT Gas Wells. *Applied Thermal Engineering* 118: 600-611. <https://doi.org/10.1016/j.applthermaleng.2017.02.075>
- Zheng, Y., 1995. Displacement Mechanism of Laminar Flow Cementing in Deviated Wells. *Acta Petrolei Sinica* 16 (4): 133-139.

Appendix: Biography

Yuxing Wu is a PhD graduate in Petroleum Engineering with a focus on geomechanical analyses of wellbores (Specialization, Well Integrity) at the University of Oklahoma, USA. He holds an MS degree in Petroleum Engineering (Specializing in Geomechanics) from the Missouri University of Science and Technology and two BS degrees in Petroleum Engineering from the Missouri University of Science and Technology and China University of Geosciences (LinkedIn).

Yuxing has professional experience in Drilling and Well Completion with 5 years of multidisciplinary experience in domestic and international oil and gas projects executed in China and the United States. He published 10 papers, 1 Elsevier book chapter, and 3 poster presentations during graduate studies (Google Scholar). He has received 6 awards, including Robberson Travel Grants from the University of Oklahoma (2020), International Student Grants from the Missouri University of Science and Technology (2014, 2015, and 2016), Excellent Dissertation Award from the China University of Geoscience (Beijing) (2016), and China University of Geoscience (Beijing) Academic Scholarship (2013).

His professional experience record was from the internship in Pegasus Vertex. Inc., Houston, TX. I worked as a computational drilling engineer in a geothermal project in which the drilling design (i.e., casing and cementing job design based on mechanical analysis) was a significant achievement. He also has an experience in the SINOPEC Sheng Li Drilling Technology Corporation, Shandong, China, working as a drilling intern. Besides working in the industry, he worked as a graduate research assistant at the Missouri University of Science and Technology during my Master. He was responsible for a project

that is investigating the development of geological folds (NSF funded). Currently, at the University of Oklahoma, he focuses on the improvement of cementing and drilling fluids in the area of drilling and completion (specialization, well integrity) of the TMS area (DOE funded). He is an active member of SPE, AADE, and also serves as a technical reviewer for leading journals by Elsevier, SPE, MDPI, ASME, SAGE etc.